Surface Forces in Thin Liquid Films of H-Bonding Liquids Confined between Hydrophobic Surfaces

by

Zhenbo Xia

Dissertation submitted to the faculty of the

Virginia Polytechnic Institute and State University

in partial fulfillment of the requirements for the degree of

Doctor of Philosophy

In

Material Science and Engineering

Roe-Hoan Yoon, Committee Chair,

Dwight D. Viehland,

Gerald H. Luttrell,

Guan-Quan Lu,

25th, September, 2015

Blacksburg, Virginia

Keywords: Hydrophobic force, Thermodynamic, Wetting film, Colloid film, Thinning, extended DLVO, Xanthate, Chalcopyrite, Galena, Gold

Surface Forces in Thin Liquid Films of H-Bonding Liquids Confined between Hydrophobic Surfaces

Zhenbo Xia

ABSTRACT

Hydrophobic interaction plays an important role in biology, daily lives, and a variety of industrial processes such as flotation. While the mechanisms of hydrophobic interactions at molecular scale, as in self-assembly and micellization, is relatively well understood, the mechanisms of macroscopic hydrophobic interactions have been controversial. It is, therefore, the objective of the present work to study the mechanisms of interactions between macroscopic hydrophobic surfaces in H-bonding liquids, including water, ethanol, and water-ethanol mixtures.

The first part of the present study involves the measurement of the hydrophobic forces in the thin liquid films (TLFs) confined between two identical hydrophobic surfaces of contact angle 95.3^{o} using an atomic force microscope (AFM). The measurements are conducted in pure water, pure ethanol, and ethanol-water mixtures of varying mole fractions. The results show that strong attractive forces, not considered in the classical DLVO theory, are present in the colloid films formed with all of the H-bonding liquids tested. When an H-bonding liquid is confined between two hydrophobic surfaces, the vicinal liquid molecules form clusters in the TLFs and give rise to an attractive force. The cluster formation is a way to minimize free energy for the molecules denied of H-bonding with the substrates. Thus, solvophobic forces are the result of the antipathy between the CH_2- and CH_3-coated surface and H-bonding liquid confined in the film. A thermodynamic analysis of the solvophobic forces measured at different temperatures support this mechanism, in which solvophobic interactions entail decreases in the excess film enthalpy and entropy. The former represents the energy gained by building clusters, while the latter represents loss of entropy due to structure building.

Thus, hydrophobic interaction may be a subset of solvophobic interaction. The solvophobic forces are strongest in pure water and pure ethanol, and decrease when one is added to the other. Adding a very small amount of ethanol to water sharply reduced the solvophobic force due to the adsorption of the former with an inverse orientation. An exposure of the OH-group toward the aqueous phase decreases the antipathy between the surface and H-bonding liquid and hence causes the hydrophobic (or solvophobic) forces to decrease.

The second part of the study involves the measurement of the hydrophobic forces in the wetting films of water using the force apparatus for deformable surfaces (FADS). This new instrument recently developed at Virginia Tech is designed to monitor the deformation of bubbles to determine the surface forces in wetting films. In effect, an air bubble is used a force sensor. The measurements have been conducted with gold, chalcopyrite, and galena as substrates. The results obtained with all three minerals show that hydrophobic force increases with increasing water contact angle, suggesting that hydrophobic forces are inherent properties of hydrophobic surfaces rather than created from artifacts such as preexisting nanobubbles and/or cavitation. A utility of the intrinsic relationship between hydrophobic force and contact angle is to predict flotation kinetics from the hydrophobicity of the minerals of interest.

ACKNOWLEDGEMENTS

First, I would like to express my sincere gratitude to my respected advisor, Dr. Roe-Hoan Yoon, for his support throughout the course of this doctoral work. I also benefited a lot from his patient guidance and inspiration.

In addition to my advisor, I would like to thank the remainder of my dissertation committee: Dr. Gerald Luttrell, Dr. Dwight Viehland and Dr. Guo-Quan Lu for their kindly suggestion, insightful comments and penetrating questions, throughout my qualify exam, prelim exam and final exam.

I am also deeply grateful to Dr. Eriksson for his suggestion and data analysis instruction of AFM experiments.

Sincere appreciation is extended to Juan Ma and Jialin Wang for training on AFM force measurements. I also want to warmly thank Lei Pan for insightful training of wetting film using FADS and helping solving a lot of problems I encountered with. I also wish to thank Zuoli Li for her help when I have questions about AFM and electrochemical reaction. This work couldn't have been done without their help.

I also acknowledge the many contributions from my fellow lab-mates and the staff at the CAST Center—both for their help and for all the fun we have had in the last few years— Biao Li, Kaiwu Huang, Seungwoo Park, Riddhika Jain, Gaurav Soni, Chris Hull, and Kirsten Titland.

Last but not least, I owe my loving thanks to my family for their encouragement and understanding.

Contents

List of Figures

List of Tables

CHAPTER 1.
Introduction

1.1 General

Hydrophobic interaction is a phenomenon of the tendency of two hydrophobic moieties in water attracting with each other. The hydrophobic interaction occurring between two hydrophobic moieties of radius less than 1 nm as between hydrocarbon chains, the process involves increase in configurational entropy. It has been shown recently that the hydrophobic interaction occurring between macroscopic surfaces entails enthalpy decrease.[1,2,4,5] Both the molecular- and macroscopic-scale hydrophobic interactions play important roles in daily lives and industry, *e.g.*, detergent, super-hydrophobic coatings for water proofing, nano-scale coatings for electronics, flotation, protein folding, *etc*.[1,2,5-9] However, there are much unknowns in the hydrophobic interactions, particularly at macroscopic scale.[5,10,11]

One of the most interesting features of hydrophobic interaction at macroscopic scale is that the meta-stability or instability of thin wetting film of water formed on hydrophobic surfaces, can be traced back to the study about mineral flotation carried out by Blake and Kitchener[12] in 1972. They used the bubble-against-plate technique developed originally by Derjaguin and Kusakov [13] to measure the thickness of wetting films. It was the first time experimentally showing that when an air bubble advanced towards a hydrophobic silica plate, meta-stable films are formed. However according to the DLVO theory, both the double-layer and Van der Waals forces were positive and hence the disjoining pressure should be positive, which should result in a stable thin liquid film (TLF). Yet, the film ruptured when the double-layer force was compressed in KCl solutions due to the presence of hydrophobic force.

Thus, they suggested that in the case of film rupturing on the hydrophobic surfaces, disjoining pressure must be negative due to the hydrophobic interaction. Thermodynamically, the condition for wetting film to rupture can be written as,[12,14,15]

$$\Pi(h) = -\left(\frac{\partial \Delta G}{\partial h}\right)_{p,T,\mu_2} < 0 \qquad [1\text{-}1]$$

at constant pressure, temperature and chemical potential, where ΔG is the free energy of the thin film system and h is the separation distance. The film will become stable in the case of $\Pi(h) > 0$ or $\partial \Delta G / \partial h < 0$.

Later, many investigators developed tools to measure the disjoining pressures in the thin liquid films (TLFs) of water confined between two air bubbles as foam films, between a bubble and a solid surface as in wetting films, and between two solid surfaces as in colloidal films. The wetting film is often referred to as flotation film as it plays an important role in flotation. Israelachivili and Pashley were the first to directly measure the hydrophobic forces in the colloid films formed between two curved mica surfaces in a cationic surfactant solution in 1982 using the *surface force apparatus* (SFA),[16,17] a widely used device allowing for the force between two crossed cylindrical surfaces to be directly measured as a function of distance. Ducker et al. used an unmodified *atomic force microscopy* (AFM) to measure the attractive force on a small silica sphere as it approached a flat silica surface.[18] Matthew et al. used *colloid probe AFM* to study the interaction between the silica particles and air bubbles.[19] There were also several other instruments used for the

hydrophobic surface interaction measurement modified based on surface force apparatus, MASIF (measurement and analysis of surface interaction and forces),[20] the interfacial gauge (IG),[20] and the method of crossed-quartz filaments.[21]

If the measurements were carried out on the hydrophilic surface using the devices introduced above, repulsive disjoining pressure was obtained and most of the data could be well explained by the classical Derjaguin-Landau-Verwey-Overbeek (DLVO) theory or Lifshitz theory. However, if the experiments were carried out on the surface of hydrophobic surface, negative disjoining pressure or attractive forces were observed.[16,18,19,22,23] Despite such diverse experimental facts or theory explanations, most of the hydrophobic force results can be fitted by using empirical single or double exponential force law or power law, after subtracting the classical DLVO forces.

Up to now, more and more researchers have conducted experiments measuring the hydrophobic forces on different systems and various theories have been developed to explain these results. All of these attractive force measured can be classified into two categories:

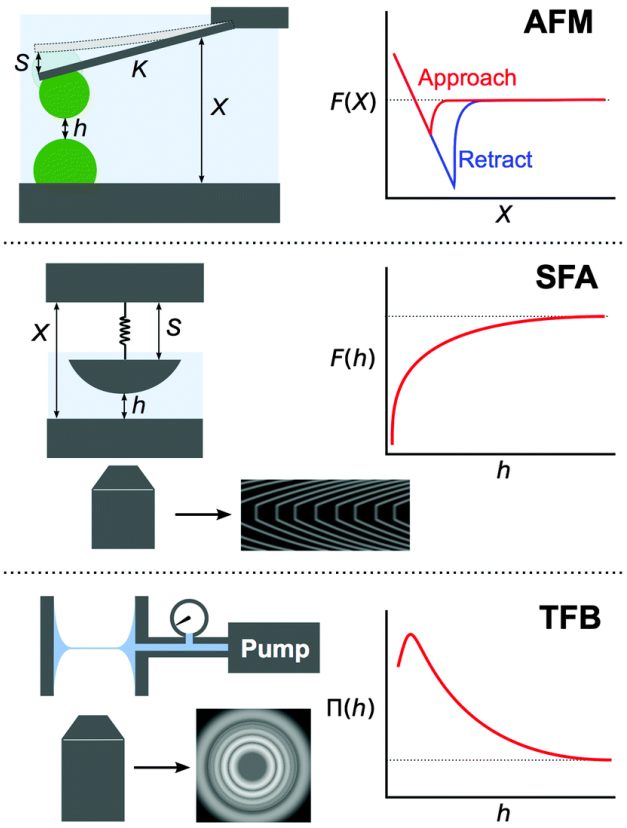

Figure 1.1 The three most common force measurement methods that have been historically used to obtain information on the range and strength of the hydrophobic force. On the left is shown a schematic of the instrument itself, and on the right is schematically shown the typical form of the data obtained. There are also a lot of modified measurement device or methods. Used under the fair use, 2015.

(1) A short range and strong attractive hydrophobic force between stable surfaces, recognized as 'intrinsic' hydrophobic force. This kind of force is due to solely considered as the orientation of water molecules on hydrophobic surfaces, the decay length of which is less than 10Å.[3,9,12,24-29]

(2) A very long-range, attractive hydrophobic force with exponential decay. This kind of forces is usually found exponentially decaying with a decay length of 10 Å ~1000 Å. Though the origin of this force is almost a mystery, the water structure reorganization effect might play a key role in these kinds of forces.[24,30-37]

1.2 Literature Review

Since the first direct measurement of hydrophobic force by Israelachvili in 1982, there have been heated debates on its origin. Some suggest that hydrophobic forces originate from the structural changes of water in the vicinity of hydrophobic surfaces,[2,38] while others believe that it is due to the air bubbles preexisting on hydrophobic surfaces.[39,40] Still others believe that it is due to the enhanced dielectric constant of water between confined hydrophobic surfaces[43]. There are also controversies on the ranges of hydrophobic forces observed. Like the double-layer force, hydrophobic force increases with decreasing film thickness. Some investigators measured short-range forces with decay length of ~1 nm, while others reported decay lengths as large a 40 nm. Since no one knows the origin of the hydrophobic force, there are no theories that can predict decay lengths.

What is making the situation more complicated is that there are also other forces, classical DLVO forces, present on the surfaces: van der Waals force is present between all confined liquid surfaces, and electrical double layer forces are present if the surfaces are charged. These forces are relatively well understood and their presence is widely accepted, and might play a pivotal role for some systems of thin liquid films. Thus, it is necessary to review these classical colloidal forces briefly before comprehensively reviewing the hydrophobic forces, mainly to introduce formulas to estimate the contribution of these forces.

1.2.1 Colloidal Forces in Confined Thin Film

a. Van der Waals Force

The literature on this subject of Van der Waals forces is quite voluminous, and quite a few scientists have written reviews and books, such as London (1937)[41], Mahanty and Ninham (1976)[42], Parsegian (2005)[43], Israelachvili (2011)[44]. Thus, I will just summarize those literatures, pointing out some most basic features or those useful aspects for my data analysis.

Van der Waals between two macroscopic objects are contributed by part or all of the three interactions, each varying with inverse sixth power of the distance:

i). The *orientation* force, also known as Keesom's dipole-dipole interaction. This is due to the permanent charge distribution in the molecules or atoms, such as ion-dipole or dipole-dipole interaction.

ii). The *induction* force, also knowns as Debye's dipole-induced dipole interaction. This force is between a dipole molecule and a nonpolar molecule, which is polarized by the permanent dipole.

iii). The well-known *dispersion* force, also known as London force, charge-fluctuation forces, electrodynamic forces, or induced-dipole-induced-dipole forces. The origin of this force is related to the dispersion of light in the visible and UV regions of the spectrum. This also is might be the most important contribution to the total van der Waals force between atoms and molecules, since they are always present.

The basic Van der Waals interaction between two atoms or small molecules can be expressed as:

$$W(r) = -C/r^6 \qquad [1\text{-}2]$$

Where C is the coefficient in the atom-atom or molecule-molecule pair potential. One may sum the interactions of all the atoms or molecules between two bodies, and the final function of the obtained 'two-body potential' is dependent on geometries. However, the resulting interaction laws can be given in terms of conventional *Hamaker constant*, (Hamaker, 1937)[45]

$$A = \pi^2 C \rho_1 \rho_2 \qquad [1\text{-}3]$$

Where ρ_1, ρ_2 are the number of atoms per unit volume in the two bodies.

After decades' effort by McLachlan, Hamaker, and Lifshitz el al, the nonretarded Hamaker constant for the interaction of two media 1, and 2, across a third medium, 3, combining the general equation for nonretarded van der Waals interaction and equation of the bulk or volume polarizability of planar dielectric medium 1 or 2 in medium 3, can be calculated from the Lifshitz equation[42-44]:

$$\begin{aligned} A = \pi^2 C \rho_1 \rho_2 &= \frac{6\pi^2 kT \rho_1 \rho_2}{(4\pi\varepsilon_0)^2} \sum_{n=0,1,2,\ldots}^{\infty} \frac{\alpha_1(iv_n)\alpha_2(iv_n)}{\varepsilon_3^2(iv_n)} \\ &= \frac{3}{2} kT \left(\frac{\varepsilon_1 - \varepsilon_2}{\varepsilon_1 + \varepsilon_2}\right)\left(\frac{\varepsilon_2 - \varepsilon_3}{\varepsilon_2 + \varepsilon_3}\right) + \frac{3h}{4\pi} \int_{v_1}^{\infty} \left(\left(\frac{\varepsilon_1(iv) - \varepsilon_2(iv)}{\varepsilon_1(iv) + \varepsilon_2(iv)}\right)\left(\frac{\varepsilon_2(iv) - \varepsilon_3(iv)}{\varepsilon_2(iv) + \varepsilon_3(iv)}\right)\right) dv \end{aligned} \qquad [1\text{-}4]$$

Where $\varepsilon_1, \varepsilon_2 \; and \; \varepsilon_3$ are the static dielectric constants of the three media, $\varepsilon(iv)$ are the values of ε at imaginary frequencies and v is the adsorption frequency. The first term includes the Keesom and Debye dipolar contributions and the second term includes the London energy contribution. Though this is not an exact equation, its accuracy is generally better than 95%.

If assuming the adsorption frequencies (v_e) of all three media are the same, and substituting the expression of $\varepsilon(iv)$ in terms of refractive indices (n) and adsorption frequencies[42-44],

$$\varepsilon(iv) = 1 + (n^2 - 1)/(1 + v^2/v_3^3) \qquad [1\text{-}5]$$

An approximate expression for the nonretarded Hamaker constant for two macroscopic phase 1 and 2 interacting across a medium 3, which is also frequently used for simple calculation, can be derived:

$$A \approx \frac{3}{2} kT\left(\frac{\varepsilon_1 - \varepsilon_2}{\varepsilon_1 + \varepsilon_2}\right)\left(\frac{\varepsilon_2 - \varepsilon_3}{\varepsilon_2 + \varepsilon_3}\right) + \frac{3h\nu_e}{8\sqrt{2}} \frac{(n_1^2 - n_3^2)(n_2^2 - n_3^2)}{(n_1^2 + n_3^2)^{1/2}(n_2^2 - n_3^2)^{1/2}[(n_1^2 + n_3^2)^{1/2} + (n_2^2 + n_3^2)^{1/2}]} \quad [1\text{-}6]$$

In the case of symmetric surfaces, or phase 1, crossing medium 3, the expression can be further reduced as,

$$A \approx \frac{3}{2} kT\left(\frac{\varepsilon_1 - \varepsilon_2}{\varepsilon_1 + \varepsilon_2}\right)\left(\frac{\varepsilon_2 - \varepsilon_3}{\varepsilon_2 + \varepsilon_3}\right) + \frac{3h\nu_e}{16\sqrt{2}} \frac{(n_1^2 - n_3^2)^2}{(n_1^2 + n_3^2)(n_1^2 + n_3^2)^{1/2}} \quad [1\text{-}7]$$

There are also a few aspects that should be noted for the van der Waals force, most of which can be deducted from these equations above:

i). Van der Waals force can be either attractive or repulsive since the Hamaker constant can be positive or negative, the sign of which is determined by the physical properties of surfaces and interactive mediums. In the case of the air-water-gold system, Hamaker constant is negative and van der Waals is repulsive. However, in the case of symmetric phase 1 and 2, Hamaker constant is always positive, resulting in an always attractive force.

ii). When the dielectric constant value is low for all the three phases or in the system of dispersion force domain interfaces, combining relations or combining rules are frequently used to estimate the unknown Hamaker constant from known ones. Usually, the geometric mean expression is used and some useful relations are listed as following:

$$A_{132} \approx \pm\sqrt{A_{131}A_{232}} \quad [1\text{-}8]$$

$$A_{132} \approx \pm(\sqrt{A_{11}} - \sqrt{A_{33}})(\sqrt{A_{22}} - \sqrt{A_{33}}) \quad [1\text{-}9]$$

$$A_{131} \approx \pm(\sqrt{A_{11}} - \sqrt{A_{33}})^2 \quad [1\text{-}10]$$

iii). A typical magnitude of Hamaker constant is about 10^{-20} J, the value of which might fluctuate within two orders. And the magnitude of van der Waals force is relative small comparing to the other colloidal forces or long range hydrophobic force at large separation distances, but it will become large enough and cannot be ignored when analyzing short range hydrophobic forces (<5 nm).

b. Electrical double layer forces

Besides the universal van der Waals force, there are electric forces on the thin liquid film, if the surface is charged. The surface charging in a liquid usually originates from in several ways.[44,46]

i) Adsorption or binding of ions from solution onto a previously uncharged surface, such as the adsorption of OH^- onto silica surfaces in water.

ii) The ionization or dissociation of surface groups, such as the ionization of surfactant ending with amine group ($-NH_2 \rightarrow -NH_3^+$).

iii) Charge exchange mechanism, occurring between two dissimilar surfaces very close, which is due to the hopping from one surface to another, such as 'acid-base' type interaction.

The fundamental equations describing the counterion distribution between two charged surfaces in solution is the well-known Poisson-Boltzmann equation,[42,44-47]

$$\varepsilon\varepsilon_0\nabla^2\psi = -e\sum z_i\rho_i(\infty)\exp(-\frac{ez_i\psi}{kT}) \qquad [1\text{-}11]$$

And the electrostatic interaction length between two charged surfaces is described by Debye Length, $1/\kappa$:

$$\kappa = \left(\sum_i \rho_i(\infty)e^2 z_i^2 / \varepsilon_0\varepsilon kT\right)^{1/2} \text{ m}^{-1} \qquad [1\text{-}12]$$

Where ε is the dielectric constant of the solution, ε_0 is the permittivity of vacuum, ψ is the electrostatic potentials ($\psi_0 = 0\ at\ midplane, x = 0$), and $\rho(\infty)$ is the number density of electrolyte ions with valence z.

At least two boundary conditions are needed to solve the PB equation to obtain the interaction pressure or double layer force. The solution is usually very complex and analytical, requiring tedious graphical or numerical integrations, which are not easily applicable to practical systems. Thus, some simplified models using proper approximation has been promoted to analysis the real systems. In the following paragraph, several approximations or special surfaces will be introduced and the equations for calculating double layer force will be shown.

i) Weak overlap approximation or linear superposition approximation (SLA)

If the separation distance is larger than or about one Debye length between those two identically charged surfaces, and when the potential of midplane potential ψ_m is small (< 25 mV. Be aware this is not the surface potential ψ_0, which is constant in the approximation.), which is estimated as the sum of the potentials from both surfaces at x=0.5D and giving $\psi_m = 2\left(\frac{4kT\tanh\left(\frac{ze\psi_0}{4kT}\right)}{e}\right)e^{-\frac{\kappa D}{2}}$, the repulsive pressure between two planar surfaces can be calculated as,[42,44]

$$P = 54kT\rho_\infty(\tanh(\frac{ze\psi_0}{4kT}))^2 e^{-\kappa D} \text{ (Pa)} \qquad [1\text{-}13]$$

Where κ is Debye length, ψ_0 is surface potential, D is the separation distance of the two surfaces, k is Boltzmann constant, and T is temperature.

By applying the Derjaguin approximation, the interaction energy between sphere and planar can also be calculated by $W_{flat-sphere} = F_{flat-flat}/2\pi R$. More results about other geometries can be found in the book written by Israelachvili, *intermolecular and surface forces, edition III.*[44]

ii) Contact Value Theorem

This equation calculated by contact value theorem is always valid if there is no interaction between the counterion and the surfaces, or the charge density on the surface remains constant and independent of D. The pressure for two planar surfaces, both with surface charge of σ, can be expressed as,[44-46]

$$P = kT\rho_0 = 2\varepsilon_0\varepsilon(\frac{kT}{ze})^2 K^2 \qquad [1\text{-}14]$$

With K the solution of equation $\left(\frac{2kTK}{ze}\right)\tan\left(\frac{KD}{2}\right) = -\sigma/\varepsilon_0\varepsilon$,

Where σ is the charge density of the surface. And Derjaguin approximation is also valid for converting the force on planar surface into energy of planar-sphere when D<< R, radius of the sphere.

iii) Low constant surface potential approximation

The equations above are valid only when the separation distance is beyond about one Debye length. At smaller separations, no simple expression that covers all possible situation can be obtained by solving PB equations and one has to resort to numerical solutions. One issue of this is the charge regulation at a small distance. In general, neither the surface charge nor the potential remain constant as two surfaces come close together. The situation will become more complex when it comes to asymmetric surfaces, such as the water thin film confined by air-bubble and plate surfaces.

However, if the surface potential is low, usually less than 100mV, approximation of the constant potential can still be applied and equations for the interactions between two surfaces of unequal but constant potential have already been given by Hogg et al., Parsegian and Gingell,[48] Ohshima et al.,[49] Chan et al.,[50] separately. The equation derived by Hogg, Healy and Fuerstenau, or HHF equation[48], was used for my data analysis. The pressure calculated by equations of the HHF between two planar surfaces is as follow:

$$\frac{F_{el}}{R} = 4\pi nkT\kappa^{-1}\left\{y_{0+}^2\left[i - tanh\left(\frac{\kappa h}{2}\right)\right] - y_{0-}^2\left[coth\left(\frac{\kappa h}{2}\right) - 1\right]\right\} \qquad [1\text{-}15]$$

Here it is specialized for the case of monovalent ions; $\kappa^{-1}$is the Debye length and $y_{0+} = (\varphi_{01} + \varphi_{02})/2$ and $y_{0-} = \frac{\varphi_{01}-\varphi_{02}}{2}$. Non-DLVO Force

c. Limitation of DLVO theory and development of non-DLVO theory

As introduced in the background section, the DLVO theory has been successfully predicted the stability of thin liquid films (TLFs) in the system involving classical colloidal forces only. A lot of followers explained their experimental results with DLVO theory, though the stability and

equilibrium film thickness might have minor differences.[1,17,30,51-53] However, scientists studying flotation in the mining industry found that the stability of the TLFs between air bubble and minerals, the surfaces of which are modified to be hydrophobic, cannot be explained by the DLVO theory.[12,54] Other researchers measuring surface forces between hydrophobic surfaces also confirmed this to be the case.[15,16,21,35,55,56] In the system of air/water/mineral (modified to be hydrophobic), the TLFs are unstable and hence rupture at short separation distance, even though both the van der Waals and the electrical double layer forces are repulsive according to the DLVO theory. Furthermore, the DLVO theory also fails to predict the stability of particle suspensions when the particles are very hydrophilic or hydrophobic.[57-60].

To better understand these discrepancies, some scientists proposed the existence of hydrophobic force in the TLFs formed between air bubble and hydrophobized mineral surfaces. Although Kitchener and Blake may be the first to suggest the presence of the non DLVO forces in 1972, it was not until 1990 that Van Oss and his colleagues extended the DLVO theory (ExDLVO or eDLVO) by accounting for the Lewis acid-base interaction,[61] which successfully explained the stability of hectorite (1 wt. %) suspension in NaCl aqueous solutions of different molarities. Later, Yotsumoto and Yoon (1994)[59] found out that the hydrophobized silica particles were unstable compared to the hydrophilic silica. They extended the DLVO theory to explain the stability of silica suspension over a wide range of pH and electrolyte concentration by incorporating a term related to the hydrophobic force:[60]

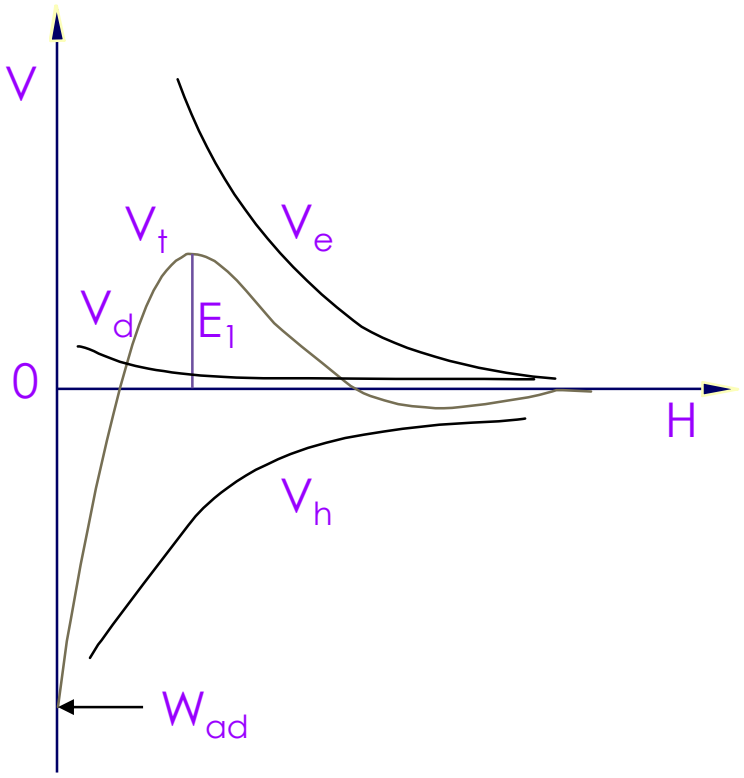

Figure 1.2 Energies promoted in none-DLVO theories, which is capable to explain experimental results obtained on hydrophobic surface.

$$V_t = V_e + V_d + V_h \qquad [1\text{-}16]$$

Where V_e is the potential energy of interaction due to electrical double-layer force, V_d is the term due to the van der Waals force, and V_h is the term due to the hydrophobic forces. The attractive energy term (V_h) was responsible for the instability of the hydrophobic silica suspensions.

These pioneering investigations provided evidences for the existence of the hydrophobic force in TLFs. Many other scientists devoted themselves to find out the origin of the non-DLVO force.

d. Direct hydrophobic force measurements and empirical expressions

Direct hydrophobic force measurement was first carried out by Israelachivili and Pashley[16] on the surface of mica in equilibrium with cetyltrimethylammonium bromide (CTAB) solution using SFA. The surface of mica will become hydrophobic after this treatment. The hydrophobic forces measured were relatively short-range and decay exponentially with decayed length less than 10 nm. They also promoted the exponential law to fit the experimental data:

$$\frac{F}{R} = -C\,exp\left(-\frac{h}{D}\right) \qquad [1\text{-}17]$$

Where D is the decay length and C is the fitting parameter, relating to the surface tension of the solid/water interfaces.

Later some other researchers showed the existence of long-range hydrophobic forces which can be fitted by a double-exponential function. Yoon and Ravishankar measured the long range hydrophobic forces between Dodecylamine-coated mica surfaces.[36,57] The fitting equation used is:

$$\frac{F}{R} = -C_1\,exp\left(-\frac{h}{D_1}\right) - C_2\,exp\left(-\frac{h}{D_2}\right) \qquad [1\text{-}18]$$

Where one set of C and D represents short-range hydrophobic force parameters, and the other set of C and D represents long-range hydrophobic force parameters.

In some cases, the hydrophobic force can be described by power law: [34,58,59]

$$\frac{F}{R} = -K_{131} / 6H^2 \qquad [1\text{-}19]$$

Where K_{131} is a fitting parameter, and H is the separation distance of the two surfaces. These three equations are still frequently used for fitting hydrophobic force. However, they are still considered as empirical though several decades have pasted.

e. Controversies on the origins of hydrophobic forces

Reports published over the past several decades strongly suggested the existence of these long-range attractive forces between macroscopic hydrophobic surfaces immersed in water. [20,57,59,62-64] These forces are orders of magnitude larger than the van der Waals force. Much efforts have been made to prove that hydrophobic force is a molecular force, but it is still not well understood today. Possible origins considered some twenty years ago included, water structuring ,

ion-ion or dipole-dipole interactions, and vapor cavitation .[62,63] More recently, scientists considered the possibilities of changes in H-bonded structures of in the vicinity of hydrophobic surfaces, correlation between charged patches, and nanobubble. [3,10]

In recent years, the nanobubble theory received the most attention. It was first hypothesized by Parker, Classon and Attard in 1994.[39] The discontinuities observed in their force vs. distance curves appeared to suggest that hydrophobic interaction is a consequence of bubble-bubble interaction involving capillary forces. They suggested that the data could be quantitatively described by a model with very low surface coverage of bubbles. However, the existence of nanobubbles has been intermittently debated and is still not unequivocally confirmed due to experimental limitations. Some researchers claimed the existence of nanobubbles based on direct observations using AFM or some other spectroscopies. The existence of air bubbles as "nanscopic gaseous bubbles" was not accepted until Ducker applied spectroscopic measurements showing the surface of nanobubbles were indeed composed of gas,[65] rather than being simply bulk contamination.

To date, the nanobubbles reported in literature can be classified as three types: surface nanobubbles, bulk nanobubbles, and micropancakes, as shown in Figure 1.3.[65-67] Micropancakes are found to be at the solid/liquid interface, with typical widths of several hundred nanometers to micrometers, but only 1-2 nm in height. Surface nanobubbles are also found at the solid/liquid interface and have typical radii of curvature of 100-1000 nm, with heights and width of 5-20 nm and 50-100 nm, respectively. Bulk nanobubbles are found in bulk solutions, with typical radii of curvature of 50-100 nm. Though the existence of surface nanobubbles is generally accepted, theories about these observed nanobubbles at the solid/liquid interfaces are still facing some great challenges.

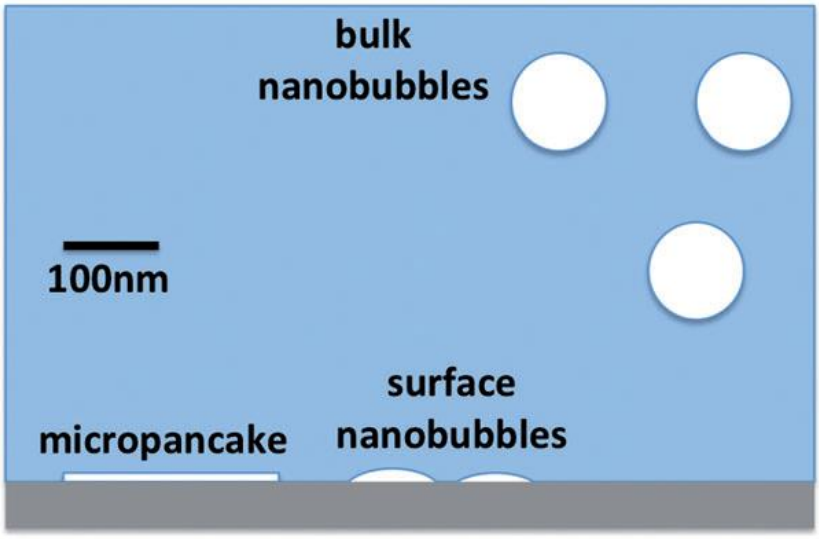

Figure 1.3 The three types of nanoscopic gaseous domain recently observed in the literature: micropancakes found at the solid/liquid interface; surface nanobubbles also found at the solid/liquid interface; bulk nanobubbles found in bulk solutions. The stability of micropancakes and surface nanobubbles are facing challenge of classical physical and chemical concept. Used under fair use, 2015.

These nanobubbles seem to violate established concepts both physically and chemically. They exhibit highly unusual nano-scopic contact angles and unexpected stability. According to the classical diffusion theory, these types of nanobubbles will dissolve in liquid in a few seconds or less due to such high curvature; however, these nanobubbles were reported to be stable for hours, days and even weeks. The gas-side contact angles do not change much regardless of the surface hydrophobicity and hydrophilicity, which contradicts the general concept of water contact angle depending strongly on the solid, liquid and gas. Some theories have been promoted to field the gap between these experimental facts and the established physical and chemical basic concepts, including ionic shielding, diffusive shielding, or theories including both.[65-67] The biggest challenge associated with the nanobubble theory is that there is still a lot of papers reporting the measurement of hydrophobic forces under conditions where bubbles cannot exist, e.g., in degassed solutions. There is a distinct characteristics of the force curves recoded when nanobubbles exit: the forces curves showed discontinuous curves, while the force curves obtained degassed water still showed strong and smooth hydrophobic force vs. distance curves.

Another theory used to try to explain the hydrophobic force is charge or ion related theory. There are also several different theoretical frameworks about charge related theories: electrostatic effects,[34,68] correlated charge fluctuations[69,70] and correlated dipole interactions[62].

Meyer et al. proposed that there were charges on the liquid/solid interfaces.[71] Unlike the traditional double layer electrical force, the charges on this theory frame is mobile and will rearrange when the film thickness varies, as shown in Figure 1.4.[3] The attractive force can be explained by the correlated in-plane dipoles. Tsao et al.[62] carried out the force measurement between hydrophobic surfaces and a polar surface on mica, on which two hydrophobic monolayers were formed. They proposed that the ions adsorbed onto mica adopt a solid configuration, a tilt will necessarily develop, which in turn will generate an electrical field. When the fields penetrate to the second surface, they will respond and generate an attractive force. This theory is capable of explaining the attractive force in the symmetrical and asymmetrical case. And, based on the model, the extended in-plane correlation length is long enough to account for 80 nm decay length. It also predicts the fact that force will become weaker when the electrolyte concentration is higher, which screens the electrical field but also influences in-plane correlations.

Podgornik[69] studied some consequences of a generalized theory of electrostatic interactions between two macroscopic surfaces immersed in dilute electrolyte. According to the assumption, the ionic interaction close to the two surfaces were supposed to be specifically affected by the presence of the surfaces, leading to a surface contribution to the total energy density of the system. By applying the analysis on the grand canonical partition functions, they also described the thermodynamic of their model in terms of a mean-field solutions and fluctuations around the surface. More interestingly, some regime of the correlation attractions obtained shows thermodynamically unstable though the global stability of the mean field solution is still stable. If the coupling of charge of inhomogeneities is strong enough that they can approach those unstable regions, the system will lead to an anomalously high attractive interaction, or the very long-range hydrophobic attraction, with decay length half of the Debye length.

Another theory widely discussed is water structuring effect, and people supporting this theory argued that the physical driving force underlying hydrophobic phenomena was that water specifically orients near non-polar surfaces, affecting its 3D hydrogen bonding network and losing configurational entropy or enthalpy.[5,60] However, not a single model promoted so far is able to

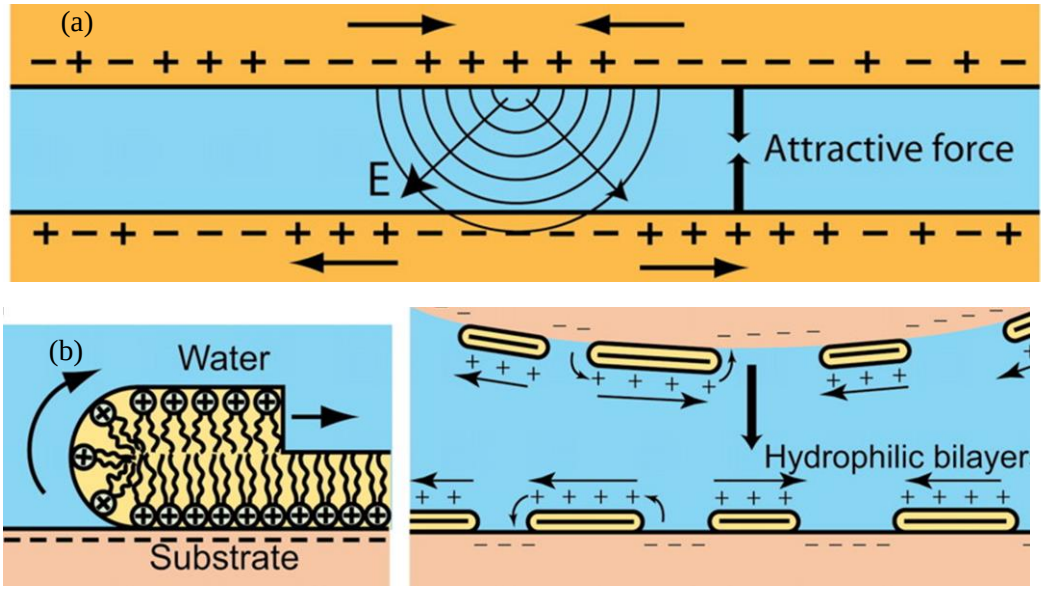

Figure 1.4 Local charge fluctuations at one surface can influence the charge density of the opposing surface, causing a long-range attractive electrostatic interaction.[3] Copyright (2006) National Academy of Sciences, U.S.A.

explain all the attractive force between two hydrophobic surfaces for all described experimental data. I will introduce some theoretical frameworks based on water structuring in the paragraphs coming.

By promoting a coarse-grained (CG) model, Shell[72] introduced a fundamental thermodynamic framework for multi-scale simulations, which is considered a candidate for analyzing the multi-scale nature of the hydrophobic interactions. The key concept in this approach is the relative entropy, S_{rel}, which is given by:

$$S_{rel} = \sum_{v} p_v \cdot \ln \frac{p_v}{\tilde{p}_v} \qquad [1\text{-}20]$$

Where p_v is the probability of a particular configuration v in a detailed, fully atomistic molecular system while $\tilde{p}_v$ is the corresponding value on a simplified, coarse-grained molecular system. S_{rel} measures the extent the configurational ensemble of the simplified system.[73] Given a reference detailed model, a simplified model can be optimally determined by minimizing the relative entropy. Then, Shell and coworkers used this approach to examine particular spherically-symmetric model of water, the Lennard-Jones-Gaussian (LJG) model.[73] The pair potential of water, *u(r)*, has a simple function form, containing only five adjustable parameters,

$$u(r) = 4\varepsilon[(\frac{\sigma}{r})^{12} - (\frac{\sigma}{r})^{6}] + B^{*}\varepsilon \exp[-(\frac{r/\sigma - r_0^{*}}{\Delta^{*}})^{2}] \qquad [1\text{-}21]$$

The usual Lennard-Jones parameters, ε and σ define the energy and length scales of the repulsive-dispersive interactions, the parameter B^* sets the relative strength of the Gaussian while r_0^* and Δ^* govern its center and spread, respectively. Consequently, Shell and coworkers optimized the LJG

potential parameters by minimizing S_{rel}. Surprisingly, they found that the region of the first coordination shell varies significantly in energy across the state condition, which was interpreted as the effective spherically-averaged hydrogen bonding interactions stabilizing the close approach of water molecules. At lower density, tetrahedrally-coordinated configurations of water structure was required for the effective potential to be minimal, while at higher density, this minimum vanishes as favorable and hydrogen-bonding configurations are less accessible. Actually, the hydrogen bonding is not specifically treated or assumed to be existing in their model at the beginning, but the presence of hydrogen bonding interaction is naturally effective for stable state conditions.[40]

Later, Hammer et al.[40] applied the approach developed by Shell to examine the ability of spherically-symmetric water in describing the hydrophobic interaction on the molecular scale, by using the experimental data obtained with the SFA. Several basic features of hydrophobic interaction on the molecular scale were captured. They confirmed that the spherically-symmetric water bath appears to yield an effective hydrophobic interaction that is comparable with the hydrophobic interaction of fully-atomistic water media.[72] Though water vibration frequency and amplitude is moderately different, the binding energy is found to be the same in order of magnitude. Their analysis also disclosed that the spherically-symmetric water model must manifest a particular variation state when contacting its nearest-neighbors in order to capture water-like properties, which allowed effective hydrogen bonding interaction to produce a number of signatures on the water's anomalous bulk properties. Based on the analysis of this model, they suggested several hydrophobic force laws on three regimes.[74] 1). The 'short' range force is overwhelming in the distance from zero (contact) up to 10 Å and is related to water structuring effects associated with surface-induced changes: the variation of water molecule orientation, fluctuation of water molecules, and the density the H-bonds network at the water/hydrophobic solid interfaces. 2). The second hydrophobic force regime with a range of 10-20 Å up to 100-200 Å is probably due to enhanced Hamaker constant associated with the proton-hopping polarizability, which is still considered to be a pure hydrophobic force. 3). The longest range hydrophobic force with effective range over several thousand angstroms is not a pure hydrophobic force, which might be due to electrostatic effects or bridging effects of cavities. However, the third conclusion is an indirect deduction, rather than a conclusion from the experimental data obtained.

Thus, the hydrophobic effect at short ranges has great probability relating to the water molecular reorientation and forming hydrogen-bonding at longer ranges to achieve a stable state condition of water. The density of water is smaller when forming hydrogen-bonding domain structures, which is called low density liquid (LDL) by other researchers. Though the shell's model doesn't predict much about the long range hydrophobic force, it is still possible the hydrogen-bonding domain structures will have significant effecting contribution.

Eriksson et al.[75] have tried to connect the long range hydrophobic force to the water structuring effect. By attributing the hydrophobic force to the presence of surface-induced water structures and employing a well-established square-gradient variational approach (Landau expansion), Eriksson et al. derived the following expression for the surface force *F*/*R* (plate-sphere or cylinder-cylinder geometry):

$$F / R = -B\left[coth\left(bh / 2\right) - 1\right] \qquad [1\text{-}22]$$

Where R is the radius of the spherical surface involved, B is decisive for the strength of the surface force, whereas b^{-1} accounts for the decay length at large surface separations. B and b are constants that reflect the free energy changes raised in the thin film as a result of the state of water order varying. The surface-induced water structure is given by the dimensionless parameter functions of s(z), mathematically by the expression:

$$s(z)=\left(\frac{B}{\pi a}\right)\frac{\cosh(bz)}{\sinh(bh/2)} \qquad [1\text{-}23]$$

Where the constant an equals the rate of lowering the Gibbs contact energy with respect to raising the order parameter in the contact monolayers. It is seen from the denominator of this expression that the order parameter tends to increase rapidly upon reducing the film thickness h. This is in qualitative agreement with the results obtained by Wang et al.[1] by employing hydrophobized gold surfaces submerged in water, showing that the differences with respect to the excess film entropy and excess enthalpy per unit area (both negative quantities) constantly become more negative as the water film gets thinner. In short, this theory can be a candidate to explain the long range hydrophobic force.

There are also a lot more literatures developing other models that explain the origin of the hydrophobic force. Nevertheless, the influence of hydrogen bonding looks like inevitable when developing a model to explain the origin of hydrophobic force, as mentioned in the model of Shell,[72,76] the hydrogen bonding and water cluster changing is naturally required for water in order to capture water-like properties, even though it is not preliminarily assumed to exist. Thus, the water structure changing through hydrogen bonding might be the intrinsic reason the hydrophobic force rises, or at least hydrogen bonding could be the key to figuring out the origin of the hydrophobic force. Hence, we are on the side of assuming that the appearance of this kind of surface force depends crucially on the hydrogen bond pattern within aqueous films.

Besides modelling, researchers, supporting the theory of hydrophobic force raising from the water structure changing, have carried out several experiments to support their point of view either with some direct or indirectly experimental method. Incapable of observing the rearrangement of water structure directly due to current technique limitations, some applied spectroscopy to characterize the hydrogen binding frequency variation of water confined in small area or on the surface of hydrophobic molecules, as a relatively direct method. Others tried to measure and calculate the thermodynamic properties, as there would be some enthalpy and entropy cost as a result of water structure changing, as indirect methods.

Spectroscopy studies have been carried out to probe the structure of water either in bulk liquid water[38,77] or water on hydrophobic surfaces,[5,78,79] and inspected whether the water is in a state of high density water or low density water.[80] Quite a few technologies have been used for the water structure transformation analysis, including x-ray absorption spectroscopy (XAS),[80] Raman multivariate curve resolution (Raman-MCR)[38,78] and sun-frequency generation (SFG). Though the model of water structures used in these references are not exactly identical, and the features of the spectroscopy are also not the same due to the different techniques applied, there are discoveries or assumptions consistent among these studies.

First, water is a dynamic liquid where H-bond are continuously broken and reformed. Second, two series of O-H vibrations on the spectroscopy were recorded in most studies and discussed in

these paragraphs. One is solute (water) intramolecular O-H stretch vibration, or free (dangling) O-H stretch band, and the other is hydrogen-bonded O-H vibration. In Raman spectroscopy, the vibration position of free O-H is typically at 3660 cm^{-1}, and hydrogen-bonded OH is near 3200 cm^{-1}.[38,78] Actually, both vibration modes exist in bulk liquid water. By introducing hydrophobic species and detecting the vibration on the air-liquid interface or liquid-hydrophobic surface, enhanced vibrations of hydrogen-bonded OH was observed. This indicates that there are more water structures that are changed due to perturbations of hydrophobic species induced or hydrophobic surfaces. Third, those papers[58,71-73] studying the temperature effect of O-H vibrations agree well with others, that the hydrogen-bonded OH vibration are enhanced at lower temperatures compared with the intensity observed of dangling OH. And the enhanced order of water surrounding hydrophobic molecular groups is even more strongly dependent on temperature than the strength of the average hydrogen bond interaction, as Simona et al. concluded.[78] Fourth, H-bonding dominating water-network or core-shell structure will form when water molecules are associated with hydrophobic species or surface, and the average length of O-H bonding is relatively longer than those in bulk water. The oxygen atoms of neighboring water molecules are ~2.8 Å at standard temperature and pressure and this value will shift to ~3.5 ± 0.5 Å when forming H-bonding structures. This will result in more O-H groups with lower vibration energy detected.

The discussion above showed evidences of water structure changing by forming some hydrogen-bonded clusters, hydration shell or clusters or other possible formation. The density of liquid cluster formed on hydrophobic surfaces is lower than bulk water, by forming the so called "ice-like" low-density liquid (LDL) species through hydrogen bonding. These LDLs are also present in bulk water with low population; however, the formation of LDL is much more favored in the vicinity of hydrophobic surfaces.

f. Evidence for the hydrophobic force originating from water structuring

A lot of surface force measurements have been carried out on hydrophobic surfaces and the experimental results are supporting the model of water structuring. Thermodynamic properties of several thin film systems confined between hydrophobic surfaces have also been analyzed.

Wang, et al.[6,81] used AFM to directly measure the hydrophobic forces in the TLFs of water confined between hydrophobic surfaces. The surfaces were hydrophobized with alkane xanthate or n-alkane thiol. In general the hydrophobic forces measured at temperatures in the range of 10 to 40 ℃ became more attractive with decreasing temperature. The authors measured the hydrophobic forces at several different temperatures and determined thermodynamic functions for the macroscopic hydrophobic interactions. They found that both enthalpy and entropy are negative and that $|\Delta H^f| > |T\Delta S^f|$ as sown in Figure 15a. The latter indicates that macroscopic hydrophobic attraction is enthalpic, which is contrary to what is known for the hydrophobic interaction at microscopic scale. The enthalpy changes are due to the formation of H-bonded structures, and the entropy changes represent the cost of building the structures. It has been suggested that the H-bonded structures are low-density liquid (LDL), which is prevalent at low temperatures. This interpretation is in line with the concept of Rabinovich and Derjaguin.[30]

More surprisingly, it has been shown Li and Yoon[2] that the hydrophobic force is also present in the TLFs of ethanol confined between alkylthiol-treated gold surfaces. The results obtained in pure ethanol are similar to those obtained in water, as shown in Figure 1.5b. The results are similar to those obtained by Wang et al.,[1] with TLFs of water. The thermodynamic analysis conducted by

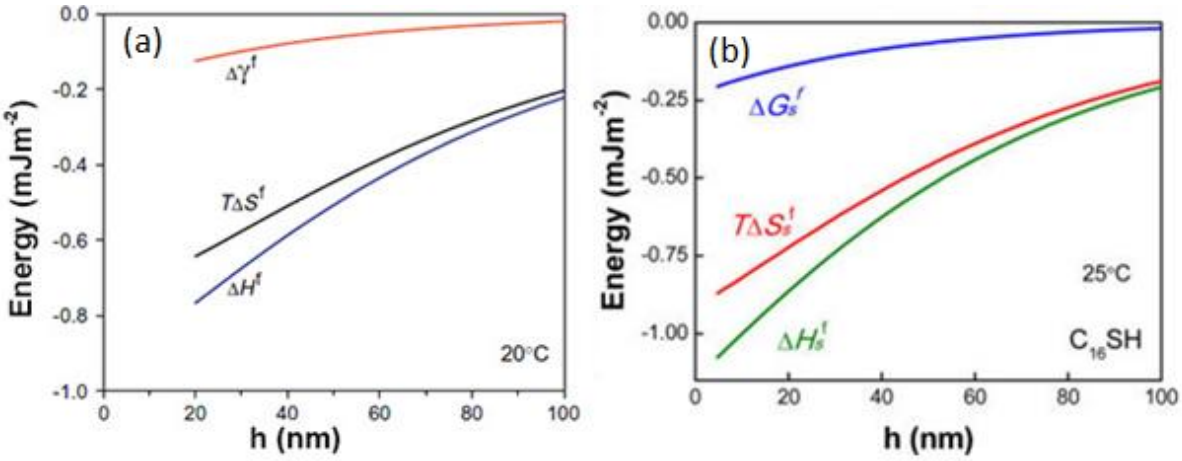

Figure 1.5 Changes in the excess thermodynamic functions, free energy (ΔG^f), enthalpy (ΔH^f) and entropy (ΔS^f), for the hydrophobic interaction between $C_{16}SH$-coated gold surfaces measured in (a): water (20ºC)[1] and (b): ethanol (25ºC)[2]. Entropy and enthalpy terms show some similarity between water and ethanol medium, both of which are hydrogen bonding liquids. This might indicate some similar performance for hydrogen bonding liquids when confined between hydrophobic surfaces. Used under fair use, 2015

Li, et al.[2] showed also that the attractive forces are due to the structuring of the solvent (ethanol) confined between hydrophobic surfaces. That the two different liquids gave rise to strong attractive forces suggest that both forces arise from the antipathy between the hydrocarbons on hydrophobic surfaces and the solvent. Both water and ethanol are H-bonding liquids, and hydrophobic surfaces cannot host H-bonding of the solvent. Thus, hydrophobic force may be considered a subset of a solvophobic force.

A possible water structure changing model was promoted by Wang and Yoon[1], as shown in Figure 1.6. This model implies that the instantaneous concentration of LDL increases with decreasing *h*, which is consistent with the thermodynamic analysis discussed above. These species represent H-bonded structures that are more extensive than the high-density liquid (HDL) that are found at higher temperatures. When a TLF becomes thinner, more LDLs will form in a closer proximity to a hydrophobic surface. The model presented in Figure 1.6 suggests that LDLs become stronger if there are gas molecules dissolved in water, as shown in Figure 1.6 (b). The LDLs, which may be considered partial clathrates, become more stable due to the van der Waals interaction between the guest (dissolved gas molecule) and the host (LDL). Indeed, many investigators showed that the hydrophobic forces measured in air-saturated water are considerably stronger than those measured in degassed water.

The thermodynamic analysis of macroscopic hydrophobic interactions coupled with the spectroscopic studies of confined water provide evidence that hydrophobic force originates from the changes of hydrogen bond networks in confined spaces relative to those in bubble liquid. Thus, hydrophobic force is a solvent- rather surface-mediated force.

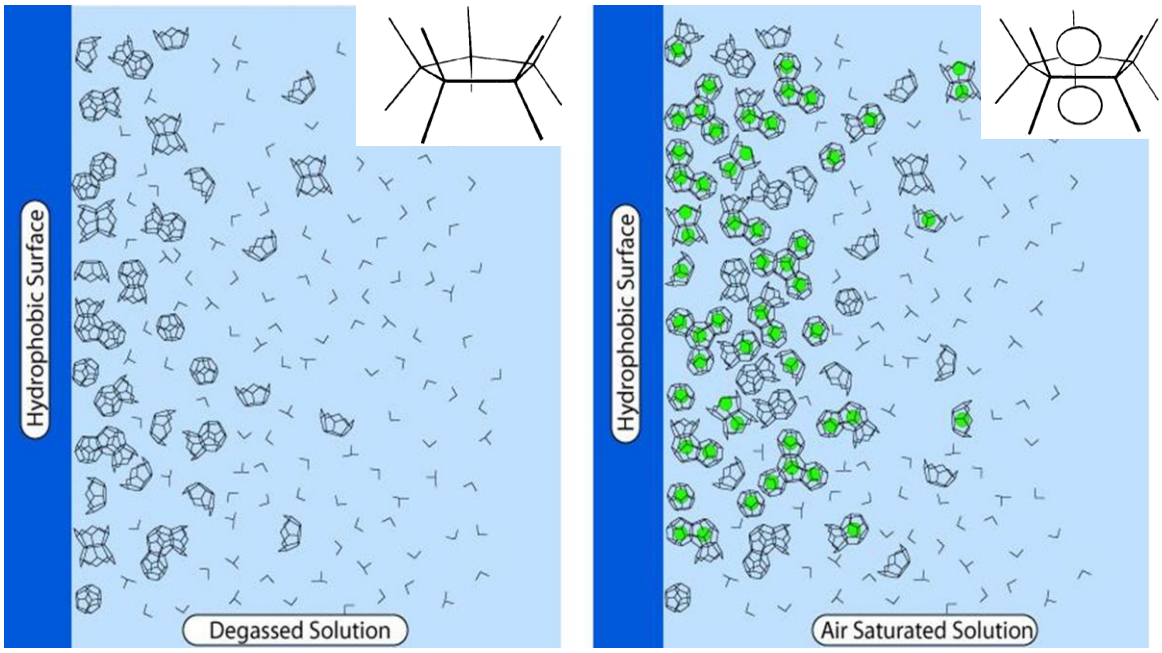

Figure 1.6 A possible model for the formation of partial water clathrates (or LDLs) in the vicinity of hydrophobic surfaces in the absence (a) and presence (b) of dissolved gas molecules (●).[1] Used under fair use, 2015.

1.2.2 Thin Films Thermodynamics

The following is an analogue of the Gibbs-Duhem equation for the interaction between two flat surfaces,

$$SdT - Vdp + Ad\gamma + \sum_i n_i d\mu_i = 0 \qquad [1\text{-}24]$$

Dividing Equation [1-24] by the interfacial area (A) of interaction,

$$\frac{S}{A}dT - \frac{V}{A}dp + d\gamma + \sum_i \frac{n_i}{A}d\mu_i = 0 \qquad [1\text{-}25]$$

Which can also be rewritten as,

$$S^f dT - hdP + d\gamma^f + \sum_i \Gamma_i d\mu_i = 0 \qquad [1\text{-}26]$$

Solving Equation [1-26] for $d\gamma^f$,

$$d\gamma^f = -S^f dT + hdP - \sum_i \Gamma_i d\mu_i \qquad [1\text{-}27]$$

For the thin liquid films (TLFs) of water confined between two surfaces, we must also consider the interaction between the surfaces, characterized by disjoining pressure, Π,

$$d\gamma^f = -S^f dT + hdP - \Pi dh + \sum_i \Gamma_i d\mu_i \qquad [1\text{-}28]$$

When h changes from an infinite distance (h = ∞) to a finite film thickness h, $\Delta\gamma^f$ rather than γ^f may be used

$$d\Delta\gamma^f = -\Delta S^f dT + hdP - \Pi dh + \sum_i \Gamma_i d\mu_i \qquad [1\text{-}29]$$

Where

$$\mu_i = \mu_i^0 + RT \ln a_i \qquad [1\text{-}30]$$

For an aqueous solution of a surfactant s,

$$d\Delta\gamma^f = -\Delta S^f dT + hdP - \Pi dh + \Gamma_w d\mu_w + \Gamma_s d\mu_s \qquad [1\text{-}31]$$

Assuming that the chemical potential of water (μ_w) does not change during the macroscopic interaction under consideration,

$$d\Delta\gamma^f = -\Delta S^f dT + hdP - \Pi dh + \Gamma_s d\mu_s \qquad [1\text{-}32]$$

Differentiating Equation [1-30]

$$\begin{aligned} d\mu_s &= RT\, ln a_s \\ &= \frac{\partial \mu_s}{\partial ln a_s} d\, ln a_s \end{aligned} \qquad [1\text{-}33]$$

Substituting Equation [1-33] into Equation [1-32],

$$\begin{aligned} d\Delta\gamma^f &= -\Delta S^f dT + hdP - \Pi dh + \Gamma_s d\mu_s \\ &= -\Delta S^f dT + hdP - \Pi dh + \Gamma_s \frac{\partial \mu_s}{\partial ln a_s} d\, ln a_s \\ &= d\Delta G^f \end{aligned} \qquad [1\text{-}34]$$

At a constant P, h, Γ_s and a_s,

$$\left(\frac{\partial d\Delta\gamma^f}{\partial T}\right)_{P,h,\Gamma_i,a_i} = -\Delta S^f \qquad [1\text{-}35]$$

When two surfaces move from an infinitely large distance to a finite h, film tension changes by $\Delta\gamma^f$ which represents the work (or negative free energy) done against the disjoining pressure Π as follows,

$$\begin{aligned} \Delta\gamma^f &= \gamma_h^f - \gamma_\infty^f \\ &= -\int_\infty^h \Pi \mathrm{dh} \\ &= -\int_\infty^h \left(\Pi_e + \Pi_d + \Pi_h\right) \mathrm{dh} \\ &= \Delta G^f \end{aligned} \qquad [1\text{-}36]$$

Where Π_e, Π_d, and Π_h represent the disjoining pressure due to electrostatic, van der Waals dispersion and hydrophobic forces, respectively. Equation [1-36] is useful when P, h, Γ_s and a_s are constant.

Derjaguin approximation relates $\Delta\gamma^f$ to the force of interaction as follows,

$$\frac{F}{R} = 2\pi\Delta\gamma^f = 2\pi\Delta G^f \qquad [1\text{-}37]$$

While experimentally measured forces are often represented by a single-exponential force law:

$$\frac{F}{R} = -C\exp\left(-\frac{h}{D}\right) \qquad [1\text{-}38]$$

From Equations [1-37] and [1-38],

$$\Delta\gamma^f = \frac{F}{2\pi R} = -\frac{C}{2\pi}exp\left(-\frac{h}{D}\right) = \Delta G^f \qquad [1\text{-}39]$$

Which gives free energy change associated with two macroscopic surfaces moving from a distance h = ∞ to h.

Differentiating Equation [1-34],

$$\left(\frac{\partial\Delta G^f}{\partial T}\right)_{P,h,\Gamma_i,a_i} = \left(\frac{\partial\left(F/2\pi R\right)}{\partial T}\right)_{P,h,\Gamma_i,a_i} = -\Delta S^f \qquad [1\text{-}40]$$

Substituting Equation [1-38] into Equation [1-40],

$$\Delta S^f = -\frac{F}{2\pi R}\left(\frac{d\,lnC}{dT} + \frac{h}{D}\frac{d\,lnD}{dT}\right) \qquad [1\text{-}41]$$

Which gives entropy change.

One can then obtain enthalpy change from the following relation,

$$\Delta G^f = \Delta H^f - T\Delta S^f \qquad [1\text{-}42]$$

1.3 Research objectives

It is believed that hydrophobic interaction (or attraction) is related exclusively to the thin films of water (or dilute aqueous solutions) that are confined between two hydrophobic solid surfaces. Majority of researchers including the author of this thesis believes that the appearance of the hydrophobic force has something to do with the hydrogen bond networks in the TLFs of water. A

surprising discovery was made recently by Wang et al.[6] that surface forces which were similar in strength and range do arise not just in water but also in the TLFs of short-chained alcohols confined between two hydrophobic surfaces. Later on, these results were confirmed by Li and Yoon[2], who investigated the temperature-dependent surface forces in the TLFs of pure ethanol confined between alkylthiol-treated gold surfaces.

Although short-chain alcohols are also H-bonded liquids like water, each alcohol molecule forms only two H-bonds as opposed to three for water. Furthermore, the former larger than the latter. As a consequence, the H-bond density is lower than that of water. Nevertheless, the magnitudes and the ranges of the non-DLVO force are comparable to those observed with water. One distinguishing difference between alcohol and water is that the former can adsorb on hydrophobic surfaces via molecular-scale hydrophobic interaction and expose the OH-group toward the aqueous phase. If this happens indeed, the hydrophobic force can decay quickly with increasing film thickness. Therefore, it is critical to conduct more careful measurement of surface forces to discern the difference between the non-DLVO attractive forces measured in water and alcohols.

In the present project, I will generate detailed surface force data by directly measuring the surface forces in water-ethanol mixtures using AFM. I will use the gold surfaces hydrophobized with potassium amyl xanthate (KAX) as confining surfaces. The measurements will be conducted using ethanol solutions of varying mole fractions ranging from zero to unity. The measurements will be conducted at several different temperatures to determine the thermodynamic functions of the interaction. Thermodynamics is often useful for deriving information on the structural changes associated with film thinning.

Another objective of this project is to study the hydrophobic force between air and solid surfaces in water. The experiments will be carried out using the Force Apparatus for Deformable Surfaces (FADS), a device developed in our lab. The new apparatus is capable of determining the hydrophobic force and the disjoining pressure from the spatiotemporal film profiles generated due to changes in local curvature during film thinning. By measuring the hydrophobic forces in the wetting films of water formed on hydrophobized mineral surfaces, one can better understand the fundamental mechanisms involved in flotation. The results obtained in the present work will be useful for understanding the role of two of the most widely used and studies hydrophobizing agents, *i.e.*, KAX and KEX, for the flotation of sulfide minerals, *i.e.*, chalcopyrite, galena. The measurement of hydrophobic forces on opaque minerals has not been possible until this new instrument has been developed.

1.4 Dissertation outline

This dissertation will be outlined as following:

In Chapter 2, AFM force measurement of solvophobic force in water/ethanol thin films confined between hydrophobized gold surfaces will be introduced as Non-DLVO theory will be applied to analyze the system. Thermodynamic analysis will also be carried out to confirm the solvent structure change on hydrophobic surfaces

In Chapter 3, all AFM force measurement results covering the whole water/ethanol composition and temperature will be carried out. Thermodynamic analysis will be applied to figure out the origination of hydrophobic forces.

In Chapter 4, the new device of FADS will be introduced briefly. The experimental results carried out on the asymmetric surfaces between air and gold using FADS will be introduced.. Double exponential fittings will be used to describe the contribution of hydrophobic forces in these systems. Finally, the adsorption mechanism of surfactant (KEX and KAX) on gold surfaces will be characterized by combing the cyclic voltammogram and FADS results.

In Chapter 5, hydrophobic force of wetting film between bubble and chalcopyrite surfaces will be measured and analyzed. Both effects of applied potential and reaction time will be investigated. Similar to the case of air/gold systems, extended DLVO theory was applied to describe the hydrophobic forces.

In Chapter 6, hydrophobic force of wetting film between bubbles and galena surfaces will be introduced. The film wetting process will be introduced in detail by using non-DLVO theory. The adsorption mechanism of KAX on galena surfaces will also be disclosed.

1.5 Reference

1 Wang, J. L., Yoon, R. H. & Eriksson, J. C. Excess thermodynamic properties of thin water films confined between hydrophobized gold surfaces. *J. Colloid Interface Sci.* **364**, 257-263 (2011).

2 Li, Z. & Yoon, R.-H. Thermodynamics of Solvophobic Interaction between Hydrophobic Surfaces in Ethanol. *Langmuir* **30**, 13312-13320 (2014).

3 Meyer, E. E., Rosenberg, K. J. & Israelachvili, J. Recent progress in understanding hydrophobic interactions. *Proceedings of the National Academy of Sciences of the United States of America* **103**, 15739-15746 (2006).

4 Muller, P. Glossary of terms used in physical organic chemistry (IUPAC Recommendations 1994). *Pure Appl. Chem.* **66**, 1077-1184 (1994).

5 Chandler, D. Interfaces and the driving force of hydrophobic assembly. *Nature* **437**, 640-647 (2005).

6 Wang, J., Li, Z., Yoon, R.-H. & Eriksson, J. C. Surface forces in thin liquid films of< i> n</i>-alcohols and of water–ethanol mixtures confined between hydrophobic surfaces. *J. Colloid Interface Sci.* **379**, 114-120 (2012).

7 Liu, Y. Y., Chen, X. Q. & Xin, J. H. Super-hydrophobic surfaces from a simple coating method: a bionic nanoengineering approach. *Nanotechnology* **17**, 3259-3263 (2006).

8 Sawhney, A. *et al.* Modern applications of nanotechnology in textiles. *Textile Research Journal* **78**, 731-739 (2008).

9 Silverstein, T. P. The Real Reason Why Oil and Water Don't Mix. *J. Chem. Educ.* **75**, 116 (1998).

10 Tabor, R. F., Grieser, F., Dagastine, R. R. & Chan, D. Y. C. The hydrophobic force: measurements and methods. *PCCP* **16**, 18065-18075 (2014).

11 Derjaguin, B. V. & Churaev, N. V. STRUCTURE OF WATER IN THIN-LAYERS. *Langmuir* **3**, 607-612 (1987).

12 Blake, T. D. & Kitchener, J. A. Stability of aqueous films on hydrophobic methylated silica. *Journal of the Chemical Society, Faraday Transactions 1: Physical Chemistry in Condensed Phases* **68**, 1435-1442 (1972).
13 Derjaguin, B. V. & Kusakov, M. M. *Acta Physicochim. URSS* **10**, 153-174 (1939).
14 Derjaguin, B. & Landau, L. Theory of the stability of strongly charged lyophobic sols and of the adhesion of strongly charged particles in solutions of electrolytes. *Prog. Surf. Sci.* **43**, 30-59 (1993).
15 Pan, L., Jung, S. & Yoon, R. H. Effect of hydrophobicity on the stability of the wetting films of water formed on gold surfaces. *J. Colloid Interface Sci.* **361**, 321-330 (2011).
16 Israelachvili, J. & Pashley, R. The hydrophobic interaction is long range, decaying exponentially with distance. *Nature* **300**, 341-342 (1982).
17 Israelachvili, J. N. & Pashley, R. M. Measurement of the hydrophobic interaction between two hydrophobic surfaces in aqueous electrolyte solutions. *J. Colloid Interface Sci.* **98**, 500-514 (1984).
18 Ducker, W. A., Senden, T. J. & Pashley, R. M. Direct measurement of colloidal forces using an atomic force microscope. *Nature* **353**, 239-241 (1991).
19 Fielden, M. L., Hayes, R. A. & Ralston, J. Surface and Capillary Forces Affecting Air Bubble−Particle Interactions in Aqueous Electrolyte. *Langmuir* **12**, 3721-3727 (1996).
20 Christenson, H. K. & Claesson, P. M. Direct measurements of the force between hydrophobic surfaces in water. *Adv. Colloid Interface Sci.* **91**, 391-436 (2001).
21 Yaminsky, V. V., Ninham, B. W. & Stewart, A. M. Surface Activity and Ion Exchange. A Study via Surface Tension, Wetting Tension, and Surface Force Techniques. *Langmuir* **12**, 836-850 (1996).
22 Pan, L. & Yoon, R.-H. Hydrophobic forces in the wetting films of water formed on xanthate-coated gold surfaces. *Faraday Discuss.* **146**, 325-340 (2010).
23 Parker, J. L. Surface force measurements in surfactant systems. *Prog. Surf. Sci.* **47**, 205-271 (1994).
24 Lum, K., Chandler, D. & Weeks, J. D. Hydrophobicity at small and large length scales. *J. Phys. Chem. B* **103**, 4570-4577 (1999).
25 Tabor, R. F., Wu, C., Grieser, F., Dagastine, R. R. & Chan, D. Y. C. Measurement of the Hydrophobic Force in a Soft Matter System. *Journal of Physical Chemistry Letters* **4**, 3872-3877 (2013).
26 Kaggwa, G. B., Nalam, P. C., Kilpatrick, J. I., Spencer, N. D. & Jarvis, S. P. Impact of Hydrophilic/Hydrophobic Surface Chemistry on Hydration Forces in the Absence of Confinement. *Langmuir* **28**, 6589-6594 (2012).
27 Dedinaite, A. in *Interface Science and Technology* Vol. Volume 14 (ed Imae Toyoko) 23-53 (Elsevier, 2007).
28 Djikaev, Y. S. & Ruckenstein, E. The variation of the number of hydrogen bonds per water molecule in the vicinity of a hydrophobic surface and its effect on hydrophobic interactions. *Current Opinion in Colloid & Interface Science* **16**, 272-284 (2011).
29 Huang, X., Margulis, C. J. & Berne, B. J. Dewetting-induced collapse of hydrophobic particles. *Proc. Natl. Acad. Sci.* **100**, 11953-11958 (2003).
30 Rabinovich, Y. I. & Derjaguin, B. V. Interaction of hydrophobized filaments in aqueous electrolyte solutions. *Colloids and Surfaces* **30**, 243-251 (1988).

31 Meyer, E. E., Lin, Q., Hassenkam, T., Oroudjev, E. & Israelachvili, J. N. Origin of the long-range attraction between surfactant-coated surfaces. *Proceedings of the National Academy of Sciences of the United States of America* **102**, 6839-6842 (2005).

32 Eriksson, J. C. & Henriksson, U. Bridging-cluster model for hydrophobic attraction. *Langmuir* **23**, 10026-10033 (2007).

33 Eriksson, J. C. & Henriksson, U. Thermodynamic Properties of Bridging Clusters in Thin Films of Water between Hydrophobic Surfaces Assessed from Surface Force Isotherms. *Langmuir* **29**, 4789-4795 (2013).

34 Eriksson, J. C., Ljunggren, S. & Claesson, P. M. A phenomenological theory of long-range hydrophobic attraction forces based on a square-gradient variational approach. *Journal of the Chemical Society, Faraday Transactions 2: Molecular and Chemical Physics* **85**, 163-176 (1989).

35 Zhang, J. H., Yoon, R. H. & Eriksson, J. C. AFM surface force measurements conducted with silica in C(n)TACl solutions: Effect of chain length on hydrophobic force. *Colloids and Surfaces a-Physicochemical and Engineering Aspects* **300**, 335-345 (2007).

36 Rabinovich, Y. I. & Yoon, R. H. Use of Atomic-Force Microscope for the Measurements of Hydrophobic Forces. *Colloids and Surfaces a-Physicochemical and Engineering Aspects* **93**, 263-273 (1994).

37 Leite, F. L., Bueno, C. C., Da Róz, A. L., Ziemath, E. C. & Oliveira, O. N. Theoretical models for surface forces and adhesion and their measurement using atomic force microscopy. *International journal of molecular sciences* **13**, 12773-12856 (2012).

38 Davis, J. G., Gierszal, K. P., Wang, P. & Ben-Amotz, D. Water structural transformation at molecular hydrophobic interfaces. *Nature* **491**, 582-585 (2012).

39 Parker, J. L., Claesson, P. M. & Attard, P. Bubbles, Cavities, and the Long-Ranged Attraction between Hydrophobic Surfaces. *J. Phys. Chem.* **98**, 8468-8480 (1994).

40 Hammer, M. U., Anderson, T. H., Chaimovich, A., Shell, M. S. & Israelachvili, J. The search for the hydrophobic force law. *Faraday Discuss.* **146**, 299-308 (2010).

41 London, F. The general theory of molecular forces. *Trans. Faraday Soc.* **33**, 8b-26 (1937).

42 Mahanty, J. & Ninham, B. W. *Dispersion forces*. Vol. 5 (IMA, 1976).

43 Parsegian, V. A. *Van der Waals forces: a handbook for biologists, chemists, engineers, and physicists*. (Cambridge University Press, 2005).

44 Israelachvili, J. N. *Intermolecular and surface forces: revised third edition*. III edn, 260-261 (Academic press, 2011).

45 Hamaker, H. The London—van der Waals attraction between spherical particles. *physica* **4**, 1058-1072 (1937).

46 Chaikin, P. M. & Lubensky, T. C. *Principles of condensed matter physics*. Vol. 1 (Cambridge Univ Press, 2000).

47 Kjellander, R. & Marcelja, S. Double-layer interaction in the primitive model and the corresponding Poisson-Boltzmann description. *The Journal of Physical Chemistry* **90**, 1230-1232 (1986).

48 Hogg, R., Healy, T. W. & Fuerstenau, D. W. Mutual coagulation of colloidal dispersions. *Trans. Faraday Soc.* **62**, 1638-1651 (1966).

49 Ohshima, H., Healy, T. W. & White, L. R. Improvement on the Hogg—Healy—Fuerstenau formulas for the interaction of dissimilar double layers: I. Second and third approximations for moderate potentials. *J. Colloid Interface Sci.* **89**, 484-493 (1982).

50 Chan, D. Y. & Horn, R. G. The drainage of thin liquid films between solid surfaces. *The Journal of chemical physics* **83**, 5311-5324 (1985).
51 Verwey, E. O. J. T. Theory of the stability of lyophobic colloids. *The Journal of Physical Chemistry* **51**, 631-636 (1947).
52 Derjaguin, B. V., Abrikosova, I. I. & Lifshitz, E. M. Direct measurement of molecular attraction between solids separated by a narrow gap. *Quarterly Reviews, Chemical Society* **10**, 295-329 (1956).
53 Khilar, K. C., Vaidya, R. N. & Fogler, H. S. Colloidally-induced fines release in porous media. *Journal of Petroleum Science and Engineering* **4**, 213-221 (1990).
54 Laskowski, J. & Kitchener, J. A. The hydrophilic—hydrophobic transition on silica. *J. Colloid Interface Sci.* **29**, 670-679 (1969).
55 Shi, C. *et al.* Measuring Forces and Spatiotemporal Evolution of Thin Water Films between an Air Bubble and Solid Surfaces of Different Hydrophobicity. *ACS Nano* **9**, 95-104 (2015).
56 Carambassis, A., Jonker, L. C., Attard, P. & Rutland, M. W. Forces Measured between Hydrophobic Surfaces due to a Submicroscopic Bridging Bubble. *Phys. Rev. Lett.* **80**, 5357-5360 (1998).
57 Yoon, R.-H. & Ravishankar, S. A. Application of Extended DLVO Theory: III. Effect of Octanol on the Long-Range Hydrophobic Forces between Dodecylamine-Coated Mica Surfaces. *J. Colloid Interface Sci.* **166**, 215-224 (1994).
58 Yotsumoto, H. & Yoon, R.-H. Application of Extended DLVO Theory: II. Stability of Silica Suspensions. *J. Colloid Interface Sci.* **157**, 434-441 (1993).
59 Yotsumoto, H. & Yoon, R.-H. Application of Extended DLVO Theory: I. Stability of Rutile Suspensions. *J. Colloid Interface Sci.* **157**, 426-433 (1993).
60 Yoon, R.-H. & Mao, L. Application of Extended DLVO Theory, IV: Derivation of Flotation Rate Equation from First Principles. *J. Colloid Interface Sci.* **181**, 613-626 (1996).
61 Vanoss, C. J., Giese, R. F. & Costanzo, P. M. Dlvo and Non-Dlvo Interactions in Hectorite. *Clays Clay Miner.* **38**, 151-159 (1990).
62 Tsao, Y. H., Evans, D. F. & Wennerstroem, H. Long-range attraction between a hydrophobic surface and a polar surface is stronger than that between two hydrophobic surfaces. *Langmuir* **9**, 779-785 (1993).
63 Tsao, Y., Evans, D. & Wennerstrom, H. Long-range attractive force between hydrophobic surfaces observed by atomic force microscopy. *Science* **262**, 547-550 (1993).
64 Li, Z. L. & Yoon, R. H. Thermodynamics of hydrophobic interaction between silica surfaces coated with octadecyltrichlorosilane. *J. Colloid Interface Sci.* **392**, 369-375 (2013).
65 Zhang, X. H., Khan, A. & Ducker, W. A. A nanoscale gas state. *Phys. Rev. Lett.* **98** (2007).
66 Weijs, J. H., Seddon, J. R. T. & Lohse, D. Diffusive Shielding Stabilizes Bulk Nanobubble Clusters. *Chemphyschem* **13**, 2197-2204 (2012).
67 Ducker, W. A. Contact Angle and Stability of Interfacial Nanobubbles. *Langmuir* **25**, 8907-8910 (2009).
68 Attard, P. Long-range attraction between hydrophobic surfaces. *The Journal of Physical Chemistry* **93**, 6441-6444 (1989).
69 Podgornik, R. Electrostatic correlation forces between surfaces with surface specific ionic interactions. *The Journal of Chemical Physics* **91**, 5840-5849 (1989).
70 Podgornik, R. & Parsegian, V. A. An electrostatic-surface stability interpretation of the "hydrophobic" force inferred to occur between mica plates in solutions of soluble surfactants. *Chem. Phys.* **154**, 477-483 (1991).

71 Meyer, E. E., Rosenberg, K. J. & Israelachvili, J. Recent progress in understanding hydrophobic interactions. *Proc. Natl. Acad. Sci.* **103**, 15739-15746 (2006).
72 Shell, M. S. The relative entropy is fundamental to multiscale and inverse thermodynamic problems. *J. Chem. Phys.* **129** (2008).
73 Chaimovich, A. & Shell, M. S. Anomalous waterlike behavior in spherically-symmetric water models optimized with the relative entropy. *PCCP* **11**, 1901-1915 (2009).
74 Hammer, M. U., Anderson, T. H., Chaimovich, A., Shell, M. S. & Israelachvili, J. The search for the hydrophobic force law. *Faraday Discuss.* **146**, 299-308 (2010).
75 Eriksson, J. C., Ljunggren, S. & Claesson, P. M. A Phenomenological Theory of Long-Range Hydrophobic Attraction Forces Based on a Square-Gradient Variational Approach. *J. Chem. Soc. Farad. T. 2* **85**, 163-176 (1989).
76 Djikaev, Y. S. & Ruckenstein, E. A probabilistic approach to the effect of hydrogen bonding on the hydrophobic attraction. *J. Chem. Phys.* **130** (2009).
77 Gierszal, K. P. *et al.* pi-Hydrogen Bonding in Liquid Water. *Journal of Physical Chemistry Letters* **2**, 2930-2933 (2011).
78 Strazdaite, S., Versluis, J., Backus, E. H. G. & Bakker, H. J. Enhanced ordering of water at hydrophobic surfaces. *J. Chem. Phys.* **140** (2014).
79 Soper, A. K. & Ricci, M. A. Structures of high-density and low-density water. *Phys. Rev. Lett.* **84**, 2881-2884 (2000).
80 Wernet, P. *et al.* The structure of the first coordination shell in liquid water. *Science* **304**, 995-999 (2004).
81 Wang, J. L., Li, Z. L., Yoon, R. H. & Eriksson, J. C. Surface forces in thin liquid films of n-alcohols and of water-ethanol mixtures confined between hydrophobic surfaces. *J. Colloid Interface Sci.* **379**, 114-120 (2012).

CHAPTER 2.

Solvophobic Forces in the Thin Liquid Films of Ethanol Solutions Confined between Hydrophobic Gold Surfaces

2.1 Abstract

Attractive forces between hydrophobic macroscopic surfaces have been measured using atomic force microscope (AFM) in water, water-ethanol mixture, and ethanol. The forces were recorded with long-range decay lengths in the range of 40 to 70 nm. The curves obtained are showing excellent continuity, providing evidence that the forces recorded are hydrophobic forces raised from hydrophobic interaction, rather than artifacts of the nano-bubbles and cavities associated with the hydrophobic surfaces. Researchers have assumed previously that the appearance of hydrophobic surface force depends crucially on the hydrogen bond pattern within aqueous films, since most previous work was measured in water. However, long-ranged, attractive surface forces were also reported to be present in thin films of alcohol with a short carbon chain. This hints that hydrophobic force is solvent-mediated force that exist in all solvent containing hydrogen-bonding.

In the present work, we have measured long-range attractions in water-ethanol mixtures between gold surfaces hydrophobized in potassium ethyl xanthate (KEX) solutions at pH 9.2 under controlled potential conditions. The results of our AFM force measurements are consistent with those of the contact angle and voltammetry experiments, indicating that the long-range attractions are closely related to gold surface hydrophobicity. This makes it solid to say that these long-rang attractions measured are due to the hydrophobic (or solvophobic) forces.

Thermodynamic analysis of the surface forces measured at different temperatures and solvent compositions show that solvophobic interaction entail decreases in configurational entropy, and that the entropy decreases become more significant with decreasing film thickness. These results indicate that the thin liquid films of H-bonding solvent becomes more structured as the film becomes thinner, which is a response of the solvent molecules in the vicinity of a surface than cannot host H-bonds with vicinal solvent molecules to reduce its free energy by forming H-bonded structures with neighboring solvent molecules.

The propensity to build structures decreases in the presence of another type of solvent as manifested with the decrease in entropy change becoming less significant at higher concentrations of the second solvent. On the other hand, the entropy change becomes more significant at lower temperatures as it is easier to build structures at lower temperatures. The results obtained in the present work suggests that hydrophobic forces (or solvophobic forces in general) originate from the antipathy between the hydrocarbon-coated surfaces and the H-bonding solvents in thin liquid films.

2.2 Introduction

Hydrophobic effect, antipathy between water and hydrophobic surfaces or molecules, underlies many interfacial processes: separation of oil and water, protein folding, self-assembly, and mineral flotation.[1-4] Strong interactions exist between hydrophobic surfaces with remarkable range and magnitude, as intensively reported during the last few decades,[5-10] following the early

observations made by Israelachvili and Pashley[11] after the advent of the surface force apparatus (SFA).

Researchers have tried both theoretically and experimentally to figure out the intrinsic reason for the existence of the hydrophobic force. In the early 1960s, Klotz and Kauzmann *et. al.* suggested a general theory of 'hydrophobic bond' between two non-polar molecules to explain hydrophobic force, which was viewed as a spontaneous tendency of attraction in water to minimize the system's surface tension.[12-14] This is a widely accepted idea and seems the reason to cause the clustering of hydrophobic units. Based on this kind of view, most scientists at that time considered the hydrophobic interaction as the properties of particles themselves, rather than that of solvent medium.[15] Though it holds true that hydrophobes play pivotal role in this kind of interactions, the model of 'hydrophobic bond' could no longer be capable of explaining the experimental results obtained in dilute solution[9,16] and it is not consistent with molecular simulation results,[17] which shows clearly that the hydrophobic interaction is related to what happens in solvent media.

Nonetheless, some years ago, Considine and Drummond[18] reported surface force measurement results recorded for Teflon-coated surfaces submerged in n-alkanes and various polar liquids using an AFM. The forces measured in the former (hexane and hexadecane) showed no attractive long-ranged forces, while those measured in the latter (water, glycerol, formamide, ethanol, and methanol) showed evidences of attractive forces with jump-in distances in the range of 9 to 500 nm. No satisfactory theory has been promoted to explain these results at that time. Nowadays, substantial progress has been made and our understanding of the hydrophobic force is also greatly improved. It is recognized that the physical driving force that underlies the hydrophobic force is that the water specifically orients near non-polar surfaces, which further affects the 3D hydrogen bonding network and loses configurational entropy.[19,20] In short, hydrophobic effect is an interaction influenced by both hydrophobic surfaces and the interacting media. And, it is very likely that liquids containing hydrogen-bonds have the potential to exhibit hydrophobic forces when confined between hydrophobic surfaces.

Chandler et al[17,21] configured a molecular-dynamics simulations of liquid water molecules near hydrophobic cavities and applied statistical thermodynamic to predict the relations between solvation free energy and spherical cavity in water. The rearrangement of the hydrogen bonding network between hydrophobe and the water molecule surrounding it provided the basic physical understanding of hydrophobic hydration effect. The diminishment of hydrogen bonding at high temperature also provided a reasonable explanation of hydration of small alkane and water,[22] and the fundamental behavior of the water network around the hydrophobe might also be able to explain the hydrophobic interaction between macroscopic bodies.[16] Chandler[17] claimed that the water is a unique solvent, and it is difficult to find other liquids with the attractive force imbalance similar to that found in water and oil.

However, it was reported by Wang et al. [23] that long-ranged, attractive surface forces exist between thin film confined between hydrophobic surfaces with relatively strong magnitude and range to those seen for water also. Later, Li and Yoon[24] also confirmed that hydrophobic interaction generated for pure ethanol films between alkylthiol-treated gold surfaces. Both of these findings are discovered in hydrogen-bonding liquid. It might be that Chandler's concept of hydrophobic interaction can be extended to all solvent containing hydrogen bonding liquid. Thus, it is possible that the hydrophobic surface force, or hydrophobic interaction, may be a general phenomenon that arises for a wider set of liquids than presupposed so far. Obviously, it will be

very important to confirm that which kind of liquid containing hydrophobic bonding will show hydrophobic interaction, and which containing hydrogen bonding will not.

In this chapter, we will show that attractive hydrophobic forces have been measured using an AFM between hydrophobized gold surfaces in the thin films of water-ethanol mixtures, besides pure water and pure ethanol. This is evidence that hydrophobic force might be existent in other hydrogen bonding liquids.

2.3 Methods and materials

2.3.1 Materials Preparation

Hydrophobizing agent potassium amyl xanthate (KAX, >90%, TCl America) was recrystallized twice before reaction with gold using HPLC grade acetone (Fisher Scientific, Inc.) and diethyl ether (99.99%, Sigma-Aldrich, Inc.).[25,26] A thin film of gold was coated on 1cm×1cm silicon substrates by electron beam physical vapor deposition (EB-PVD 250), with film layer thickness of 100 nm. 5 nm chromium thin film was coated as adhesion layer. Gold-coated substrates were cleaned in piranha solutions (7:3 by volume of H_2SO_4/H_2O_2) for 10 minutes, then rinsed by DI water and finally dried by ultrapure N_2 gas (Air gas, lnc.) before hydrophobization reaction.

Gold spheres were made from gold wires (0.0127 mm diameter, 99.9%, Alfa Aesar) by following the method described by Raiteri et al.[24,27] Only those gold spheres with diameter of approximately 10 μm were selected for AFM surface force measurement. In a given experiment, a gold sphere was glued onto a cantilever (AIOE-10, NanoAndMore, USA) with epoxy resin (EPON 1004F), and the sphere-cantilever assembly was immersed in pure ethanol for 1 minutes before exposing it to 245 nm UV light for 1 hour, as a means of destroying possible organic contaminants on the gold surface. The sphere-cantilever assembly was mounted into an AFM liquid cell for a force measurement.

2.3.2 In-situ hydrophobic surfaces preparation

A KAX solution was injected into the liquid cell to hydrophobize gold surface. In all of the force measurements conducted in the present work, gold spheres were immersed in a 10^{-5} M KAX solution for 10 minutes. The equilibrium contact angle of the gold was 95.3º. The contact angle measurement was conducted on a gold plate treated under the same condition.

2.3.3 AFM force measurement

Force measurement were carried out when the temperature of the system reached equilibrium, which was controlled by a thermal application controller (TAC) assembled in the Nano-Scope Iva AFM (Multi Mode, Digital Instrument, Inc.). The spring constant of cantilever will be determined by the resonant frequency technique. During measurement, both the vertical movement of the piezoelectric scanner and the deflection of the cantilever will be recorded simultaneously. The recorded information is subsequently converted to normalized force (*F/R*) vs. film thickness curves.

In the present work, the force measurements were conducted at 10, 20, 30 and 40ºC in ethanol solutions of ethanol mole fraction (x_2) of 0, 0.03, 0.18and 1. During each measurement, the spring constant were calibrated using thermal tuning program that came with the instrument.

2.4 Results and Discussion

2.4.1 AFM Force Measurement Results

It is critically important to carefully control the surface hydrophobization condition to be able to detect the intrinsic hydrophobic force.[16,28] Either a long reaction time or a high surfactant concentration will result in multilayer surfactant formation on gold surfaces, and the force curve measured will be the artifact of the nanobubbles trapped on these hydrophobic surfaces. In this study, hydrophobic gold substrates were prepared in a 10^{-5} M KAX for only 10 minutes. The equilibrium water contact angle of the hydrophobic surfaces fabricated is 95.3º. This procedure effectively avoided the formation of a dixanthogen multilayer on gold surface. These gold surfaces prepared are also free of nano bubbles after this treatment.

In this chapter, AFM force measurement will be conducted on alkyl-functionalized gold surfaces to detect the solvophobic forces. The extended-DLVO theory will be used to analyze the experimental results. In the next chapter, comprehensive thermodynamic analysis of the data will be applied to investigate the origin of the solvophobic forces. Figure 2.1 shows the measured forces, *F/R*, *vs* minimum separation distance (*h*) curves, obtained from water-ethanol mixtures at different temperatures in AFM. Long range attractive forces have found existence in these solvents investigated: pure water, pure ethanol, and ethanol/water mixture. Results shown in Figure 2.1 (a) and (d) are consistent with those reported by Wang et al.[16] and Li et al.[24] More importantly, attractive forces are found to be present in the solvent of ethanol/water mixtures, containing 3% ethanol and 18% ethanol, as show in Figure 2.1 (b) and (c). However, the magnitudes of the forces

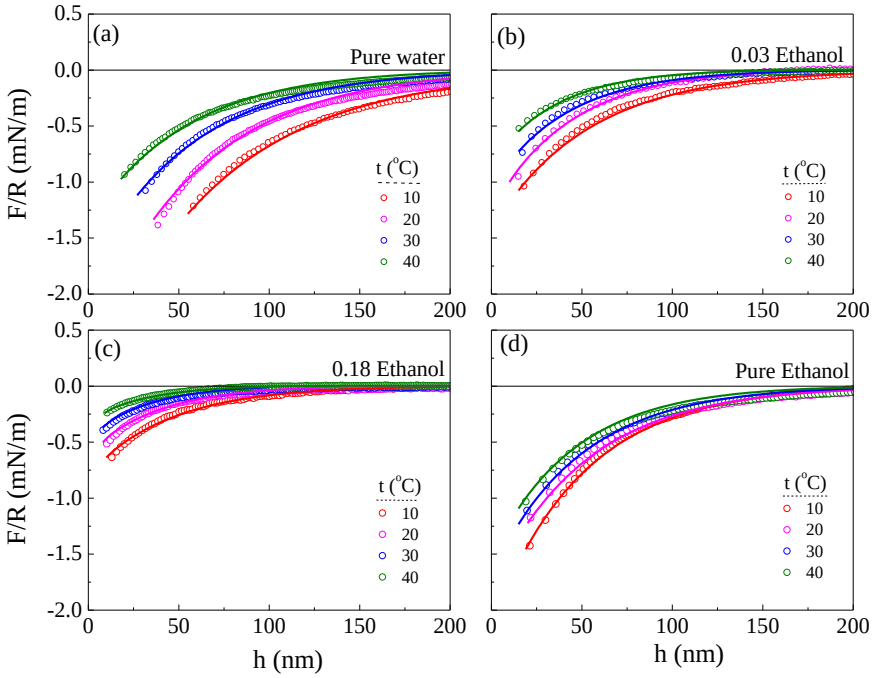

Figure 2.1 Normalized surface force (*F/R*) isotherms at different temperatures as functions of the film thickness for water-ethanol mixtures of different mole percentages of ethanol. The equilibrium water contact angle of the surfaces measured is 95.3º.

recorded are smaller than those obtained in pure liquid. From these results, we can tell that the hydrophobic forces generated in the ethanol-water mixtures are not a simple addition of the contribution of both liquids. Otherwise, the magnitude recorded should lie between the two pure liquids and are closely related to their mole fraction. Obviously, these results disclose that the water and ethanol molecules will interact with each other, changing the hydrogen bond network in the vicinity of hydrophobic surfaces. Nevertheless, these results provide evidence that the solvophobic forces can be present in H-bonding solvents other than water; in other words, the theoretical approach promoted by Chandler et al.[17,21] should be extended to other liquid containing hydrogen bonding. However, it might not be proper to say that this conclusion is suitable for all liquids containing hydrogen-bonding, since this would require further study.

2.4.2 Solvophobic Forces

According to extended-DLVO theory, the surface forces measured between two hydrophobic surfaces should include contributions from the hydrophobic force, van der Waals force, and double layer forces, i.e.,

$$F = F_e + F_d + F_s \qquad [2\text{-}1]$$

where, F_e represents electrical force, F_d van der Waals force or dispersion force, F_s solvophobic force, and F is the force measured as shown in Figure 2.1.

Figure 2.2 shows the contributions from three different surface forces in the water/ethanol mixtures at ethanol mole fractions of 0, 0.03, 0.18 and 1.0 at 20ºC. The dash line represents the Van der Waals force, with Hamaker constant of 1.92×10^{-20} J.[16,24,29] The magnitude of van der Waals is less than 0.1% of solvophobic force measured when the separation distance is about 25 nm and thus its contribution can be ignored.

Double layer electrical force is calculated by using HHF equation[30] as introduced in Equation [1-15], and in the case of symmetric surface, it can be rewritten as,

$$\frac{F_{el}}{R} = 4\pi\, \mathrm{n}kT\kappa^{-1}\mathrm{y}_{0+}^{2}\left[1-\tanh\left(\frac{\kappa h}{2}\right)\right] \qquad [2\text{-}2]$$

Where, κ is Debye length, y_0 is the surface potential of gold achieved and R is the radius of the gold probe used. Several parameters are needed to calculate the Debye length and thus the normalized electrical forces. Taking into account the water solubility and dissociation of atmospheric, the value we get of $c_\infty \cong 2.4\times10^{-6}$ M of CO_2 for pure water at 25ºC, applying the solubility data for CO_2 in water-ethanol in the literature[31]. These data are used for Debye length calculation. Static dielectric constant of water-ethanol data are also required for the calculation of Debye length, and the data is complex in water/ethanol mixtures, compared to that of pure water or pure ethanol cases. Here, the data measured by Moriyoshi[32] will be used for calculation directly. The range of Debye length calculated are between 70 nm and 200 nm for all experimental setting. ζ-potential of gold surfaces were also measured in water/ethanol mixture under different temperatures, as shown in Table 2-1. Here, it is assumed that the ζ-potential is close to the surface potential. Based on all the parameters obtained, double layer electrical forces were calculated and shown in Figure 2.2.

Single exponential fitting was used to fit the solvophobic force,

$$F / R = -Ce^{-h/D} \qquad [2\text{-}3]$$

C is a term relating to surface energy of wetting film and D is the decay length of solvophobic force in the water/ethanol mixture. The solid line shown in Figure 2.1 is the extended-DLVO plots for the data obtained at 20°C. The results obtained at other temperatures are also processed likewise. In general, most of the experimental data can be fitted to the extended DLVO theory.

The plotting of the double layer forces given in Figure 2.2 shows that the magnitude of the double layer forces are only 1/10 or even 1/50 of the solvophobic force obtained. Although only the data obtained at 20°C are shown, the same conclusion can be drawn for the data obtained at other temperatures. In other words, the contribution of electrical force to the surface force is very small and can be ignored.

Figure 2.3 shows the solvophobic forces contributing the measured surface forces shown in Figure 2.1. All of these forces increase as the wetting film separation distance decreases. At a given film thickness and solution composition, the magnitude of the force is smaller at higher temperatures. This finding is not difficult to understand, because the population of LDLs decrease with increasing temperature. The H-bonding network will be disrupted and the confined water will behave like bulk liquid.[16,24]

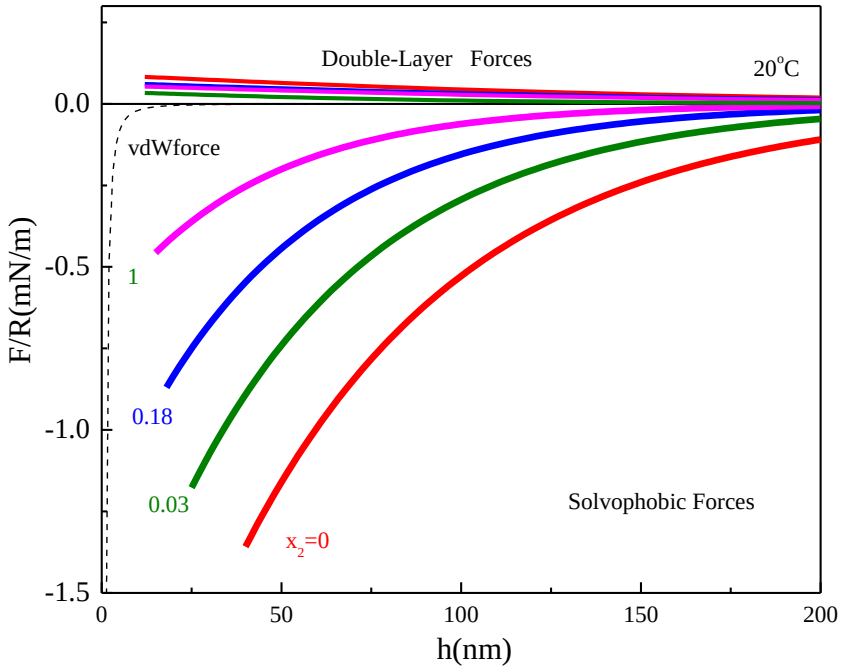

Figure 2.2 Normalized solvophobic force (F/R) and DLVO forces in thin water-ethanol film confined between hydrophobic surfaces as functions of film thickness (h) at 20°C for different ethanol mole fraction.

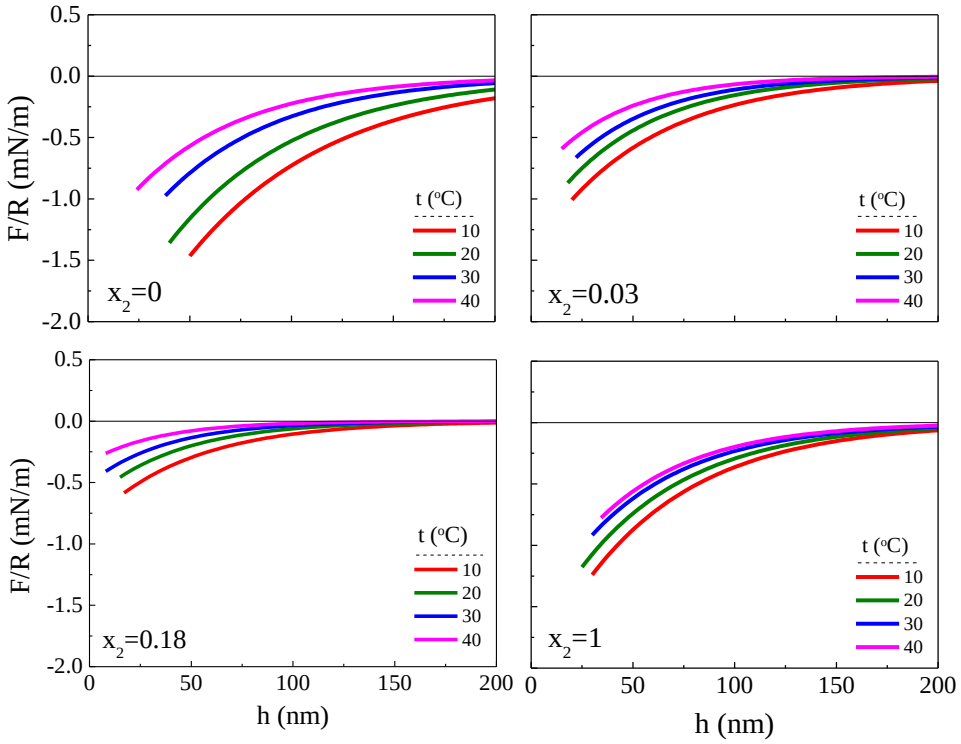

Figure 2.3 Normalized solvophobic force (F/R) in thin water-ethanol film confined between hydrophobic surfaces as functions of film thickness (h) under different temperatures for different ethanol mole fractions.

The C and D data are also obtained during the fitting process, as shown in Figure 2.4. The results indicate that the hydrophobic force parameters decrease with temperature.

2.4.3 Influence of Media Composition

Besides the temperature, there are other factors affecting the magnitude and range of solvophobic force. All of the factors affecting the H-bonded network should also affect the solvophobic force. One intrinsic factor should be the structure of alcohol molecules, e.g., the lengths of hydrocarbon chain. Water structure may also change in the presence of electrolytes such as NaCl.

In this chapter, the effect of solution composition will be studied. The data presented in Figure 2.3 andFigure 2.4 suggest that solvophobic forces are the strongest in pure water and ethanol and

Table 2-1. ζ-potential (mV) of the gold probe and the gold substrate in different mixed water-ethanol media at different temperatures

Ethanol mole fraction	*t (°C)*			
(x_2)	10	20	30	40
0	-47.3	-44.5	-39.1	-33.9
0.03	-42.8	-38.8	-36.5	-32.0
0.18	-40.9	-37.2	-34.6	-31.3
1	-43.8	-39.2	-35.0	-29.3

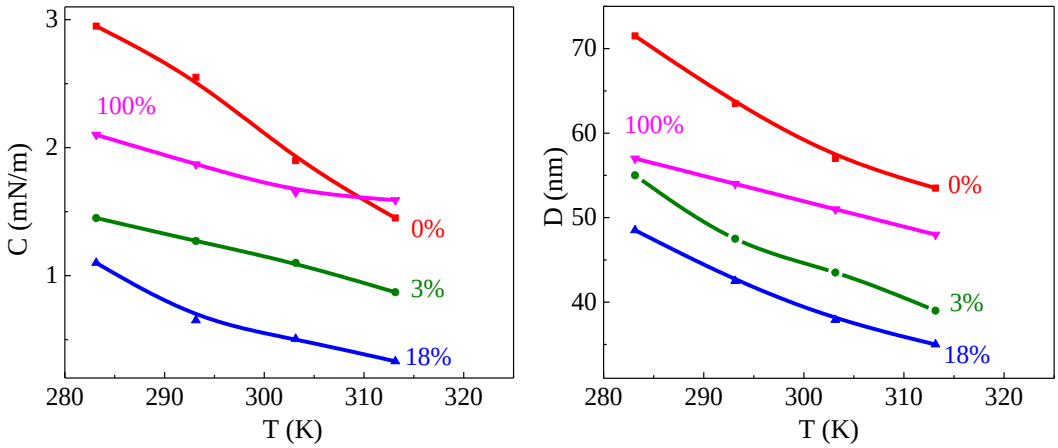

Figure 2.4 Fitting parameters of *C* (mN/m) and *D* (nm) of hydrophobic force law *vs.* different temperatures for selected ethanol mole fractions.

becomes weaker in the presence of the other. The same data have been replotted in Figure 2.5 to show the effect of mole fraction of ethanol (x_2) on C and D values. As shown, both of these parameters reach minima at $x_2 = 0.18$ at all temperatures studied.

Shi et al.[20] conducted the force measurement between an air bubble and an OTS-coated mica surface, and found that the parameter *C* of the single-exponential force law, representing the strength of the hydrophobic force is close to the interfacial tension at the air/water interface (72 mN/m). If the C value is close to the interfacial tension, *C* should decrease monotonically from the interfacial tension at the water/hydrophobic surface to that at the ethanol/hydrophobic surface. The results obtained in the present work show, on the contrary, that *C* varied with x_2 with a minimum at $x_2 = 0.18$. This finding suggests that solvophobic force may vary with H-bonded structure.

To clarify the relation of parameter C and the solvent/alkyl interfacial tension, it may be appropriate to apply a basic relation, Derjaguin Approximation,[33] written as follows:

$$F / R = 2\pi\left[G^f(h) - G^f(h=\infty) \right] \qquad [2\text{-}4]$$

By combing equation [2-3] and [2-4], the following relation can be derived:

$$G^f(h) - G^f(h=\infty) = -\frac{1}{2\pi} C \exp\left(-\frac{h}{D} \right) \qquad [2\text{-}5]$$

It is obvious that the equation is self-consistent when the film thickness is large, as both sides are equal zero. It can be seen from the equation that parameter *C* is a term relating to free energy difference of wetting film as compared to the bulk liquid, rather than the surface tension of the media. When the film thickness is zero, the right side will become $-\frac{C}{2\pi}$, and the left side is twice the difference of the monolayer water/ethanol-hydrocarbon interfacial tension and bulk water/ethanol-hydrocarbon interfacial tension.

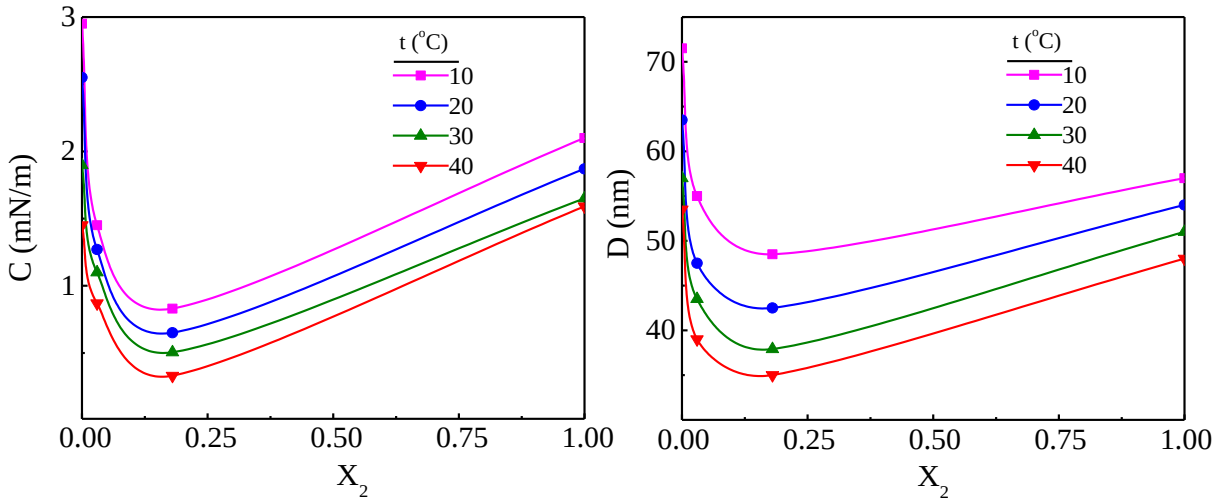

Figure 2.5 Fitting parameters C and D of the solvophobic force vs. the ethanol mole fraction (x_2) at different temperatures. Both C and D parameters are minimum when the ethanol mole fraction is about 0.18.

The film excess energies of the thin film of water/ethanol are shown in Figure 2.6. When the temperature is at 20ºC, the film excess surface energies are about 20 μN/m to 160 μN/m at film separation distance of 50 nm, compared to about 100 mN/m estimated for the overall film tension. It is only 1/50 of the water/air interfacial tension. However, such a small difference raised large solvophobic forces that cannot be ignored. Actually, the water molecule will form clusters in the vicinity of hydrophobic surfaces, according to the LDL theory, as proposed by Wang et al.,[16] and this water structure transformation will result in the changes in film tension. Actually, it might be more accurate to say that excess film tension crated the solvophobic forces and this is the reason hydrophobic force is considered surface force.

If the mole fraction of ethanol increases in the media, the interfacial tension of the water/ethanol-hydrocarbon would decrease exponentially *vs.* mole fraction of alcohol as reported by Makoto[34] and Gonzalo.[35] This means that the mixture of water and ethanol is not ideal solution. Surprisingly, the plotting shape of the excess surface tension vs. mole fraction of ethanol, for both reported by Makoto[34] and Gonzalo,[35] is very similar to the plot of parameter *C vs.* x_2 in present study: both decrease when the ethanol mole fraction increase and at some point ($x_2 \sim 0.2$), increase until the liquid is pure ethanol.

Without knowing the details of 3D hydrogen bonding network, it is still possible to deduce some properties the 3D hydrogen bonding network. First, there should be some H-bonded clusters of either water or ethanol. Second, the surface tension in the vicinity of hydrophobic surfaces should change with the population of these clusters. When the thickness of wetting film is thin, there should be more clusters. Third, the presence of ethanol will change with the population of water clusters, and thus influence their hydrogen bonding network. The energy cost for the mixture should be large, according to the solvophobic force magnitude difference shown in Figure 2.2. This can be seen from the plotting demonstrating the change of film excess energy, especially enthalpy, as shown in Figure 2.7, Figure 2.8 and Figure 2.8. From these plots, it is obviously that the structuring effect have been reduced due to the presence of ethanol. Smaller energy changes mean smaller amount of water or ethanol is changed to of H-bonding clusters. Because the ethanol

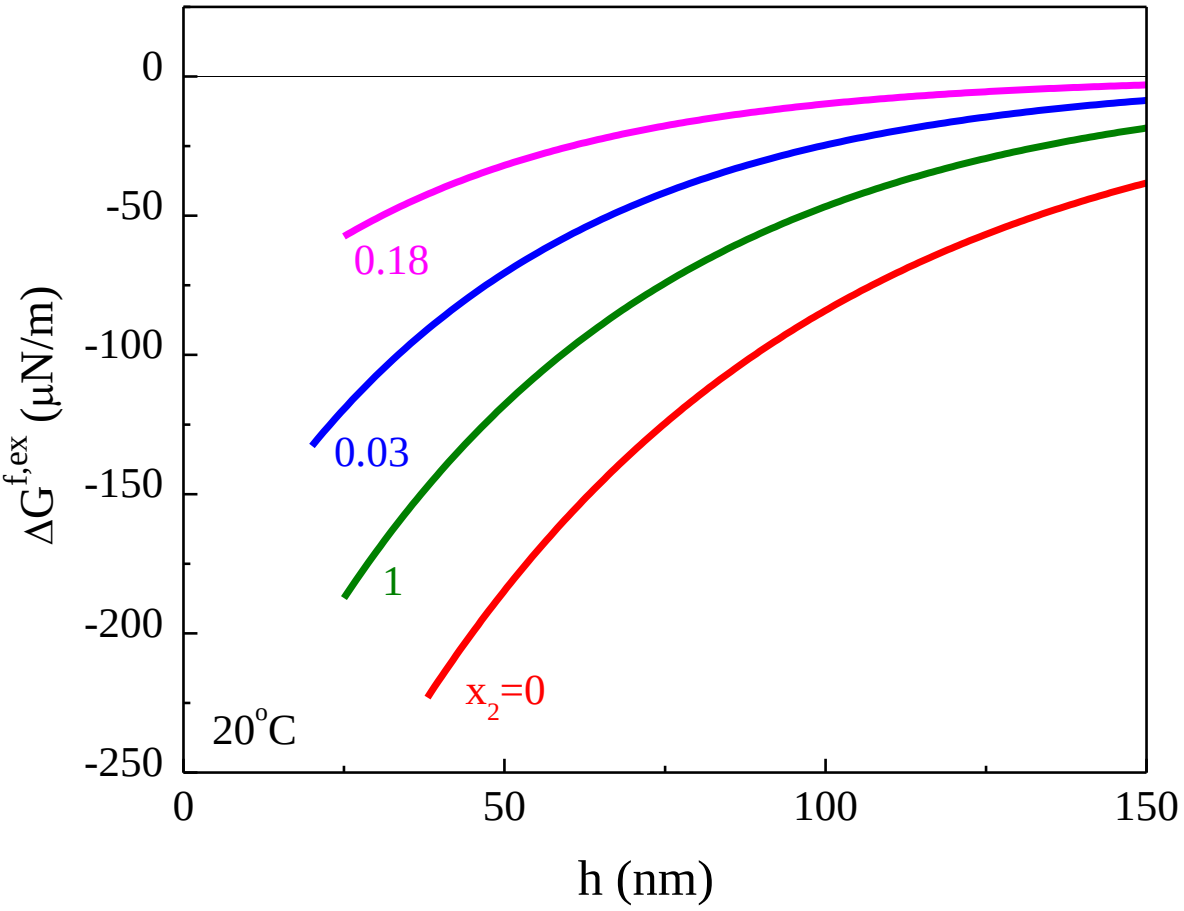

Figure 2.6 Free energies in the thin film of water/ethanol mixture at different ethanol fraction under 20º. The free energy change is minimum when the ethanol fraction is 0.18.

molecules are amphiphilic molecules. When small amount of ethanol was added into the water, the hydrophobic heads of ethanol molecules trend to adsorb preferentially onto the hydrophobic wall, leaving the hydrophilic head pointing toward the bulk water.

Figure 2.8 shows the film excess energies at the function of wetting film thickness, when the mole fraction of ethanol is 0.18. For all temperature ranges studied, we can see that $\left|\Delta H^{f,ex}\right| > T\left|\Delta S^{f,ex}\right|$. Thus the wetting process are all enthalpy driven, which means that the thinning process is accompanying the creation of new interfaces or building/breaking hydrogen bonding.[17] Obviously, H-bonded structures are formed in confined liquids. As the film thins, more and more H-bonded structures will form and reduce enthalpy. However, much of the energy gained by forming the structures will be lost due to the loss of entropy associated with the structuring. This is so-called enthalpy-entropy compensation, which was initially considered a unique property of water, but now it has been recognized as the interaction that exists in aqueous solution if they only associate with hydrogen bonding.[36,37]

A lot of theories and references has been reported to unveil how the water/ethanol structure changes their hydrogen bonding network on a hydrophobic/hydrophilic surface. According to the

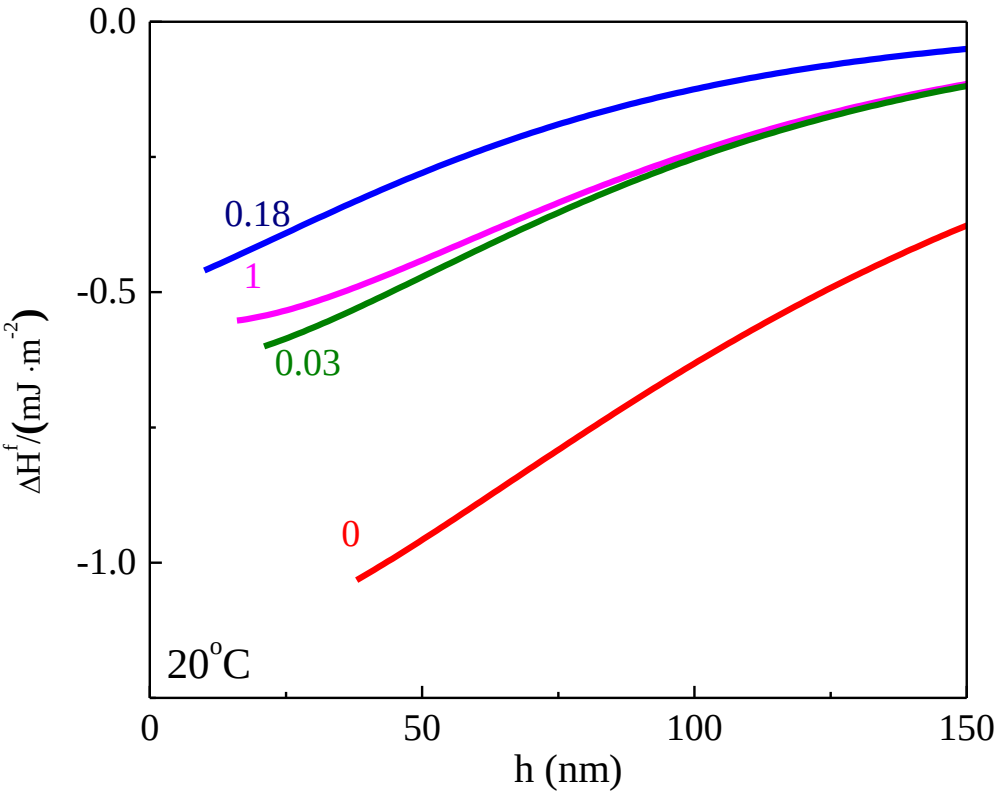

Figure 2.7 Film enthalpy *vs.* film thickness, *h*, at 20ºC at different ethanol mole fraction. The enthalpy change is minimum at ethanol mole fraction of 0.18, indicating least water cluster formed in this media.

molecular simulation by Willard and Chandler[38], for water adjacent to an extended hydrophobic surface the structure of an intrinsic interface is quantitatively similar to that of water-vapor interface, due to the incapability in forming hydrogen bonding between water and the substrate molecular. When ethanol was added, which has both hydrophobic and hydrophilic segments, ethanol would preferentially go to the surface and hydrophilic segment facing bulk water.[39] There is also other evidence supporting this kind of configuration, judged from their water/ethanol surface structure data or adsorption isotherm.[40,41] This kind of configuration will reduce the surface tension of the liquid-substrates confined in thin film comparing with those ideally mixed with water and ethanol, because more ethanol molecules were exposed on the surface. This kind of configuration will reduce the surface hydrophobicity of the gold surfaces, and reduce the antipathy between water and hydrophobic surface. In short, less water cluster will form and the water will more likely behave like bulk water. The change of film tension (or free energy of the film) will be high and the solvophobic force measured will also be small.

The phenomenon of low ethanol mole fraction preferentially adsorption hydrophobic surface or the ethanol tendency occupying the liquid surface will no long persist when the mole fraction reaches about 0.15~0.20. It is also possible when the mole fraction of ethanol is higher than 0.20, water will become unfavorable in the liquid. The statement solvophobic force magnitude variation

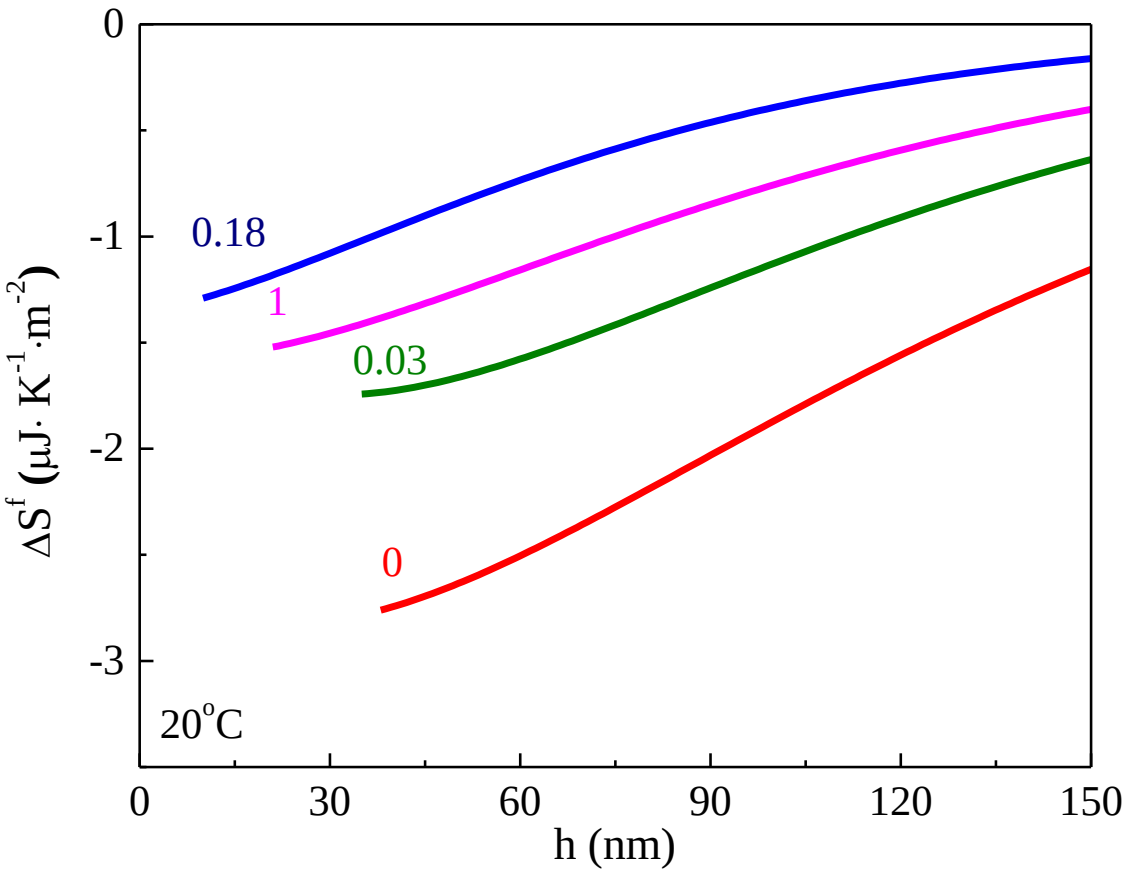

Figure 2.8 Film excess entropy *vs.* film thickness, *h*, 20°C at different ethanol mole fraction.

is true for all data presented in this chapter. The case of 0.18 ethanol mole fraction is smaller than that of 0.03, and both mixtures are smaller than pure liquids. However, a detailed study covering a whole ethanol composition range might be required to draw a more convincing conclusion, which will be introduced in the next chapter.

2.5 Summary and Conclusion

AFM force measurements have been conducted between gold probes and gold substrates, hydrophobized in KAX solutions in open circuit. Long range solvophobic forces are observed in pure ethanol, pure water, and water-ethanol mixtures, which are all hydrogen-bonding liquids. The magnitude of the solvophobic forces measured *vs.* ethanol mole fraction shows a similar variation trend of excess interfacial tensions for the water-ethanol mixtures reported previously.[38,40,41]

Thermodynamic analysis shows that the solvophobic forces measured are enthalpy driven, along with changes in hydrogen bonding network during film thinning. Ethanol addition to water affects the water-alkyl interface structure. In the presence of a small amount of ethanol, the hydrophobic moiety of the molecule is preferentially in contact with the hydrophobic substrate and leave the OH group in contact with the neighboring water phase. This kind of water-ethanol configuration results in a reduction of excess free energy and a smaller solvophobic force. The

absolute value of the excess free energy of water-ethanol mixture increases at a higher ethanol mole fraction, resulting in a larger solvophobic force.

Nevertheless, our analysis shows that solvophobic force does exist in other hydrogen-bonding liquids besides water and ethanol. However, this might require many more experiments to figure out which kind of hydrogen-bonding liquids have this property and which do not.

2.6 Reference

1 Tabor, R. F., Grieser, F., Dagastine, R. R. & Chan, D. Y. C. The hydrophobic force: measurements and methods. *PCCP* **16**, 18065-18075 (2014).

2 Dyson, H. J., Wright, P. E. & Scheraga, H. A. The role of hydrophobic interactions in initiation and propagation of protein folding. *Proc. Natl. Acad. Sci.* **103**, 13057-13061 (2006).

3 Whitesides, G. M. & Grzybowski, B. Self-assembly at all scales. *Science* **295**, 2418-2421 (2002).

4 Dill, K. A. Dominant forces in protein folding. *Biochemistry* **29**, 7133-7155 (1990).

5 White, S. H. & Wimley, W. C. Hydrophobic interactions of peptides with membrane interfaces. *Biochimica et Biophysica Acta (BBA) - Reviews on Biomembranes* **1376**, 339-352 (1998).

6 Tsao, Y. H., Evans, D. F. & Wennerstroem, H. Long-range attraction between a hydrophobic surface and a polar surface is stronger than that between two hydrophobic surfaces. *Langmuir* **9**, 779-785 (1993).

7 Tsao, Y., Evans, D. & Wennerstrom, H. Long-range attractive force between hydrophobic surfaces observed by atomic force microscopy. *Science* **262**, 547-550 (1993).

8 Attard, P. Long-range attraction between hydrophobic surfaces. *The Journal of Physical Chemistry* **93**, 6441-6444 (1989).

9 Meyer, E. E., Rosenberg, K. J. & Israelachvili, J. Recent progress in understanding hydrophobic interactions. *Proc. Natl. Acad. Sci.* **103**, 15739-15746 (2006).

10 Hammer, M. U., Anderson, T. H., Chaimovich, A., Shell, M. S. & Israelachvili, J. The search for the hydrophobic force law. *Faraday Discuss.* **146**, 299-308 (2010).

11 Israelachvili, J. & Pashley, R. The hydrophobic interaction is long range, decaying exponentially with distance. *Nature* **300**, 341-342 (1982).

12 Némethy, G. & Scheraga, H. A. Structure of Water and Hydrophobic Bonding in Proteins. I. A Model for the Thermodynamic Properties of Liquid Water. *The Journal of Chemical Physics* **36**, 3382-3400 (1962).

13 Tanford, C. *The Hydrophobic Effect: Formation of Micelles and Biological Membranes 2d Ed*. (J. Wiley., 1980).

14 Kauzmann, W. in *Adv. Protein Chem.* Vol. Volume 14 (eds M. L. Anson Kenneth Bailey C.B. Anfinsen & T. Edsall John) 1-63 (Academic Press, 1959).

15 Ben-Naim, A. Hydrophobic interactions and structural changes in the solvent. *Inorg. Chim. Acta* **40**, X35-X36 (1980).

16 Wang, J. L., Yoon, R. H. & Eriksson, J. C. Excess thermodynamic properties of thin water films confined between hydrophobized gold surfaces. *J. Colloid Interface Sci.* **364**, 257-263 (2011).

17 Chandler, D. Interfaces and the driving force of hydrophobic assembly. *Nature* **437**, 640-647 (2005).

18 Considine, R. F. & Drummond, C. J. Long-range force of attraction between solvophobic surfaces in water and organic liquids containing dissolved air. *Langmuir* **16**, 631-635 (2000).
19 Djikaev, Y. S. & Ruckenstein, E. A probabilistic approach to the effect of hydrogen bonding on the hydrophobic attraction. *J. Chem. Phys.* **130** (2009).
20 Shi, C. *et al.* Measuring Forces and Spatiotemporal Evolution of Thin Water Films between an Air Bubble and Solid Surfaces of Different Hydrophobicity. *ACS Nano* **9**, 95-104 (2015).
21 Lum, K., Chandler, D. & Weeks, J. D. Hydrophobicity at small and large length scales. *J. Phys. Chem. B* **103**, 4570-4577 (1999).
22 Murphy, K. P. Hydration and Convergence Temperatures - on the Use and Interpretation of Correlation Plots. *Biophys. Chem.* **51**, 311-326 (1994).
23 Wang, J. L., Li, Z. L., Yoon, R. H. & Eriksson, J. C. Surface forces in thin liquid films of n-alcohols and of water-ethanol mixtures confined between hydrophobic surfaces. *J. Colloid Interface Sci.* **379**, 114-120 (2012).
24 Li, Z. & Yoon, R.-H. Thermodynamics of Solvophobic Interaction between Hydrophobic Surfaces in Ethanol. *Langmuir* **30**, 13312-13320 (2014).
25 Li, Z. & Yoon, R.-H. AFM force measurements between gold and silver surfaces treated in ethyl xanthate solutions: Effect of applied potentials. *Miner. Eng.* **36**–**38**, 126-131 (2012).
26 Pan, L., Jung, S. & Yoon, R. H. Effect of hydrophobicity on the stability of the wetting films of water formed on gold surfaces. *J. Colloid Interface Sci.* **361**, 321-330 (2011).
27 Raiteri, R., Preuss, M., Grattarola, M. & Butt, H.-J. Preliminary results on the electrostatic double-layer force between two surfaces with high surface potentials. *Colloids and Surf. A: Physicochemical and Engineering Aspects* **136**, 191-197 (1998).
28 Li, Z. L. & Yoon, R. H. Thermodynamics of hydrophobic interaction between silica surfaces coated with octadecyltrichlorosilane. *J. Colloid Interface Sci.* **392**, 369-375 (2013).
29 Wang, J. L., Yoon, R. H. & Morris, J. AFM surface force measurements conducted between gold surfaces treated in xanthate solutions. *Int. J. Miner. Process.* **122**, 13-21 (2013).
30 Hogg, R., Healy, T. W. & Fuerstenau, D. W. Mutual coagulation of colloidal dispersions. *Trans. Faraday Soc.* **62**, 1638-1651 (1966).
31 Dalmolin, I. *et al.* Solubility of carbon dioxide in binary and ternary mixtures with ethanol and water. *Fluid Phase Equilib.* **245**, 193-200 (2006).
32 Moriyoshi, T., Ishii, T., Tamai, Y. & Tado, M. Static dielectric constants of water + ethanol and water + 2-methyl-2-propanol mixtures from 0.1 to 300 MPa at 298.15 K. *Journal of Chemical & Engineering Data* **35**, 17-20 (1990).
33 Derjaguin, B. Untersuchungen über die Reibung und Adhäsion, IV. *Kolloid Z.* **69**, 155-164 (1934).
34 Aratono, M. *et al.* Thermodynamic Study on the Surface Formation of the Mixture of Water and Ethanol. *J. Colloid Interface Sci.* **191**, 146-153 (1997).
35 Vazquez, G., Alvarez, E. & Navaza, J. M. Surface Tension of Alcohol Water + Water from 20 to 50 .degree.C. *Journal of Chemical & Engineering Data* **40**, 611-614 (1995).
36 Dunitz, J. D. Win Some, Lose Some - Enthalpy-Entropy Compensation in Weak Intermolecular Interactions. *Chemistry & Biology* **2**, 709-712 (1995).
37 Lumry, R. & Rajender, S. Enthalpy-Entropy Compensation Phenomena in Water Solutions of Proteins and Small Molecules - a Ubiquitous Property of Water. *Biopolymers* **9**, 1125-& (1970).

38 Willard, A. P. & Chandler, D. The molecular structure of the interface between water and a hydrophobic substrate is liquid-vapor like. *J. Chem. Phys.* **141** (2014).
39 Ballal, D. & Chapman, W. G. Hydrophobic and hydrophilic interactions in aqueous mixtures of alcohols at a hydrophobic surface. *The Journal of chemical physics* **139**, 114706 (2013).
40 Yano, Y. F. Correlation between surface and bulk structures of alcohol-water mixtures. *J. Colloid Interface Sci.* **284**, 255-259 (2005).
41 Li, Z. X. *et al.* The Structure of the Surface of Ethanol-Water Mixtures. *Mol. Phys.* **80**, 925-939 (1993).

CHAPTER 3.
Thermodynamic Analysis of Solvophobic Forces Measured in the TLFs of Ethanol Solutions of Different Mole Fractions

3.1 Abstract

Attractive surface forces have been recorded by means of an AFM for the thin liquid films (TLFs) of water-ethanol mixtures confined between two gold surfaces that are hydrophobized by chemisorption of potassium amyl xanthate (KAX). Thermodynamic properties of the TLFs have been derived from the AFM force measurements conducted at temperature in the range 10 to 40℃ and at different ethanol mole fractions (x_2). Strong hydrophobic force are observed in pure water. However, its magnitude decreases rapidly upon ethanol additions, reaching a minimum at x_2=0.2.

It has been found also that film thinning entails decreases in excess film enthalpy, entropy and Gibbs energy, indicating that two KAX-coated surfaces placed in an ethanol-water mixture are brought together spontaneously. That both the excess film enthalpy an entropy changes are negative while free energy changes remain negative indicates an enthalpy-entropy compensation, which may be associated with building H-bonded structures in the TFLs confined between two hydrophobic surfaces. Building structure is a response from the H-bonding liquid or mixtures thereof in the vicinity of a macroscopic surface that is incapable of hosting H-bonds with the solvent(s). The structuring effect is compromised in the presence of a solute, resulting in a decreased solvophobic force. Thus, the data obtained in the present work suggests that solvophobic (or hydrophobic) forces originate from the structuring of the TFLS confined by hydrophobic surfaces. There is no evidence of the solvophobic interaction being caused by pre-existing nanobubbles.

3.2 Introduction

3.2.1 Brief Background

It has been widely believed for decades that hydrophobic attraction is a unique property of water and thus the prefix *hydro*. Hence, a majority of researchers, including ourselves, have tacitly assumed that appearance of hydrophobic force depends crucially on the *H*-bond networks within *aqueous* films.[1,2]

Nonetheless, some years ago Considine and Drummond[3] reported as follows as to surface forces recorded for Teflon-coated surfaces submerged in n-alkanes and various *H*-bonding liquids using an AFM. The forces measured in the former (hexane and hexadecane) showed no attractive long-ranged force, while those measured in the latter (water, glycerol, formamide, ethanol, and methanol) showed evidence for attractive forces with large jump-in distances in the range of 9 to 500 nm. The aforementioned authors concluded, however, that these attractive forces were due to coalescence of nano-bubbles preexisting on the Teflon-coated surfaces.

Later on, it was observed by Wang et al.[4] that long-ranged, attractive surface forces which are similar in strength and range to those seen for water also arise in thin liquid films (TLFs) of short-chained alcohols between hydrophobic surfaces devoid of any signs of preexisting nanobubbles.

These results were confirmed by Li and Yoon[5] in a recent investigation of the temperature-dependent surface forces generated for pure ethanol films between alkylthiol-treated gold surfaces.

Although changes in H-bond networks should undoubtedly be of significance also for the TLFs of alcohol, the network structures may be quite different from those for water films.[6] Thus, it is possible that the comparatively strong and long-ranged surface force which we (and others) usually refer to as hydrophobic force (or solvophobic force) may well turn out to be a fairly general phenomenon that arises for a wider set of liquids than presupposed so far. It is obviously an important matter to find out more precisely as to which classes of liquids-liquid mixtures one can anticipate solvophobic forces for the TLFs confined between hydrophobic solid surfaces.

Throughout the past three decades, following upon the early observations made by Israelachvili and Pashley[7] after the advent of the surface force apparatus (SFA), the origin of the hydrophobic attraction has been recognized as a scientific issue of vast importance for a variety of technologies. A number of review papers have been devoted to this fundamental theme. Among them we note recent articles from the research group headed by Israelachvili,[8,9] a survey of experimental results written some time ago by Claesson and Christenson,[10] a couple of book chapters originating from the research group at Virginia Tech headed by Roe-Hoan Yoon,[11,12] and a comprehensive survey of the theoretical endeavors in this field due to Boinovich and Emelyanenko.[13]

Early on, some investigators suggested that bridging of (nano-sized) air bubbles are at the root of the hydrophobic attraction.[14] Today, however, there is plenty of solid theoretical and experimental evidences speaking against such a proposition.[15,16]

In this chapter, I report and discuss novel data generated by means of force measurements for the TLFs of water-ethanol mixtures confined between hydrophobized gold surfaces, carried out using an AFM-device with a plate-sphere geometry. The entire composition range was covered raging from zero to one mole fractions. The measurements were carried out at temperatures in the range of 10 to 40 ℃ in order to derive thermodynamic information. Thermodynamics analysis is an excellent tool for better understanding reaction mechanisms.

3.2.2 Derivation of Thermodynamic Relations for Binary Thin Liquid Film

At constant ambient pressure, the thermodynamic fundamental equation (in the Gibbs sense) for a thin, planar film of thickness *h* formed from a binary liquid mixture, can be written conveniently as follows,[12]

$$-dG^{f} = \Delta S^{f} dT + \pi_{D} dh + \Delta\Gamma_{2}^{f}\left(\frac{\partial \mu_{2}}{\partial \ln x_{2}}\right) d\ln x_{2} \qquad [3\text{-}1]$$

Where ΔG^{f} is the excess Gibbs energy per unit area of the thin film minus the excess Gibbs energy per unit area of a corresponding film of large thickness. Similarly, ΔS^{f} stands for the excess entropy difference per unit area, whereas π_{D} is the disjoining (interaction) pressure that approaches zero for films of sufficient thickness. The symbol $\Delta\Gamma_{2}^{f}$ denotes the film excess of ethanol per unit area for a thin liquid film of a certain thickness, *h*, minus the film excess of ethanol per unit area for similar liquid film of large thickness. The ethanol mole fraction is symbolized

by x_2, and the ethanol chemical potential by μ_2. Furthermore, in the theoretical treatment we use the equimolecular dividing surfaces with respect to the solid component (which are located at the hydrophobic walls which confine the film) to delimit the film in the normal direction, thus excluding the solid component from explicit consideration.

It is worth noting that, for an *ideal* binary solution, the coefficient within parenthesis on the rhs of Eq.[3-1] is equal to R_gT, R_g standing for the gas constant. For water-ethanol mixtures we have ideality in this sense below about $x_2 = 0.1$ as well as above about $x_2 = 0.9$.[6] Furthermore, it should be recognized that Eq.[3-1] entails the correct number of independent variables insofar as the ambient pressure is held constant, that is 3 (T, x_2, plus the film thickness h).

It is important to fully acknowledge that the differences denoted by Δ in Eq.

[3-1] are differences between thermodynamic film excess properties for a thin, planar liquid film of thickness h, and the corresponding properties of a thick film devoid of any surface-to-surface interactions but formed at the same temperature and chemical potentials as the thin film of thickness h. Thus, in our formal framework we have the following relations:

$$\Delta G^f \equiv G^f(h) - G^f(\infty) = \Delta\left(G^f - \Gamma_1^f \mu_1 - \Gamma_2^f \mu_2\right) \qquad [3\text{-}2]$$

$$\Delta S^f \equiv S^f(h) - S^f(\infty) = \Delta\left(S^f - \Gamma_1^f \hat{s}_1 - \Gamma_2^f \hat{s}_2\right) \qquad [3\text{-}3]$$

$$\Delta\Gamma_2^{f,ex} \equiv \Gamma_2^{f,\mathrm{ex}} - \Gamma_2^{f,ex}(\infty) = \Delta\left(\Gamma_2^f - \Gamma_1^f c_1 / c_2\right) \qquad [3\text{-}4]$$

In these relations, superscript ^{f} denotes a true film property. Hence, G^f in Eq. [3-2] is *not* an excess property but rather the actual Gibbs energy per unit area of a film of a certain thickness h. Furthermore, in Eq. [3-2] the chemical potentials μ_1 and μ_2 are determined in the bulk of the liquid mixture, and, likewise so, of course, the partial molar entropies $\hat{s}_1$ and $\hat{s}_2$ included in Eq.[3-3]. The superficial film densities ($\mathrm{mol \cdot m^{-2}}$) of the two components of the film are denoted Γ_1^f and Γ_2^f, whereas c_1 and c_2 are the bulk concentrations ($\mathrm{mol \cdot m^{-3}}$) of water and ethanol, respectively. Moreover, in line with Eq. [3-2], $G^f - \Gamma_1^f \mu_1 - \Gamma_2^f \mu_2$ obviously represents the work per unit area of forming a thin film of a certain thickness from the bulk of the liquid mixture. Although it is hardly self-evident, one can readily prove that $\Gamma_2^{f,ex}(\infty)$ is the same as $\Gamma_2^{f,ex}(h)$ for the imaginary case of zero surface-to-surface interaction.

Insofar as the hydrophobic solid surfaces that confine the film show inertness toward the liquid components, implying that the constituent molecules are free to change orientation, and that there are no hindrance for their diffusive transport along the surfaces, one should not encounter any problem concerning the applicability of the fundamental Eq.[3-1] for the thin film systems under investigation which have a thickness over about 10 nm (cf. Ref. [17,18]). Thus, the integral resulting from Eq.[3-1], viz.,

$$\Delta G^f(h) = \int_h^\infty (\pi_D)_{T,P,x_2}\, dh \qquad [3\text{-}5]$$

to a good approximation, will yield the overall lateral (mechanical) tension operating in a thin liquid film of thickness h, minus the lateral tension of a thick enough film, devoid of surface-to-

surface interaction. This would not be the case, however, for liquid films showing strongly localized, as opposed to mobile, attachment of some constituent(s).

In the same vein, for the case of mobile adsorption, the ordinary Gibbs surface tension equation for a single interface is expected to hold to a good approximation with respect to half of the film properties denoted G^f (∞), S^f (∞), Γ_2^f (∞) above. More precisely, in the Gibbs scheme we have the following expression where superscript ^{f,ex} (film excess) is replaced by ^{s,ex} (surface excess):

$$-d\Delta G^s = \Delta S^f dT + \Gamma_2^f \left(\frac{\partial \mu_2}{\partial \ln x_2} \right) d \ln x_2 \qquad [3\text{-}6]$$

and the Δ signs actually involves subtraction of the corresponding properties of a hydrophobic solid/vacuum interface[18]. Below, this standard expression will be employed to estimate the magnitude of the surface excess Γ_2^s in the concentration range close to $x_2 = 1$, aiming at a comparison with the film excess difference, $\Delta\Gamma_2^f$.

In passing we note that the above Eq. [3-5] plays a major role in derivation of the Derjaguin approximation[19] in 1934 which is frequently used in the following form:

$$F / R = 2\pi\Delta G^f \text{ (cylinder-cylinder, radius } R\text{)}, \qquad [3\text{-}7]$$

Accordingly, by making surface force measurements using a surface force apparatus based on crossed cylindrical surfaces, or an AFM device equipped with a (smooth) plate and a spherical probe tip, one can quantify the central thermodynamic film property, ΔG^f, *i.e.*, the film tension difference as defined above. Having obtained ΔG^f at different temperatures and compositions, values for ΔS^f and $\Delta\Gamma_2^f$ are easily derived by means of differentiation in agreement with Eq.[3-1]. This thermodynamic scheme also implies that we can derive the film enthalpy per unit area per square meter from the obvious relation:

$$\Delta H^f = \Delta G^f + T\Delta S^f \qquad [3\text{-}8]$$

Hence, a fairly complete thermodynamic characterization is feasible within the bounds of temperature and composition chosen, though it is, of course, a certain disadvantage that, for the most part, we are restricted to evaluating thermodynamic *film excess differences* rather than the actual film excesses themselves.

3.2.3 Solvophobic Surface Forces

The basic notions about the thermodynamic properties of thin liquid films between inert solid surfaces can be traced back to ideas proposed many years ago by Derjaguin and Churaev.[20] In addition to the dispersion and electrostatic components of the surface-to-surface interactions, they coined the term "structural component of disjoining pressure", indicating that there is also a component which is related with structural changes occurring in the liquid film. In the past, the terms hydrophobic attraction and (repulsive) hydration forces have also been in common use for the same purpose when dealing with aqueous films. On the other hand, Israelachvili suggested "solvation force" as a term of wider applicability.[21] In a recent paper from our laboratory on the

surface forces of pure ethanol films between hydrophobic surfaces,[5] we forwarded "solvophobic force", in analogy with "hydrophobic force". In order to minimize confusion, in the following we shall continue using this terminology.

As a brief reminder, let us consider a pair of plane-parallel plates made out of an (inert) hydrophobic solid composed of densely packed hydrocarbon (or fluorocarbon) moieties. The plates are kept at a distance *h* apart and are submerged in a liquid composed of non-dissociated, neutral molecules generating a thin film in the gap between the solid surfaces. Depending upon the molecular constitution, the detailed thermodynamic state of the liquid, and the particular constraints prevailing at each of the solid-liquid interfaces, a certain extent of layering develops, especially in close vicinity of the solid surfaces where the amplitudes of the thermal fluctuations are minimized. As the outcome of this scheme, some extra molecular ordering, additional to the one that predominates in the bulk state, presumably subsists in the film even for some distance. In particular, this could be the case for pure liquids composed of equal-sized, polar molecules which, for rather obvious reasons, tend to give rise to comparatively well-defined molecular layers particularly next to inert solid surfaces.[22]

The main driving force behind such a surface-induced structuring process is likely to be a reduction, relatively speaking, of the free energy related with the first couple of molecular layers that are in direct contact with the solid surfaces, causing the local density to be raised to some extent, hence providing a tightly packed (and polarized) substrate for additional adsorption.

By means of a supposedly cluster-mediated propagation mechanism, the local free energy becomes slightly raised throughout the core of the film (in a rapidly decaying manner towards the mid-plane of the film) in comparison with the bulk state. Focusing on the case of a pure liquid component we may thus claim that in order for its chemical potential to remain the same throughout the film system, the pressure tensor components inside the liquid film have to be adjusted, resulting in attraction in the normal direction and tension in the lateral direction.

It is important to appreciate the very small extent of the adjustments required of the thermodynamic properties to realize the film state. As a numerical example we may consider a thin water film of thickness 50 nm at 20°C that is confined between hydrophobic surfaces. For such a film, the lowering of the Gibbs energy excess amounts to $\approx 10^{-4}$ J·m^{-2} (cf. Figure 3.5) that corresponds to about $1.5 \times 10^{-5}\, k_B T$ per water molecule. At the same time the total Gibbs energy excess, $G^{f,ex}\,(h = 50\,\mathrm{nm})$, amounts to on average $1.5 \times 10^{-2}\, k_B T$ per molecule. Most of this excess, however, supposedly involves roughly 4 molecular layers yielding about 0.6 $k_B T$ per molecule. These considerations indicate that conventional MD simulations are excluded when it comes to exploring surface forces in molecular terms for water in thin films of medium thickness or more, above about 10 nm. Conversely, one cannot properly dismiss the notion of (weak) ordering on the basis of such simulations.

Upon bringing the two solid walls closer together, thus diminishing the film thickness *h*, we can evidently reduce the amount of liquid that is energetically influenced by the presence of the solid surfaces. Insofar as the local excess free energy function always stays about the same in the residual parts of the thin film, the total excess free energy of the film system will likewise become reduced, resulting in attraction.

3.2.4 The Marcelja-radic Approach

According to the theoretical treatment presented by Eriksson et al.[1], following up earlier work of similar kind by Marcelja and Radic,[23] the decisive mechanism at play here is, however, a little more complicated than described above. Hence, upon diminishing the separation, *h*, there would occur an increase of the magnitude of the negative free energy contribution associated with the contact with the solid surfaces and this increase will outweigh the free energy rise due to enhanced structure formation in the core of the film that simultaneously occurs. Thus, the final equilibrium state is determined by a balance between a negative contact term and a positive core term.

By invoking a (dimensionless) order parameter function, $s(z)$, where *z* is the coordinate in the normal direction perpendicular to the film, and employing a well-established square-gradient variational approach (Landau expansion),[24] the following expression emerges for the surface force *F*/*R* (plate-sphere or cylinder-cylinder geometry).

$$F/R = B\left[\coth\left(bh/2\right) - 1\right] \qquad [3\text{-}9]$$

Here *R* is the radius of the spherical surface involved, whereas *B* and *b* are constants that reflect the free energy changes that arise in the thin film as a result of varying the state of order. *B* is decisive for the strength of the surface force, whereas b^{-1} stands for the decay length at large surface separations. It is worth noting that the order parameter $s(z)$ does not appear explicitly in the above surface force expression. This parameter acts behind the scenes, so to speak, but is nevertheless given mathematically by the expression:

$$s(z) = \frac{B}{\pi a}\left[\frac{\cosh(bz)}{\sinh\left(bh/2\right)}\right] \qquad [3\text{-}10]$$

where the constant *a* equals the rate of lowering the Gibbs contact energy with respect to raising the order parameter in the contact monolayers. It is seen from the denominator of this expression that the order parameter tends to increase rapidly upon reducing the film thickness *h*. This is in qualitative agreement with the results obtained by Wang et al.[2] by employing hydrophobized gold surfaces submerged in water, showing that the differences with respect to the excess film entropy and excess enthalpy per unit area (both negative quantities) constantly become more negative as the water film gets thinner. This feature is also evident from Figure 3.4 and Figure 3.6 below.

In his statistical-thermodynamic treatment from 1997, Besseling[25] actually proposed that for the case of an "attractive hydration" (that is "hydrophobic") surface force, $s(z)$ might simply be taken as the local change in density from the bulk state divided by the density of the bulk phase. Such an approach might evidently apply to a wider choice of film-forming liquids than merely those capable of forming hydrogen-bonded clusters.

For large enough film thicknesses, Eq. [3-9] can be written in an approximate, single-exponential form, that is,

$$F/R = -C\exp\left(-h/D\right) \qquad [3\text{-}11]$$

where the constants are: $C \equiv 2B$ (strength) and $D \equiv b^{-1}$ (decay length). This expression holds satisfactorily for solvophobic surface forces arising for liquid films with a thickness *h* larger than

about 2*D*. The constants *C* and *D* are assumed to depend merely on temperature and composition. Evidently, the above single-exponential expression furnishes a suitable mathematical function for fitting to surface force data generated for different states of a thin film, provided, of course, that the film thickness is not too small. Hence, from the primary data collected with our AFM set-up we have been able to derive *C* and *D* as functions of temperature and composition (Figure 3.1Figure 3.2). Then the film excesses of entropy and ethanol were readily computed by means of the following expressions:

$$\Delta S^f = -\Delta G^f \left(\frac{\partial \ln C}{\partial \ln T} + \frac{h}{D} \frac{\partial \ln D}{\partial T} \right) \qquad [3\text{-}12]$$

$$\Delta \Gamma_2^f = -\Delta G^f \left(\frac{\partial \ln C}{\partial \ln T} + \frac{h}{D} \frac{\partial \ln D}{\partial T} \right) \left(1 + \frac{\partial \ln f_2}{\partial \ln x_2} \right)^{-1} / R_g T \qquad [3\text{-}13]$$

where, $\Delta G^f = -(C/2\pi)\exp(-h/D)$ has to be inserted. In the latter expression, f_2 stands for the activity coefficient of ethanol in the liquid mixture and R_g for the gas constant. The data needed to quantify the activity coefficient f_2 were derived from the ethanol partial pressures at 25℃ that early on were reported by Dobson and Butler & Wightman (cf. Ref.[6]). For completeness, we list the analogue expressions based on Eq. [3-9]:

$$\Delta S^f = -\Delta G^f \frac{\partial \ln B}{\partial T} - \frac{Bbh}{4\pi} \left(\frac{\partial \ln b / \partial T}{\sinh^2(bh/2)} \right) \qquad [3\text{-}14]$$

$$\Delta \Gamma_2^{f,ex} = -\left(\Delta G^f \frac{\partial \ln B}{\partial \ln x_2} + \frac{Bbh}{4\pi \sinh^2(bh/2)} \frac{\partial \ln b}{\partial \ln x_2} \right) \left(1 + \frac{\partial \ln f_2}{\partial \ln x_2} \right)^{-1} / R_g T \qquad [3\text{-}15]$$

where ΔG^f is given by Eq. [3-9].

An additional remark concerns the tacit supposition that a thin liquid film between hydrophobic surfaces is laterally homogeneous which is implicit in the above exposition. Some experimental results reported earlier appear to indicate that a water surface[26], like bulk water,[27-29] is phase-separated on the nano-scale. Toward this background we have previously shown that a water film model comprising bridging clusters, is fully compatible with the recorded surface force data at medium and long range.[30,31] In particular, a long range surface force expression of the same form as Eq. [3-11] is derived even for this case. Interfacial mixing was recognized as the main (entropic) driving force behind the generation of elongated bridging clusters.

To finally decide which of the available model descriptions that is closest to reality appears as quite a demanding task. First of all, we cannot exclude that different types of models are needed to cover different experimental situations, e. g. a pure water film *vs.* a pure ethanol film, confined between hydrophobic surfaces, or even a thin film *vs.* a thick film. Then there is a major issue to convincingly account for the long-range-ness observed, either by referring to long-range (attractive) electrostatic interactions (Miklavic et al.[32]), formation of bridging clusters, generation of low-density liquid species or dissolved gas clathrates, or exponentially decaying intermolecular correlations.

The Marcelja-Radic approach yields a variational problem that in a straightforward manner results in a simple expression for an attractive solvophobic surface force, *i.e.*, Eq. [3-9] , which is capable of reproducing experimental data in a wide film thickness range (2 – 100 nm). Nonetheless, it would be desirable to eventually forward an alternative approach that is based primarily on the actual physical conditions prevailing in the liquid films rather on some less tangible, mathematical/thermodynamic properties. Here the aim has been to broaden our experimental surface force studies to entail hydrophobic solid surfaces submerged in liquid mixtures in order to further such a development.

3.2.5 Other Potential Contributions to the Surface Force Recorded

So far we have been discussing surface force contributions that arise due to the impact of hydrophobic surfaces on the structure of the liquid in which they are submerged. In other words, up till now we have considered merely the "structural component" of the surface force/film tension, once more using the terminology due to Derjaguin. In addition, however, we need to estimate other possible surface force contributions.

It is well known that interactions of van der Waals type are strong enough only for rather short separations to yield surface forces comparable with solvophobic (that is structural) surface forces. As a rule, this might only happen below about 2 nm in film thickness. Considering especially the dispersion interactions present among surfactant-loaded gold surfaces prepared in the way described in the experimental section below, we can readily verify that surface force contributions of this nature are generally 2 to 3 orders smaller than the attractive surface forces which we observe in the thickness range 20 – 100 nm. Hence, in the present context, they are insignificant. The same conclusion holds true with respect to the viscous force that arises because of the finite speed with which the (gold-covered) spherical probe approaches the gilded plate of our AFM set-up.

However, we also have to consider the repulsive electrostatic surface force contribution that arises as a result of electrostatic double layer formation. As a point of departure, let us bring up the (low surface potential) force expression according to the treatment presented by Hogg et al.:[33]

$$F_{el} / R = 4\pi c_{\infty} R_{\infty} T \kappa^{-1} Y_0^2 \left[1 - \tanh\left(\kappa h / 2\right)\right] \qquad [3\text{-}16]$$

Here it is specialized for the case of monovalent ions and a pair of equivalent surfaces; κ^{-1} is the Debye length and Y_0 the scaled surface potential = $e\Psi_0/k_BT$. It is well known, of course, that the constant electrostatic potential boundary condition closely approximates the proper constant chemical potential condition. The notation used here is standard. In particular, c_∞ denotes the electrolyte concentration in the bulk solution that is largely determined by the dissociation of dissolved carbon dioxide. Ψ_0 is the surface potential that we have assigned the value 40mV, in approximate agreement with the zeta potentials of the gold probe and the substrate surfaces measured in different water/ethanol mixtures at different temperatures (Table 3-1). Accordingly, by taking into account the water solubility and dissociation of atmospheric CO_2, for the pure water case we get $c_\infty \cong 2.4 \times 10^{-6} M$ at 25°C, (implying a Debye length of 196 nm) and a relatively minor electrostatic contribution to the surface force for water-rich films in the thickness interval 20–100 nm: from +0.034 mN·m^{-1} at 20 nm to +0.027 mN·m^{-1} at 100 nm. The corresponding

Table 3-1. ζ-potential (mV) of the gold probe and the gold substrate in different mixed water-ethanol media at different temperatures

Ethanol mole fraction (x2)	t (°C) 10	20	30	40
0	-47.3	-44.5	-39.1	-33.9
0.002	-46.9	-44.1	-38.5	-33.6
0.01	-45.8	-42.9	-37.6	-32.8
0.03	-42.8	-38.8	-36.5	-32.0
0.18	-40.9	-37.2	-34.6	-31.3
0.5	-32.3	-30.9	-27.4	-26.4
1	-43.8	-39.2	-35.0	-29.3

recorded surface forces are about -2 mN·m^{-1} and -0.5 mN·m^{-1}, respectively, that is 50 to 20 times larger in magnitude.

Although (rather intriguing) solubility data for CO_2 in water-ethanol mixtures are available in the literature,[34] we have been unable to find experimental values for the dissociation constant of CO_2 dissolved in these mixtures, making it virtually impossible to reliably estimate the magnitude of the electrostatic surface force contribution for the films studied. A rough estimate is that it may amount to a few percent in the thickness range 20 – 100 nm. Hence, it is justifiable to claim that the AFM forces recorded, divided by the sphere radius, to a good approximation may be considered as purely solvophobic surface forces.

3.3 Method and Materials

The surface forces, $F/R = 2\pi\Delta G^f$, operating in thin films of water, ethanol and water-ethanol mixtures were determined by applying the colloidal probe technique[35] and using a Nanoscope V atomic force microscope (AFM). The following ethanol mole fractions, x_2, were chosen: 0, 0.002, 0.01, 0.03, 0.18, 0.5 and 1.0. All the force measurements were conducted at 10, 20, 30 and 40°C, respectively, regulated by means of a thermostat included in the AFM set-up.

For the AFM force measurement we used a spherical gold probe and a gilded bottom plate. The plates were treated by coating ~100 nm gold films onto 1cm × 1cm silicon substrates by means of electron beam physical vapor deposition (EB-PVD 250). Chromium was used as an intermediate adhesive layer, 5 nm in thickness, between the gold film and the silicon substrate. Gold spheres were produced from gold wires (0.0127 mm diameter, 99.9%, Alfa Aesar), following the method devised by Raiteri et al.[36] Tiny spheres with diameters from 10 to 15μm were selected for cleaning, followed by hydrophobization.

The gold-coated substrate plates were cleaned in piranha solutions (7:3 by volume of H_2SO_4/H_2O_2) for 10 minutes, rinsed by deionized water and dried in ultrapure N_2 gas. The gold spheres were glued onto a cantilever (AIOE-10, Nano and More, USA) with epoxy resin (EPON 1004F). The spring constant of the cantilever was ~0.48 N/m and was further calibrated during the force measurement by an AFM equipped with software Nanoscope V 7.3. The gold spheres with attached cantilevers were first immersed in pure ethanol for 1 minute and then further exposed under 245 nm UV light for 1 h for cleaning purpose.

The hydrophobizing agent used was potassium amyl xanthate ($C_5H_{11}OCS_2^-K^+$, KAX, >90%, TCI America). Before chemisorption onto gold it was recrystallized twice using HPLC grade acetone (Fisher Scientific, Inc.) and diethyl ether (99.99%, Sigma-Aldrich, Inc.) as described previously by Pan et al.[37] and by Li et al.[38]

After the gold-coated substrate and probe had been assembled in the AFM device, KAX/water solution was injected to carry out surface hydrophobization. The concentration of KAX was chosen equal to 10^{-5} M and the reaction time to 10 minutes. Following upon the reaction step, ethanol/water mixture (or pure water or ethanol) was carefully injected into the AFM cell to replace the KAX/water solution. By this step one avoids to expose the hydrophobized surfaces to the ambient air. Through this treatment tightly packed KAX are generated on the gilded plate as well as on the gold surface of the probe.[39] The equilibrium water contact angle of the gold plate treated in this way was 95.3º.

3.4 Results and discussion

In consistency with the Derjaguin approximation, the force data obtained were divided (normalized) by the radius of the gold sphere, thus converting them to film tension differences (ΔG^f) multiplied by the numerical factor 2π. In the present paper, we report on the effects of varying the temperature and ethanol mole fraction as studied experimentally and discussed below in terms of thermodynamic parameters. A recent, closely related, paper from our laboratory was devoted to the effect of temperature changes on the surface forces of pure ethanol films of variable thickness.[5]

Figure 3.1 shows the normalized surface force, *F/R*, *vs* the minimum separation (*h*), obtained for water-ethanol mixtures at different temperatures. Since the conditions for hydrophobization of the gold spheres and gilded substrates were by and large chosen exactly the same, the differences observed for a given separation *h* should be due exclusively to variations of the temperature and composition of the liquid mixture.

It is also worth underlining that none of the force curves recorded show any steps or discontinuities. This is strong evidence for the absence of (air-filled) nano-bubbles during the AFM runs. Whether or not air bubbles adhere to a gold surface treated with a hydrophobization agent depends strongly on the detailed conditions chosen for treatment. It has been demonstrated earlier that hydrophobization treatment using a solution of an alkyl thiol at low concentration for a short length of time (10^{-5} M for 10 minutes, in our case) does not give rise to adhering (air) nanobubbles. Yet, a satisfactory degree of hydrophobicity is attained to judge from the contact angle measured toward water.

All forces recorded for different ethanol mole fractions in the temperature range 10 – 40℃ were attractive and increasingly so upon reducing the film thickness. By adding ethanol to water, the strength of the attractive force present at first diminishes at a surprisingly rapid rate, and then attains a broad minimum where the mole fraction of ethanol is about 0.20. Thereafter, it steadily moves upward with the ethanol concentration and reaches a maximum for pure ethanol (Figure 3.5). These findings are consistent with the results obtained by Wang et al.[2] for alkyl-thiolate gold surfaces submerged in pure water by making AFM runs at 22℃ .

As to the order of magnitude of the forces recorded, at this stage it may be appropriate to remind of the basic relation [7] written as follows:

$$F / R = 2\pi\left[G^f(h) - G^f(h=\infty)\right] \qquad [3\text{-}17]$$

The purpose is to clearly display that the surface force *F/R* involves a comparison with the interfacial tension operating at the solid hydrocarbon/liquid-mixture interface for $h = \infty$. Upon assuming for the pure water case, that this latter excess free energy is approximately twice what we might expect for a water-oil interface (~50 mNm^{-1}) and, for the pure ethanol case about twice the ethanol-air surface tension (22 mNm^{-1}) minus about 2 times 20 mNm^{-1} to account for the exchange from an ethanol-air to an ethanol-hydrocarbon interface, one can roughly estimate $G^f(h = \infty)$ to diminish from ~100 mNm^{-1} to 4 mNm^{-1} as the ethanol mole fraction is raised from 0 to 1. Simultaneously, the surface force *F/R* (h = 20 nm) is found to scatter about 1 mNm^{-1} corresponding to $\Delta G^f \approx 0.1$ mNm^{-1}. This indicates that especially for low ethanol concentrations, ΔG^f corresponds to just a very minor portion of the overall surface free energy whereas this is not so for ethanol mole fractions close to unity.

The single-exponential surface force expression as given by Eq. [3-11], was used to generate force curves by fitting to the experimental data, cf. Figure 3.2. In Figure 3.3, the *C*- and *D*-functions obtained are plotted vs the ethanol mole fraction, x_2. Both these parameter functions display a minimum for about x_2 = 0.20 and maxima, one on the water side, and one (of somewhat lesser size) for pure ethanol. It is also clearly seen that the *C*- and *D*- values are smaller at higher temperatures than those at lower temperatures. It is hardly surprising, of course, that, apart from

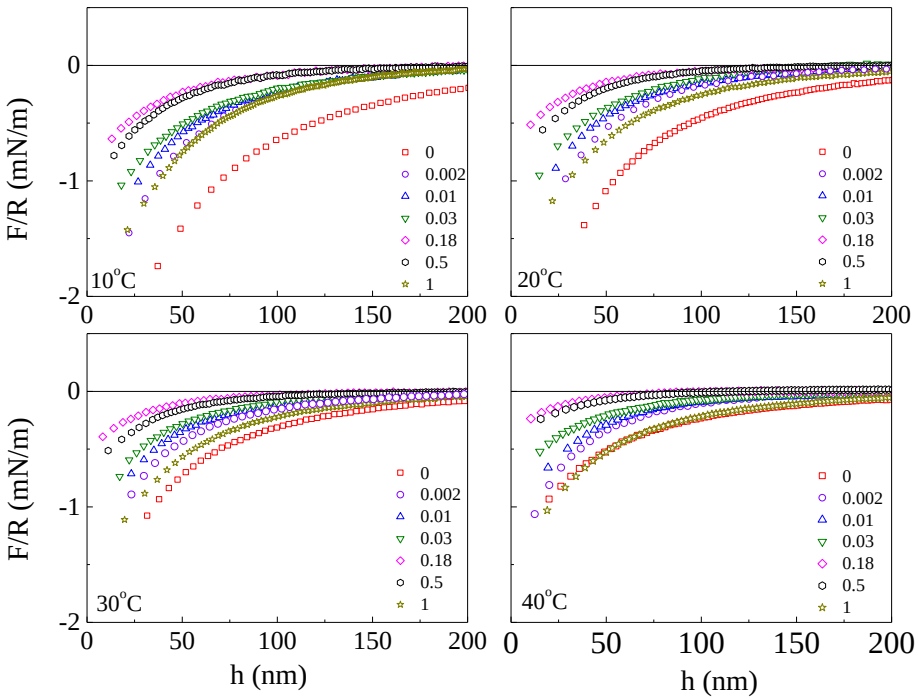

Figure 3.1 Normalized surface force (F/R) isotherms recorded at different temperatures as functions of the film thickness for water-ethanol mixtures of different mole percentages of ethanol. The AFM force measurement was carried out with a gold plate and an AFM probe hydrophobized in10^{-5} M KAX solution for 10 minutes to obtain an equilibrium water contact angle 95.3º

the sign, the x_2- dependencies of the *C*- and *D*- parameters resemble the variation of the film excess Gibbs energy difference ΔG^f with x_2, *cf.* Figure 3.5.

The most surprising feature, however, common to all the plots shown in Figs. 3 to 8, is the extraordinary rapid changes taking place in the very dilute range, below about x_2= 0.03. Thus, in the narrow interval from x_2= 0 to 0.03, the magnitude of the excess Gibbs energy (film tension) difference, ΔG^f, drops to roughly half its value for pure water (Figure 3.5), irrespective of the temperature chosen. In the same concentration range, upon adding ethanol to water, the surface tension of the water-ethanol/air interface drops in a parallel fashion[40]. Simultaneously, the "free" (non-hydrogen-bonded) OH groups are seen to be replaced by ethyl groups as studied by means of SFG (Sum Frequency Generation) vibrational spectroscopy by Tyrode et al.[41] This phase-transition-like, rather drastic change of the solid-hydrocarbon/liquid-mixture interface is indicative of a major restructuring of the hydrogen-bond pattern going on in the interface. Checking Figure 3.4, Figure 3.6 and Figure 3.7 one also notes that, in the very dilute range, the excess film entropy and enthalpy differences decrease rapidly in magnitude consequent to minor additions of ethanol. Furthermore, it is seen that ΔH^f and $T\Delta S^f$ are large in comparison with their difference ΔG^f. Taken together with the inferred, rapid disappearance of free OH groups, it seems that we are facing a kind of surface melting process induced by the presence of small amounts of ethanol in the surface. A reasonable scenario may be that the outwards directed free OH groups are repelling

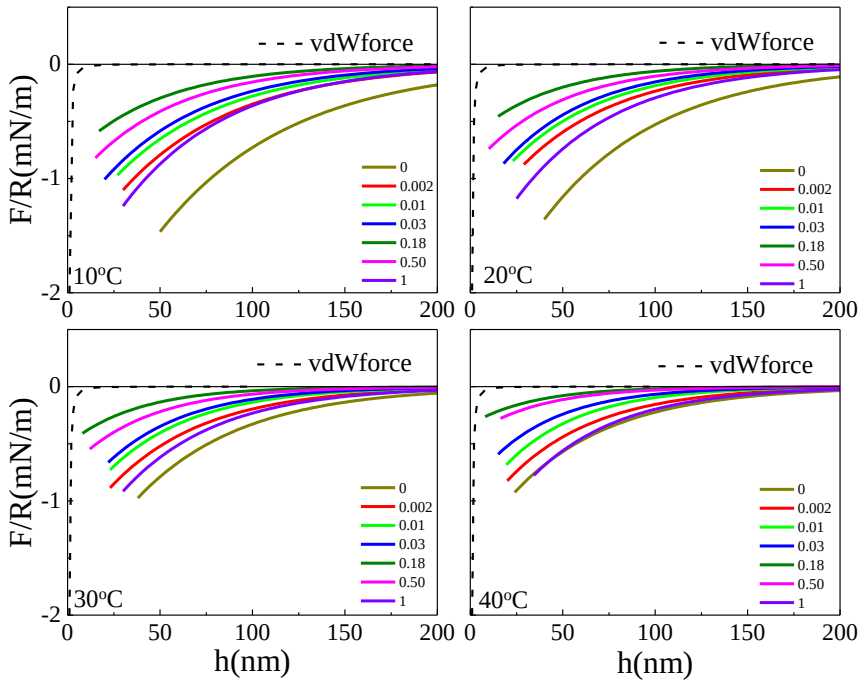

Figure 3.2 Solvophobic force (F/R) in a thin water-ethanol film confined between hydrophobic surfaces as functions of the film thickness (h) at different temperatures and for different ethanol mole percentages. Dashed lines show the van der Waals contribution with the Hamaker constant put equal to 1.2×10^{-20} J. As seen, this contribution is insignificant throughout the whole thickness range investigated.

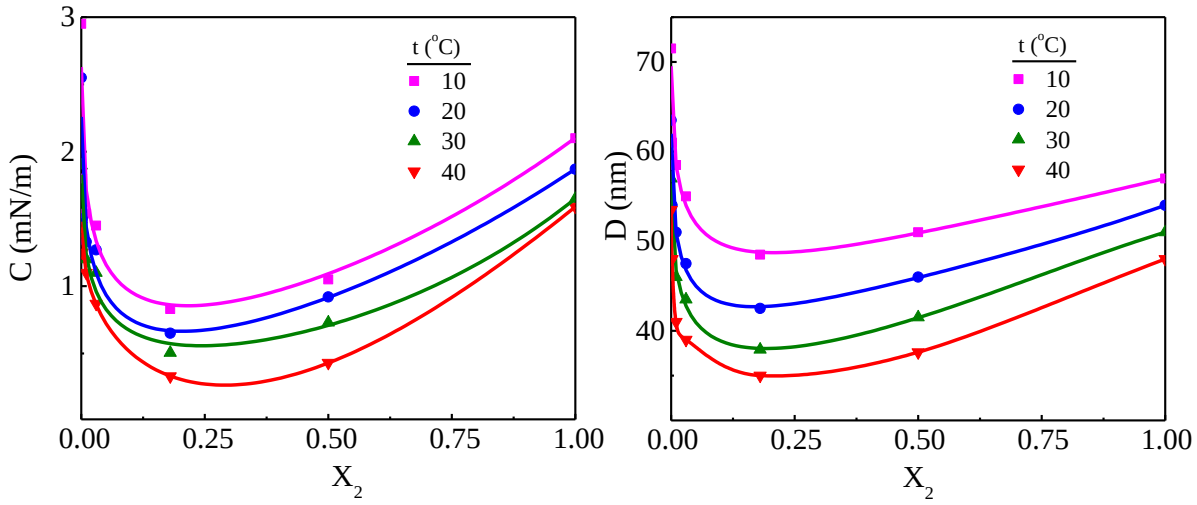

Figure 3.3 Fitting parameters C and D of the solvophobic force expression given by Eq. [3-11]. the ethanol mole fraction (x_2) for different temperatures. The solid lines represent the C and D functions obtained which were used for computing the enthalpy and entropy excess difference.

each other, causing their lateral thermal motions to become restricted, and that this restriction is removed upon replacement with ethyl groups.

According to the theoretical approach taken in Ref. [1], the *C*-parameter is strongly correlated with the response toward order parameter changes in the contact monolayers next to the hydrophobized surfaces. If a large free energy reduction is generated by increasing the order parameter to a certain extent, the *C*-value will tend to become large as well. Accordingly, the free energy response toward order parameter changes is anticipated to be large for ethanol mole fractions below about 0.03, and less so in the middle concentration range, between $0.03 < x_2 < 0.5$, but is seen to increase again in the interval $0.5 < x_2 < 1.0$ (Figure 3.5).

For films of large thickness one finds the following attractively simple relation to hold.[1]

$$G_0^f - G_\infty^f = \frac{C}{4\pi} \qquad [3\text{-}18]$$

where G_0^f represents the excess Gibbs energy per m^2 that we would have prior to restructuring the two interfaces. For pure water, the *C*-values we have derived at different temperatures cover the range $\sim 1-3$ mNm^{-1} which corresponds to $G_0^f - G_\infty^f$ spanning the range from ca 0.08 to 0.24 mNm^{-1}, to be compared with ca 100 mNm^{-1} estimated for the overall film tension. Thus, the free energy reduction due to the structural reorganization amounts to at most about a quarter of a percent of the total excess Gibbs energy of a relatively thick film. For thinner films, however, the relative contribution of restructuring becomes bigger.

The parameter *D* represents the decay length of the solvophobic (structural) surface force which in the present work was generally found to amount to several tens of nanometers (Figure 3.3). The decay length becomes shorter upon raising the temperature that signals a weakened tendency to avoid order parameter gradients, $\partial s(z)/\partial z$. Elongated trains of *H*-bonded water or

ethanol molecules or bridging clusters may well be responsible for the surprisingly long decay lengths observed, attaining a *D*-value for the pure water case that is equal to over 70 nm at 10℃. Note, in addition, the strong temperature dependence of both the *C* and *D* parameters (which is indicative of sizeable entropy contributions), and the roughly parallel courses of the *C* and *D* functions in Figure 3.5 implying that more well-ordered films are anticipated to show relatively long decay lengths and vice versa.

An important finding is, of course, that the reduction in magnitude of the excess Gibbs energy difference, ΔG^f, depends strongly on the film thickness (as seen from Figure 3.5) verifying the results obtained earlier by Wang et al.[4] This difference is negative, and, somewhat surprisingly, even more so as the film thickness is diminished. The prime reason for this behavior seems to be that the (negative) contact contribution to the film free energy shifts the balance as the counterweight of the (positive) core contribution is reduced.

Although hydrogen-bond effects on their own may not be the one and only cause of solvophobic attraction it would be most unlikely if changes of that kind were not essential for the understanding of the film properties that we consider here. On this point we might hope that further SFG spectroscopic data will be illuminating. Such work is currently in progress in collaboration with a SFG-oriented research group in Stockholm, Sweden, headed by Eric Tyrode.[41]

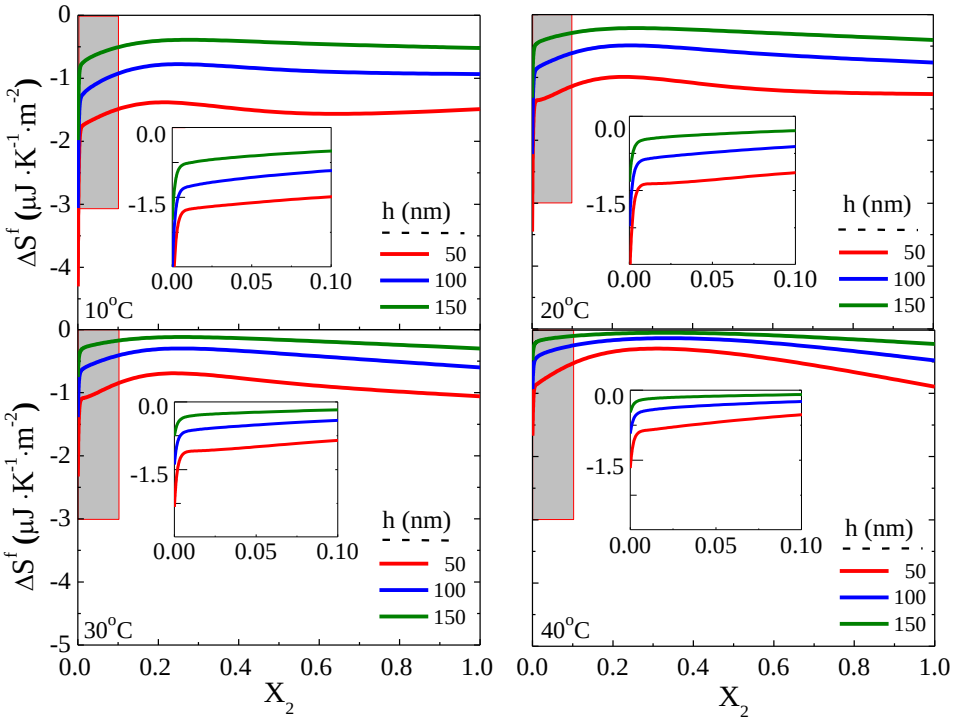

Figure 3.4 Film excess entropy for a film of a given thickness, *h*, minus the film excess entropy for a film of large thickness, plotted *vs* the ethanol mole fraction for 10, 20, 30 and 40℃. The insets are magnified figures of the low ethanol mole fraction region, showing rapid entropy increases upon adding small amounts of ethanol.

As seen from Figure 3.5, there is a general trend toward a broad minimum for $|\Delta G^f|$ in the central part of the concentration range, about x_2= 0.20. Checking Figure 3.8,one may further note that the difference as to the excess of ethanol, $\Delta\Gamma_2^{f,ex} \equiv \Gamma_2^{f,ex}(h) - \Gamma_2^{f,ex}(\infty)$, is generally negative at low mole fractions but positive above ca x_2= 0.20. On the basis of Eq. [3-4] we may thus infer that the actual film density changes related with both water as well as ethanol due to surface-to-surface interaction, for the most part become negative for the mixed states. In detail, the reasoning behind goes as follows. Firstly, at low mole fractions of ethanol, the actual film density change for ethanol, $\Delta\Gamma_2^f$, is to a good approximation obtained from the relation $\Delta\Gamma_2^{f,ex} \equiv \Delta\Gamma_2^f - \Delta\Gamma_1^f x_2/x_1 \approx \Delta\Gamma_2^f$, and is consequently, according to the experimental results, negative. Secondly, when $\Delta\Gamma_2^{f,ex}$ = 0 (that happens for about x_2= 0.20 almost independently of the film thickness), $\Delta\Gamma_1^f$ and $\Delta\Gamma_2^f$ are bound to have the same (negative) sign. Thus the uptake of ethanol in water-rich films is hindered by structuring, and the uptake of water is hindered by some structural features that appear at higher mole fractions.

From the surface tension isotherms for water-ethanol mixtures exposed to air derived by Aratono et al.,[40] it appears that above about x_2= 0.20 the courses of the isotherms are almost linear up to x_2= 1. Replacing the air contact with solid hydrocarbon should lower the interfacial tension by an almost constant amount equal to approximately 20 mNm^{-1}. Referring to the Gibbs equation,

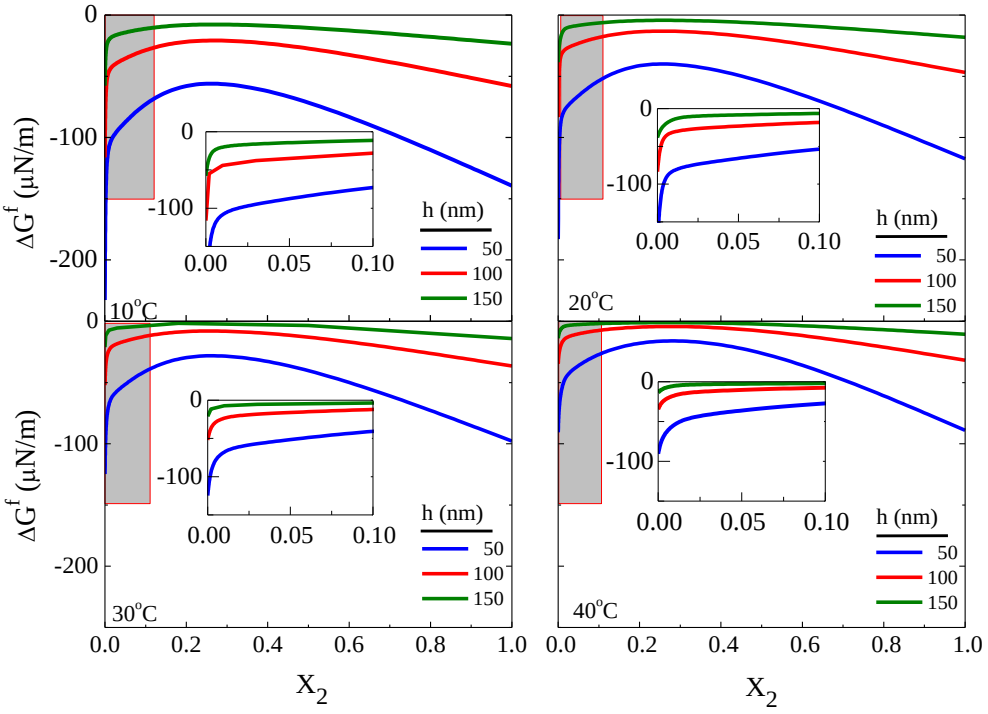

Figure 3.5 The film excess free energy difference, ΔG^f, *vs.* the ethanol mole fraction for different film thicknesses, and at different temperatures: 10, 20, 30 and 40°C. It is only the solvophobic surface force that is found to contribute to ΔG^f here. The curves that are displayed were calculated on basis of the surface forces in Figure 3.2. The insets are magnified figures of the low ethanol mole fraction regions, showing a rapid free energy change as a result of adding small amounts of ethanol.

Eq. [3-6], this observation allows us to assume that in the elevated concentrated range, the surface excess isotherm, $\Gamma_2^{s,ex}$ *vs* x_2, should be equal to half the value of the film excess of ethanol for a thick film, $\Gamma_2^{f,ex}(\infty)$. By employing the isotherm derived by Butler and Wightman[6] in this manner we find that whereas $\Delta\Gamma_2^{f,ex}$ is found to be of the order 10^{-7} mol/m^2 for pure ethanol films of thickness 50 - 100 nm, we have that $\Gamma_2^{f,ex}(\infty) \cong 2\Gamma_2^{s,ex}$ is about a factor of 50 larger, showing, once more, that we are dealing with miniscule changes of the film composition here.

It is noteworthy that the parallel formation of an adsorption layer at the water-ethanol/air interface results in a maximum for the surface excess of ethanol at about x_2= 0.18 that seemingly marks the onset of the formation of the second adsorption monolayer[6,40] with an excess of hydroxyl groups pointing toward the hydroxyls of the primary adsorption layer

It is also worth observing that the ethanol excess functions displayed in Figure 3.5 show a certain resemblance with the partial molar volume function for ethanol in water-ethanol mixtures,[42] which at 25 ℃ has a minimum value for $x_2 \cong 0.08$ equal to 52.2 cm^3/mole followed by a steady increase up to a maximum value of 58.1 cm^3/mole for pure ethanol. The minimum is presumably due to ethyl groups at first filling up and stabilizing the voids in the water clusters that initially are present in pure water. Soon enough, however, upon adding more ethanol, the formation of (low density) water clusters is hampered by the presence of an excess of ethanol. Although we cannot

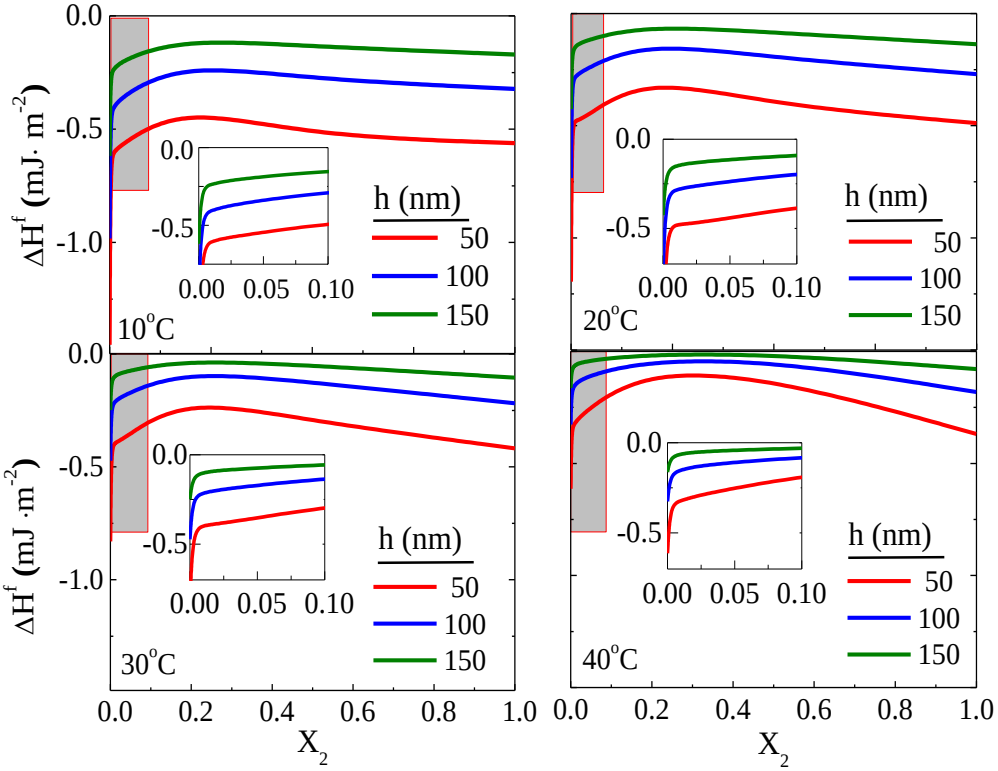

Figure 3.6 Film excess enthalpy for a film of a given thickness, *h*, minus the film excess enthalpy for a film of large thickness, plotted *vs*. the ethanol mole fraction for 10, 20, 30 and 40ºC. The insets are magnifications of the low ethanol mole fraction region, showing rapid increases upon adding small amounts of ethanol.

yet establish the full connection between the thermodynamic film properties and the density of water-ethanol mixtures it is reassuring to that these broad common features reappear for which hydrophobic and hydrogen-bonding effects in conjunction are most likely responsible.

Nevertheless, turning back to the basic mechanism for solvophobic attraction (that supposedly involves successive formation of less and less well-organized molecular layers) we may first consider the case of pure ethanol. The magnitude of the surface force is for this case broadly the same as for pure water (Figure 3.2). In line with detailed surface tension studies of water-ethanol mixtures,[40] we may imagine that a monolayer of ethanol molecules first becomes attached to each one of the two hydrophobic walls with their hydroxyl groups turned predominantly toward the interior of the thin film. A second layer is then to some extent composed of ethanol molecules turned the other way around thus enabling more of hydrogen-bonding to the first monolayer. Apparently, this process can be repeated successively but is eventually hampered by entropic factors calling for random orientation and extensive mixing of ethyl and hydroxyl groups. So far this model description is, however, merely part-wise supported and in an indirect manner by SFG studies.

On the other hand, in the dilute composition range, below about x_2= 0.03, a strongly favored exchange process is going on that apparently involves that, upon adding ethanol, initially free OH groups become *H*-bonded to a network of hydroxyl groups and largely replaced by C_2H_5O groups with their ethyl ends turned outward. This process is accompanied by a drastic reduction of the interfacial (free) energy. Our surface force data do reflect and depend on the major change of the

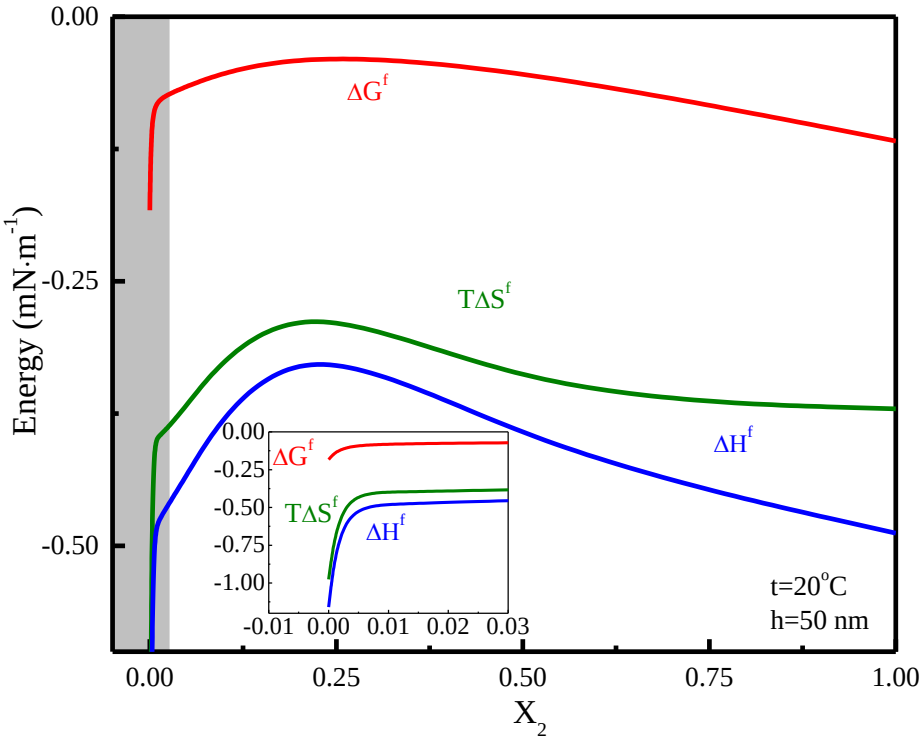

Figure 3.7 The main thermodynamic film excesses for a film with *h* = 50 nm minus the corresponding excesses for a film of large thickness plotted *vs* the ethanol mole fraction. Temperature of present data is obtained at 20ºC.

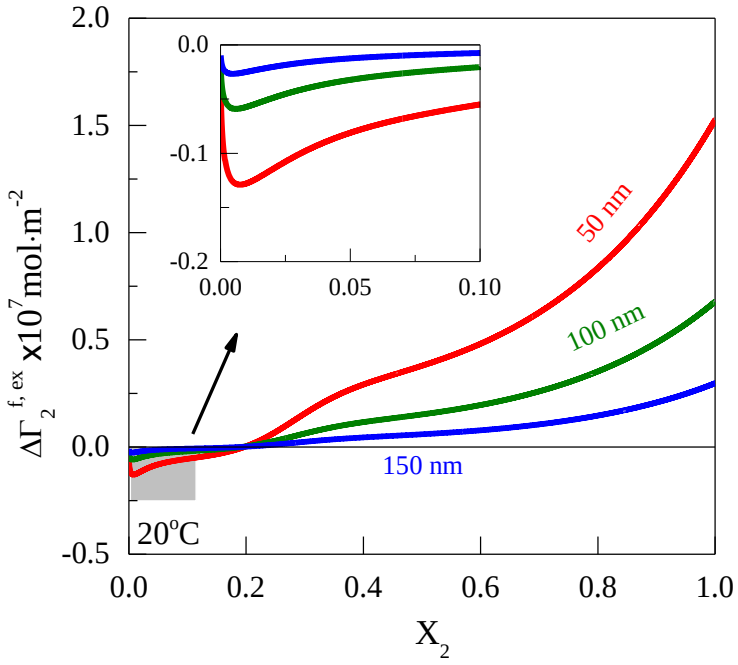

Figure 3.8 Film excess of ethanol for a film of a given thickness, h (= 50nm, 100nm and 150 nm, respectively), minus the film excess of ethanol for a film of large thickness plotted vs the ethanol mole fraction at 20ºC. The insets are magnifications of the low ethanol mole fraction region, showing minima around $x_2 \approx 0.01$.

nature of the hydrocarbon-water interface taking place in this narrow regime, from a constrained to a softer and more flexible structure of the interfaces involved.

3.5 Summary and conclusion

AFM force measurements have been conducted at different temperatures using hydrophobized gold surfaces submerged in ethanol-water mixtures. Relatively large and long-ranged solvophobic forces have been observed, in particular for pure water and pure ethanol. Our analysis of the force data generated supports the notion (originally due to Derjaguin and Churaev) that the solvophobic force arising in a confined space generally results in (weak) structuring of the liquid film. Broadly speaking, there is a fair agreement with the Marcelja-Radic approach to treating thin liquid films modified to account for the solvophobic surface force case.

The data collected also indicate that the addition of minor amounts of ethanol to pure water will have a vast reconstructive effect of the hydrocarbon/water interface and the vicinal liquid. These include increased population of free (dangling) OH groups due to the adsorption of ethanol with inverse orientation on hydrophobic surfaces and the "melting" of the interfacial liquid structure at close proximity. The forces recorded for pure ethanol is astonishingly strong but is not, however, drastically diminished upon adding water. Likewise, the strong hydrophobic force observed in pure water decays fast upon adding a small amount of ethanol. These results suggest that structuring of H-bonded liquids in the vicinity of hydrophobic surfaces is hampered in the presence of a foreign solute. The solvophobic forces recorded show a minimum value for an ethanol mole fraction about 0.2, *i.e.* close to where there is a maximum of the surface excess of

ethanol. The ethanol molecules would adsorb at the hydrophobic surface/solution interface with inverse orientation, diminishing surface solvophobicity (or hydrophobicity) and hence the solvophobic force.

3.6 References

1 Eriksson, J. C., Ljunggren, S. & Claesson, P. M. A Phenomenological Theory of Long-Range Hydrophobic Attraction Forces Based on a Square-Gradient Variational Approach. *J. Chem. Soc. Farad. T. 2* **85**, 163-176 (1989).

2 Wang, J. L., Yoon, R. H. & Eriksson, J. C. Excess thermodynamic properties of thin water films confined between hydrophobized gold surfaces. *J. Colloid Interface Sci.* **364**, 257-263 (2011).

3 Considine, R. F. & Drummond, C. J. Long-range force of attraction between solvophobic surfaces in water and organic liquids containing dissolved air. *Langmuir* **16**, 631-635 (2000).

4 Wang, J. L., Li, Z. L., Yoon, R. H. & Eriksson, J. C. Surface forces in thin liquid films of n-alcohols and of water-ethanol mixtures confined between hydrophobic surfaces. *J. Colloid Interface Sci.* **379**, 114-120 (2012).

5 Li, Z. & Yoon, R.-H. Thermodynamics of Solvophobic Interaction between Hydrophobic Surfaces in Ethanol. *Langmuir* **30**, 13312-13320 (2014).

6 Butler, J. & Wightman, A. 293. Adsorption at the surface of solutions. Part I. The surface composition of water–alcohol solutions. *J. Chem. Soc.*, 2089-2097 (1932).

7 Israelachvili, J. & Pashley, R. The hydrophobic interaction is long range, decaying exponentially with distance. *Nature* **300**, 341-342 (1982).

8 Hammer, M. U., Anderson, T. H., Chaimovich, A., Shell, M. S. & Israelachvili, J. The search for the hydrophobic force law. *Faraday Discuss.* **146**, 299-308 (2010).

9 Meyer, E. E., Rosenberg, K. J. & Israelachvili, J. Recent progress in understanding hydrophobic interactions. *Proc. Natl. Acad. Sci.* **103**, 15739-15746 (2006).

10 Christenson, H. K. & Claesson, P. M. Direct measurements of the force between hydrophobic surfaces in water. *Adv. Colloid Interface Sci.* **91**, 391-436 (2001).

11 Fuerstenau, M. C., Jameson, G. J. & Yoon, R.-H. *Froth flotation: a century of innovation*. (SME, 2007).

12 Eriksson, J. C. & Yoon, R. H. in *Colloid Stability: The Role of Surface Forces-Part I, Volume 1* (ed Tharwat F. Tadros) Ch. 5, 99-131 (Wiley-VCH, 2007).

13 Boinovich, L. & Emelyanenko, A. in *Colloid Stability: The Role of Surface Forces-Part I, Volume 1* (ed Tharwat F. Tadros) Ch. 6, 133-159 (Wiley-VCH, 2007).

14 Attard, P. Nanobubbles and the hydrophobic attraction. *Adv. Colloid Interface Sci.* **104**, 75-91 (2003).

15 Kralchevsky, P. A. Conditions for stable attachment of fluid particles to solid surfaces. *Langmuir* **12**, 5951-5955 (1996).

16 Ryan, W. L. & Hemmingsen, E. A. Bubble Formation in Water at Smooth Hydrophobic Surfaces. *J. Colloid Interface Sci.* **157**, 312-317 (1993).

17 Eriksson, J. C. Thermodynamics of surface phase systems: V. Contribution to the thermodynamics of the solid-gas interface. *Surf. Sci.* **14**, 221-246 (1969).

18 Eriksson, J. C. & Henriksson, U. Thermodynamic surface properties of single crystal faces of xenon calculated by employing the Einstein model of crystalline solids. *Colloid J.* **74**, 186-193 (2012).

19 Derjaguin, B. Untersuchungen über die Reibung und Adhäsion, IV. *Kolloid Z.* **69**, 155-164 (1934).
20 Derjagui.Bv & Churaev, N. V. Structural Component of Disjoining Pressure. *J. Colloid Interface Sci.* **49**, 249-255 (1974).
21 Israelachvili, J. Solvation Forces and Liquid Structure, as Probed by Direct Force Measurements. *Acc. Chem. Res.* **20**, 415-421 (1987).
22 Chen, H. *et al.* Determination of structure and energetics for Gibbs surface adsorption layers of binary liquid mixture 1. Acetone + water. *J. Phys. Chem. B* **109**, 8053-8063 (2005).
23 Marcelja, S. & Radic, N. Repulsion of Interfaces Due to Boundary Water. *Chem. Phys. Lett.* **42**, 129-130 (1976).
24 Binder, K. & Landau, D. Finite-size scaling at first-order phase transitions. *Physical Review B* **30**, 1477 (1984).
25 Besseling, N. A. M. Theory of hydration forces between surfaces. *Langmuir* **13**, 2113-2122 (1997).
26 Teschke, O. & de Souza, E. Water molecule clusters measured at water/air interfaces using atomic force microscopy. *PCCP* **7**, 3856-3865 (2005).
27 Wernet, P. *et al.* The structure of the first coordination shell in liquid water. *Science* **304**, 995-999 (2004).
28 Huang, C. *et al.* The inhomogeneous structure of water at ambient conditions. *Proc. Natl. Acad. Sci.* **106**, 15214-15218 (2009).
29 Huang, C. *et al.* Reply to Soper et al.: Fluctuations in water around a bimodal distribution of local hydrogen-bonded structural motifs. *Proc. Natl. Acad. Sci.* **107**, E45-E45 (2010).
30 Eriksson, J. C. & Henriksson, U. Bridging-cluster model for hydrophobic attraction. *Langmuir* **23**, 10026-10033 (2007).
31 Eriksson, J. C. & Henriksson, U. Thermodynamic Properties of Bridging Clusters in Thin Films of Water between Hydrophobic Surfaces Assessed from Surface Force Isotherms. *Langmuir* **29**, 4789-4795 (2013).
32 Miklavic, S. J., Chan, D. Y. C., White, L. R. & Healy, T. W. Double-Layer Forces between Heterogeneous Charged Surfaces. *J. Phys. Chem.* **98**, 9022-9032 (1994).
33 Hogg, R., Healy, T. W. & Fuerstenau, D. W. Mutual coagulation of colloidal dispersions. *Trans. Faraday Soc.* **62**, 1638-1651 (1966).
34 Dalmolin, I. *et al.* Solubility of carbon dioxide in binary and ternary mixtures with ethanol and water. *Fluid Phase Equilib.* **245**, 193-200 (2006).
35 Kappl, M. & Butt, H. J. The colloidal probe technique and its application to adhesion force measurements. *Part. Part. Syst. Char.* **19**, 129-143 (2002).
36 Raiteri, R., Preuss, M., Grattarola, M. & Butt, H. J. Preliminary results on the electrostatic double-layer force between two surfaces with high surface potentials. *Colloids and Surf. A: Physicochemical and Engineering Aspects* **136**, 191-197 (1998).
37 Pan, L., Jung, S. & Yoon, R. H. Effect of hydrophobicity on the stability of the wetting films of water formed on gold surfaces. *J. Colloid Interface Sci.* **361**, 321-330 (2011).
38 Li, Z. & Yoon, R.-H. AFM force measurements between gold and silver surfaces treated in ethyl xanthate solutions: Effect of applied potentials. *Miner. Eng.* **36–38**, 126-131 (2012).
39 Ederth, T. Substrate and solution effects on the long-range "hydrophobic" interactions between hydrophobized gold surfaces. *J. Phys. Chem. B* **104**, 9704-9712 (2000).
40 Aratono, M. *et al.* Thermodynamic study on the surface formation of the mixture of water and ethanol. *J. Colloid Interface Sci.* **191**, 146-153 (1997).

41 Tyrode, E., Liljeblad, J., Kumpulainen, A. & Eriksson, J. C. (To be published).
42 Atkins, P. W. *Physical Chemistry*. 8th edn, 137 (Oxford, 2006).

CHAPTER 4.
Hydrophobic Forces in the Wetting Films of Water formed on Gold Surfaces Hydrophobized with KEX and KAX

4.1 Abstract

Surface force measurements have been measured in the wetting films of water formed on gold using the force apparatus for deformable surface (FADS). The measurements are conducted by controlling the hydrophobicity of the gold plates with potassium ethyl xanthate (KEX) and potassium amyl xanthate (KAX). The measurement involves recoding the thickness of the wetting films as a function of time, which is accomplished by recording the optical fringes generated during film thinning by means of a high-speed camera. By plotting the film thicknesses across the cross sectional area of a wetting film, one obtains spatiotemporal film profiles. By analyzing the film profiles, it is possible to determine the disjoining pressure in the wetting film as a function of film thickness using the method developed by Pan et al. (2011)

From the disjoining pressures determined in this manner, the surfaces forces present in the wetting films have been determined. If the van der Waals and double-layer forces are known, one can then determine the contributions from the hydrophobic forces to the disjoining pressure in the film. Depending on the type of xanthate and the electrochemical potentials at which the gold surface electrodes are polarized, the magnitudes of the hydrophobic forces varied. The measured forces can be fitted to an exponential force law with the pre-exponential parameter, C, varying from 0.5 to 1.5 mN/m, while the decay lengths, D, varying from 35 to 50 nm. Both the C and D parameters vary in consonance to the contact angles (θ) measured under controlled potential conditions. Thus, the FADS can be used to study the effects of electrochemical potentials on sulfide minerals flotation. It appears that FADS is a more sensitive tool to detect the effect of chemical conditions on flotation than the traditional contact angle measurement. Furthermore, the FADS data can be used to predict flotation kinetics, while contact angle is a thermodynamic property.

4.2 Research Background

Wetting films are very important both in our daily lives and industry applications, such as flotation, coatings, corrosion, inkjet printing, heat transfer, nanoscale engineering, medicine, carbon storage, enhanced oil recovery with CO_2, detergency, particle suspension, [1-6]. The topic has been the focus of extensive research for over forty years. Related topics, such as the stability of attachment, film thinning kinetics and the deformation of an air bubble approaching hydrophobic/hydrophilic surfaces, have also been studied.[7-10]

Interaction between an air bubble and a solid surface that occurs in flotation is very complicated as it involves both hydrodynamic and surface forces. The latter include the double-layer, dispersion and hydrophobic forces.[11] The asymmetric properties of the air bubble and solid made it more difficult to analyze as compared to the symmetric properties in colloidal interactions. When an air bubble meets a particle in a flotation cell, the bubble deforms and form a thin liquid film (TLF) or wetting film on the particle surface. The curvature change creates an excess pressure, which causes the film to thin. As the film thins approximately below 300 nm, the film thinning is

controlled by the disjoining pressure created by the surface forces. It has been suggested that hydrophobic force facilitates film thinning and eventually cause the film to rupture.[12]

Many investigators attempted to measure surface forces in the wetting films formed during bubble-particle interactions using AFM[9,13,14] and a modified thin film pressure balance (MTFPB).[7,8] All of these studies have a consistent conclusion: the TLFs formed on the surface of hydrophobic mica or gold thin spontaneously, while those on hydrophilic surfaces form stable films that do not rupture. However, there are some different viewpoints regarding the distance range of the hydrophobic force and the magnitudes. Shi et al.[9,13] reported the decay length to be 0.8-1.0 nm in a 0.5 M NaCl solution. The results obtained at Virginia Tech show both short- and long-range hydrophobic forces with decay lengths in the range of 2.3 and 36 nm.[7,8] Wetting film will rupture when the disjoining pressure gradient is positive and disjoining pressure is negative, *i.e.*, $\partial\Pi(h)/\partial h > 0$ and $\Pi(h) < 0$. Film thinning is driven by the hydrodynamic (or excess) pressure as has already been noted. When hydrodynamic pressure exceeds the energy barrier created by the surface forces, the film should rupture spontaneously. Hydrodynamic pressure decreases with decreasing film thickness due to the increasing double-layer force. Thus, the kinetics of film thinning in wetting films is critically dependent on surface forces.

In this chapter, the kinetics of film thinning has been studied in view of the surface forces or disjoining pressures in wetting films. The force measurements are conducted using the force apparatus for deformable surface (FADS) with the wetting films formed on gold. The gold surfaces were hydrophobized with two different flotation collectors, i.e., potassium amyl xanthate (KAX) and potassium ethyl xanthate (KEX). The results will be useful for better understanding the kinetics of bubble-particle interaction in flotation. The FADS has been developed at Virginia Tech.

4.3 Force Apparatus for Deformable Surfaces

4.3.1 Device introduction

Figure 4.1 shows the scheme of force apparatus of deformable surface (FADS), recently developed in Virginia Tech. An air bubble about 2 mm radius is stabilized in the center of the cell. The liquid confined between two quartz plates is replaceable. During wetting film experiments, one plate will be driven moving toward another plate with a speed of setting value, controlled by a micro piezo. When the air bubble and substrate come close, the air bubble will deform, the shape of which is dependent on separation distance, substrate surface properties and medium composition and so on. As the substrate approaches the air bubble, interference patterns forms due to optical interferences at curved air/water interface. These interference patterns are be recorded by a high speed camera,, as shown in Figure 4.2. These interference patterns are called Newton rings fringes. The profile of the wetting film gives the separation distance between bubble and substrate, $h(r,t)$. The shape of the wetting film varies with both the capillary and surface forces in the TLFs. The surface forces in turn varies with the surface properties of the substrate. On hydrophilic surface, the TLF is stabilized at an equilibrium thickness (h_e), where the capillary force and the surface forces are balanced. On a hydrophobic surface, the surface force becomes attractive due to the hydrophobic force and ruptures, forming a finite contact angle.

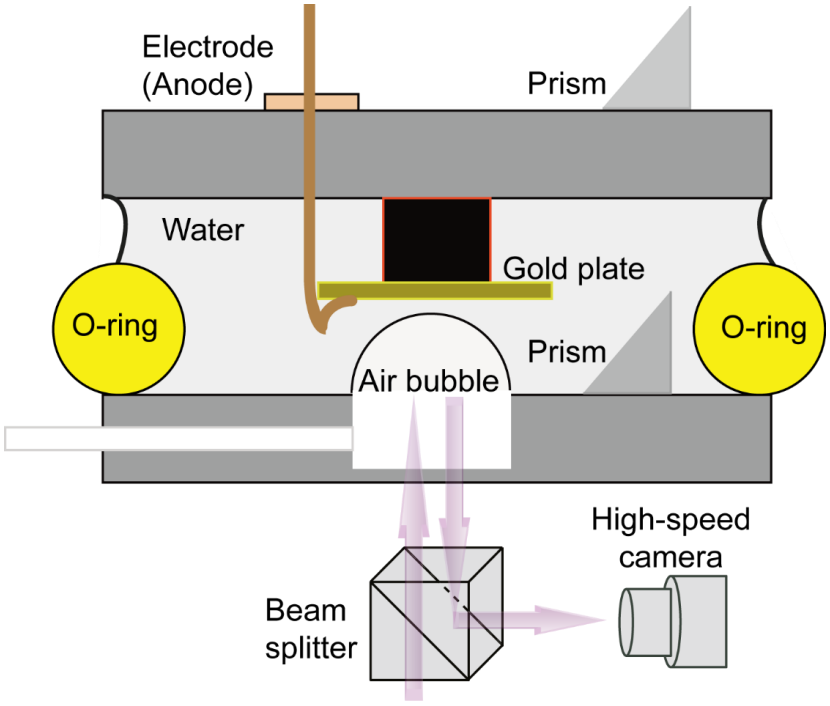

Figure 4.1 Scheme of force apparatus of deformable surface (FADS) developed in Virginia Tech. An air bubble about 2 mm radius is stabilized in the center of the cell. After the gold plate is hydrophobized and mounted on the upper plate, the lower plate is driven to move upward, controlled by a piezo. The camera recorded the interference pattern, which contains the information of the thickness *h(r,t)*, of the water film confined between air bubble and plate.

4.3.2 Calculation of Air Bubble Profile

When hundreds of interference patterns are recorded with a high speed camera, the bubble and substrate separation distance, *h(r,t)*, will be calculated from those interference patterns, by applying the micro-interferometric method developed by Scheludko and Exerowa[15] and improved by Michail[16], with the following equation:

$$h = \frac{\lambda}{2\pi n_2}\left(\frac{2m+1}{2}\pi - \frac{\delta}{2} \pm \arcsin \sqrt{\frac{\Delta}{1+4(1-\Delta)\dfrac{\sqrt{R_{12}R_{23}}}{\left(1-\sqrt{R_{12}R_{23}}\right)^2}}} \right) \qquad [4\text{-}1]$$

$$\text{Where } \Delta = \frac{I - I_{min}}{I_{max} - I_{min}} \qquad [4\text{-}2]$$

Here, m=0, 1, 2, 3… determines the order of interference, I_{min} and I_{max} are the minimum and maximum intensities of interfered light, respectively, and

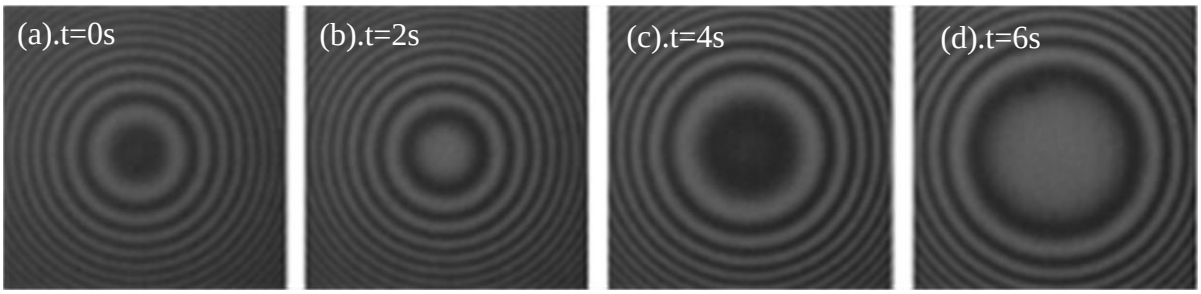

Figure 4.2 Newton ring fringes recorded by force apparatus of deformable surface (FADS). The light intensity variation is due to the interference of light reflected from air bubbles and the surface of substrates. These images are further analyzed to generate the profile of the air bubble s, *h(r,t)*.

$$R_{12} = \frac{(n_1 - n_2)^2}{(n_1 + n_2)^2} \text{ and } R_{23} = \frac{(n_2 - n_3)^2}{(n_2 + n_3)^2} \qquad [4\text{-}3]$$

δ equals 0 if $n_3 > n_2 > n_1$, δ equals π if $n_2 > n_3 > n_1$.

However, if the substrate is gold or other metals, the refractive indices will be in complex form rather than a real number, *e.g.* $n_3 = 0.3054 + 2.3391i$ for gold when the wavelength is 546nm[17]. Thus the adsorption induced phase shift term should be considered in the wetting film carried out on metal surfaces. In other words, δ might be some other values between 0 and π. And the definition of Δ and R_{12} should be expressed in a complex function. The expression of Eq. [4-1] should also be extended to complex refractive index situation.

By applying the same concept of Scheludko et al. and the fundamental treatment method of light adsorption terms, the equation capable for calculating all substrates can be derived directly from the Fresnel' equations, taking the refractive indices as a complex form. The equation I derived applicable for all substrates can be expressed as:

$$h(r,t) = \frac{\lambda}{2\pi n_2}\left(m\pi \pm ar\sin\sqrt{\frac{\Delta}{1 + 4(1-\Delta)\|\rho\|/(1-\|\rho\|)^2}} + \frac{\theta}{2} \right) \qquad [4\text{-}4]$$

where

$$\rho = r_{21}r_{23} = \frac{n_2 - n_1}{n_2 + n_1}\frac{n_2 + n_3}{n_2 + n_3} = \|\rho\| exp\{i\theta\} \qquad [4\text{-}5]$$

and $\theta = \text{angle}(\rho)$

It is very easy to verify that Equation [4-4] will become Eq. [4-1] in the case of real n_2 data. Equation [4-4] has taken the half-wave losses into consideration, which makes it easier for computer coding to realize.

By applying this equations, the film thickness profiles, *h(r,t)*, or the spatiotemporal film profiles can be obtained from these interference patterns, which in turn will be used for the

calculation of disjoining pressure in the wetting films confined between air bubble and gold substrates.

4.3.3 Theoretical Mode to Calculate Disjoining Pressure

In the system of air-water-hydrophobized solid interaction, extended DLVO is valid and the total disjoining pressure is contributed by the pressure of van der Waals force(Π_d), double layer electrical forces (Π_e), and hydrophobic forces (Π_h),

$$\Pi = \Pi_e + \Pi_d + \Pi_h \qquad [4\text{-}6]$$

Pressures contributed by van der Waals force and double layer electrical forces can be calculated from the expressions shown in Eqs. [1-2] and [1-15]. The pressure contributed by van der Waals force can be derived as[7],

$$\Pi_d = -\frac{A_{132}}{6\pi h^3} \qquad [4\text{-}7]$$

Where A_{132} is Hamaker constant and h is the closest separation distance of air bubble and substrate. The pressure contributed by electrical double layer forces can be expressed as,[7]

$$\Pi_e = -\frac{\xi\varepsilon\kappa^2}{2\sinh(\kappa h)}\left[\left(\psi_1^2+\psi_2^2\right)csc\,h(\kappa h) - 2\psi_1\psi_2\coth(\kappa h)\right] \qquad [4\text{-}8]$$

Where ψ_1 and ψ_2 are the surface potentials on the air /water interface and water/substrate interface; κ is the Debye length; h is the separation distance of air bubble and substrate; $\zeta\varepsilon$ is the dielectric permittivity of water. Both pressures contributed by van der Waals force and electrical force are positive, and there should be an attractive force present to make the disjoining pressure negative. Disjoining pressure raised from the hydrophobic force can be written as the following,

$$\Pi_h = -\frac{C}{2\pi D}exp\left(-\frac{h}{D}\right) \qquad [4\text{-}9]$$

Where *C* is a fitting parameters regarding the interfacial tension of gold and water, *D* is the decay length, and *h* is the separation distance of the air bubble and substrate.

The process of film drainage is driven by disjoining pressure, hydrodynamic pressure and curvature pressure with following relation,[7,9,13]

$$\Pi = p_{cur} - p \qquad [4\text{-}10]$$

Where Π is disjoining pressure, p_{cur} is curvature pressure and p is hydrodynamic pressure.

Curvature pressure can be calculated from the geometry of the air bubble and liquid interaction with the following expression,

$$p_{cur} = \frac{2\gamma}{R} - \frac{\gamma}{r}\frac{\partial}{\partial r}\left(r\frac{\partial h}{\partial r}\right) \qquad [4\text{-}11]$$

Hydrodynamic pressure can be calculated by using lubrication approximation, since the system fulfilled the requirements of the conditions as low Reynolds number flow. The relations of wetting film thickness and the pressure between them have the following relations,

$$\frac{\partial h}{\partial t} = \frac{1}{12\mu}\frac{\partial}{r\partial r}\left(rh^3\frac{\partial p}{\partial r}\right) \qquad [4\text{-}12]$$

Where, p is the pressure between the wetting film and μ is viscosity of liquid confined, r is the radial coordinate of the air bubble.

With some transformation and applying boundaries, the kinetics contribution to the disjoining pressure can be derived as,[8]

$$p = 12\mu\int_{r=\infty}^{r}\frac{1}{rh^3}\left[\int_{r=0}^{r} r\frac{\partial h}{\partial t}dr\right]dr \qquad [4\text{-}13]$$

Substituting Eqs. [4-13] and [4-11] into Eq. [4-10], the disjoining pressure can be calculated from the expression of *h(r,t)*, obtained in the previous section from the Newton ring images,

$$\Pi = \frac{2\gamma}{R} - \frac{\gamma}{r}\frac{\partial}{\partial r}\left(r\frac{\partial h}{\partial r}\right) - 12\mu\int_{r=\infty}^{r}\frac{1}{rh^3}\left[\int_{r=0}^{r} r\frac{\partial h}{\partial t}dr\right]dr \qquad [4\text{-}14]$$

The function provides a good approximation to calculate the disjoining pressure of the wetting film system.

If the above measured/calculated disjoining pressure is compared with the theoretical value from [4-6] , the *C* and *D* parameter can be fitted with proper system parameters.

4.4 Methods and Materials

4.4.1 Materials

Gold substrates were prepared by depositing 100 nm gold thin film on silicon surface with Electron Beam Physical Vapor Deposition (EBPVD) system, PVD 250. Then, the fresh made gold substrates were cleaned in piranha solutions (7:3 by volume of H_2SO_4/H_2O_2) for 10 minutes, rinsed by DI water (Nanopure, 18.2MΩ) and dried by ultrapure N_2 gas (Air gas) flow.

The hydrophobizing agent used was potassium ethyl xanthate ($C_2H_5OCS_2^-K^+$, KAX, >90%, TCI America) and potassium amyl xanthate ($C_5H_{11}OCS_2^-K^+$, KEX, >90%, TCI America). Before coated onto gold, they were recrystallized twice using HPLC grade acetone (Fisher Scientific, Inc.) and diethyl ether (99.99%, Sigma-Aldrich, Inc.) following the method used by Pan et al.[12] and Li et al.[18] Then KAX/KEX aqueous solution were prepared and then adjusted to 9.2 by adding 0.05 M sodium tetraborate decahydrate ($Na_2B_4O_7$, Sigma-Aldrich Inc.)

4.4.2 Cyclic Voltammogram and Electrochemical Reaction

Cyclic voltammogram was carried out in potentiostat (Model 273A, EG&G, Princeton Applied Research). Before electrochemical reaction, KAX/KEX aqueous solution (pH 9.2) and

$Na_2B_4O_7$ solution both were degassed by ultrapure nitrogen gas for 1 hour. The electrodes and substrates were first cleaned electrochemically by three rounds of cycle potential sweeps in 0.05 M $Na_2B_4O_7$ solution between -450 mV and 800 mV with a sweep rate of 20 mV/s, and then the solution was replaced by potassium amyl xanthate solution (pH 9.2) to obtain the cyclic voltammogram between -450 mV and 800 mV with a sweep rate of 20 mV/s.

When the Cyclic voltammogram was obtained, several selected potentials (200 mV to 70 mV) around the peak adsorption would be applied for surfactant and gold electrochemical reaction. The potentials were held for 2 minutes before adsorption of xanthate onto the gold reached equilibrium.

4.4.3 Contact Angle Measurement

After electrochemical reaction was finished, the substrate was moved into the cell of FADS for the film wetting experiment as soon as possible to avoid oxidization. The approaching speed of the air bubble was controlled at 0.5 μm/s. When the substrate was close to the substrate, the fringes patterns would form and be recorded by a high speed camera until the wetting film reached equilibrium or ruptured. The receding water contact angles were measured after the film ruptured and contacted with the substrate using an optical microscopy equipped in FADS.

4.5 Results and Discussion

4.5.1 Au-KEX

Figure 4.3 shows the voltammogram of gold in 0.05 M $Na_2B_4O_7$ (pH 9.2) solution with and without 10^{-3}M KEX between -450 mV and 850 mV. Sweep rate was controlled at $20mV \cdot s^{-1}$. At lower potential ranges, the charges in both curves are due to the adsorption and desorption of hydrogen. At high potentials larger than 0mV and when there is no KEX present, gold substrate will be oxidized and form some gold oxides during the anode scan and these oxides will be reduced during the cathodic scan. However, the oxidization process will be inhabited when there are KEX in the aqueous solution. The cyclic voltammogram with 10^{-3} M KEX shows an adsorption peak, which does not show in the curve without KEX. There are reports that the adsorption of KEX onto gold begins as low as -0.4 V[19]. But when the applied potential reaches about 130 mV, the adsorbed xanthate ions begin to be oxidized and form ethyl dixanthogen. This is consistent with those reported by Yoon[18], Talonen[19] and Woods[20]. The process of formation of diethyl dixanthogen, can be described as the following, according to Woods[20],

$$2C_2H_5OCS_2^- \rightarrow (C_2H_5OCS_2)_2 + 2e^- \qquad [4\text{-}15]$$

Whose E^o=-60 mV[21]. The reversible potential is 117 mV when the concentration is 10^{-3} M at 298K. This is close to the value observed in the voltammogram shown in Figure 4.3. More and more dixanthogen was formed on the gold surface afterwards, and the charge reached maximum when the potential was about 460 mV. After that, the charge began to decrease, and a multilayer of ethyl dixanthogen formed on top of the first monolayer. The large cathodic peak observed at 400 mV is because of the reduction of dixanthogen, which requires a large overpotential.[22] This large overpotential ensures the measurement of disjoining pressure in water applicable since the formed dixanthogen will be stable in water. Besides, the solubility of dixanthogen is also very small, which is only 1.14×10^{-5} M.[23] The products of electrochemical reaction above have been confirmed in-situ FTIR spectroscopy.[19,22]

Figure 4.4 shows the disjoining pressures measured in pure water between gold substrates and air bubbles, treated in 10^{-3} M KEX solution for 2 min under different applied potentials. After reaction, the gold plate is quickly put into FADS for wetting film measurement to avoid exposure. When there was no KEX adsorbed on gold substrate, only repulsive force could be observed in the wetting film as shown in Figure 4.4. However, when the surfaces of gold were hydrophobized, negative disjoining pressures were present, which were stronger than van der Waals forces. The decay length of these pressures measured were between 40 to 55 nm.

Among the potential range of 200 mV~ 450 mV, the magnitude of the disjoining pressures increase with the increase of applied potential, indicating a better hydrophobicity at higher applied potential. The receding water contact angles was measured in-situ after the wetting film ruptured, as shown in Figure 4.5. The result also confirms the increase of gold surface hydrophobicity at higher potential, as the value of water contact angle is larger. According to analysis of the voltammogram, this is the process of ethyl dixanthogen formation. More and more ethyl dixanthogen will be adsorbed on the gold surface at higher potential and will form a relative well-ordered monolayer at an applied potential of 460 mV.

However, it is surprising, the disjoining pressure decreased if the gold surfaces were hydrophobized at a higher electrical potential. When the wetting film thickness is 100 nm, the disjoining pressure decreased from 1750 Pa to 250 Pa, as the potential increased from 450 mV to 650 mV. At the same time, the receding water contact angle is also decreasing from 65º to 45º. The decrease of water contact angle stands for the decrease of surface hydrophobicity. Thus, it is evident that the disjoining pressure depends on the surface hydrophobicity. In other words, the

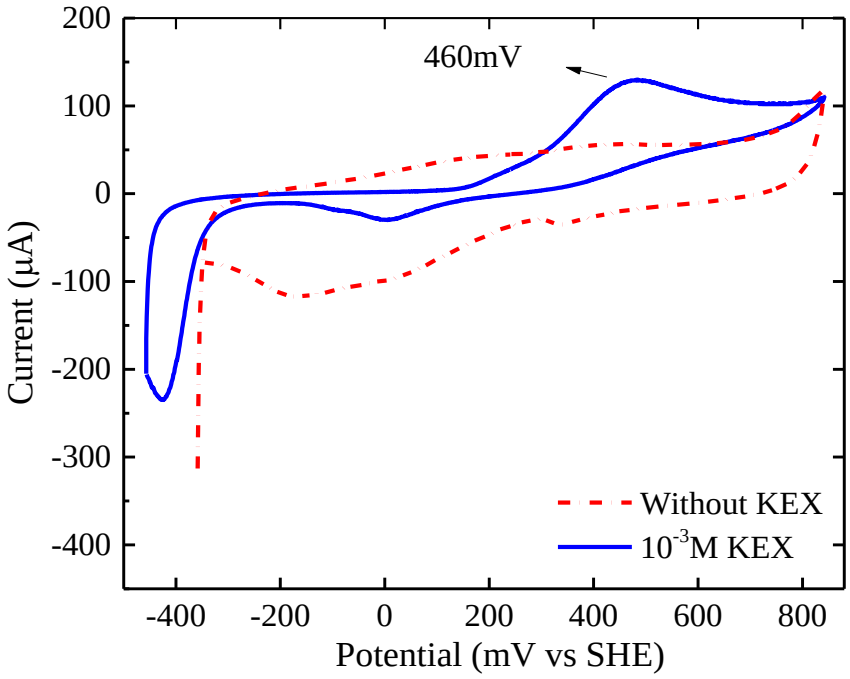

Figure 4.3 Voltammogram of gold in 0.05 M $Na_2B_4O_7$ (pH 9.2) solution with and without 10^{-3} M KEX. Sweep rate was 20 mV·s^{-1}. The adsorption peak of KEX is about 450 mV.

disjoining pressures measured in the present work depends on surface hydrophobicity rather than the artificial of nanobubbles.

As demonstrated previously, multilayers of ethyl dixanthogen forms on top of the monolayer. When ethyl dixanthogen forms multilayer, potassium ethyl xanthate molecules will be present with the hydrophilic head facing toward bulk water. This molecular level arrangement will reduce the gold surface hydrophobicity, resulting in smaller disjoining pressure measured.

Single exponential hydrophobic law was used to derive the disjoining pressure expression shown in Equation [4-9],

$$\frac{F}{R} = -C\,exp\left(-\frac{h}{D}\right) \qquad [4\text{-}16]$$

Combining Equations [4-6]~[4-10] and the disjoining pressures shown in , non-DLOV fitting results can be obtained by changing *C* and *D* values to match curves shown. The fitting results of *C* and *D* were shown in Figure 4.5. Long range hydrophobic interactions were present. The *C* and *D* values have maximum values when the applied potential is about 450 mV, which is consistent

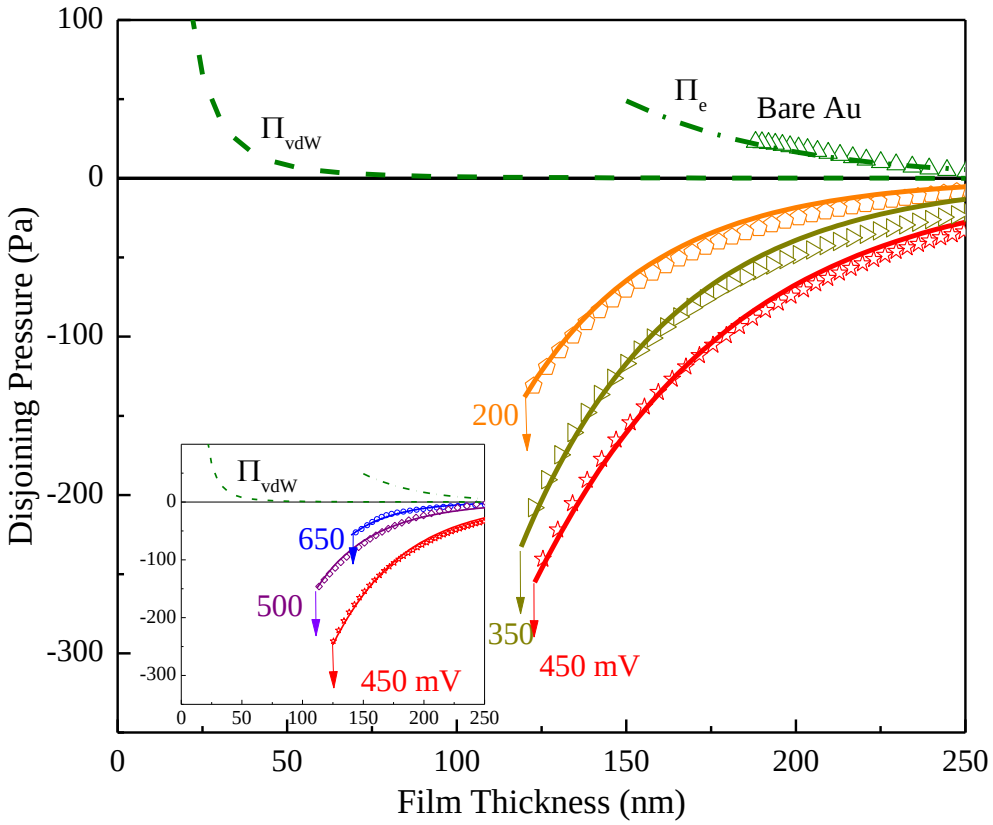

Figure 4.4 Disjoining pressure in pure water between gold coated substrates and probe, treated in 10^{-3} M KEX solution for 2 min at different potentials. Sample of pure gold is measured without KEX treatment. Dash line represents the pressure contributed by van der Waals force and Hamaker constant used here is 1.2×10^{-20} J.

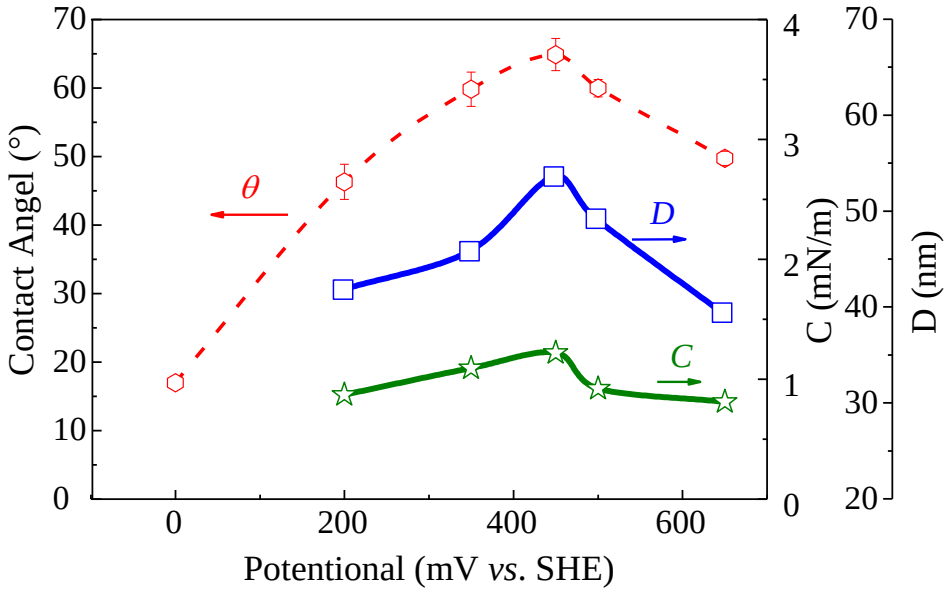

Figure 4.5 Effect of applied potentials on the receding water contact angles and the *C* and *D* constants of the hydrophobic law. The water contact angles were measured directly in the FADS after the wetting film rupture. And the *C* and *D* constants are obtained by fitting with exponential law.

with the water contact angle and disjoining pressure obtained. Be aware that *C* and *D* values obtained in FADS are not close to those obtained by AFM in pure water.[24] This is acceptable since AFM is measuring hydrophobic interactions between gold surfaces and FADS is between air bubbles and gold surfaces.

Figure 4.6 shows the spatiotemporal profiles of the wetting films formed between air bubble and hydrophilic and hydrophobic gold surfaces. Figure 4.6 (A) presents how the film profile changes during film thinning. The approach speed of the piezo was 500 nm/s. Note here that the film thinning velocity diminishes as the film becomes thinner, which can be attributed to hydrodynamic resistance and the repulsive surface force, i.e., double-layer repulsion. From t=5.6 s to 6.35 s, the film thinning velocity was ~250 nm/s. Film thinning stopped at an equilibrium thickness of 180 nm, where the capillary and surface force forces are equal in magnitude. Figure 4.6 (C) shows repulsive disjoining pressure of this experiment and the DLVO theory is applied here. Figure 4.6 (B) is the spatiotemporal profiles an air bubble when it is moving towards hydrophobized gold surfaces. The spatiotemporal profiles are totally different from those observed on hydrophilic gold surface. Firstly, the air bubble will rupture instead of becoming stable when the bubble comes close to the hydrophobic surfaces of gold, and the film rupture distances are about 113.6 nm. Secondly, the kinetics of film thinning is faster on the hydrophobic surface than that on the hydrophilic surface. The average film thinning velocity is ~450 nm/s between t=5.47 s and 5.73 s. As compared to the case of hydrophilic gold surface, there should be some other attractive force existing in the TLFs of water formed on the hydrophobic gold surface, which drive the air bubble towards galena surfaces and trigger the air bubble rupture. We consider the force to be hydrophobic force. Extended-DLVO theory is applied to fit the data and the result is shown in Figure 4.6 (D). The disjoining pressure measured matches well with the theoretical curve. There

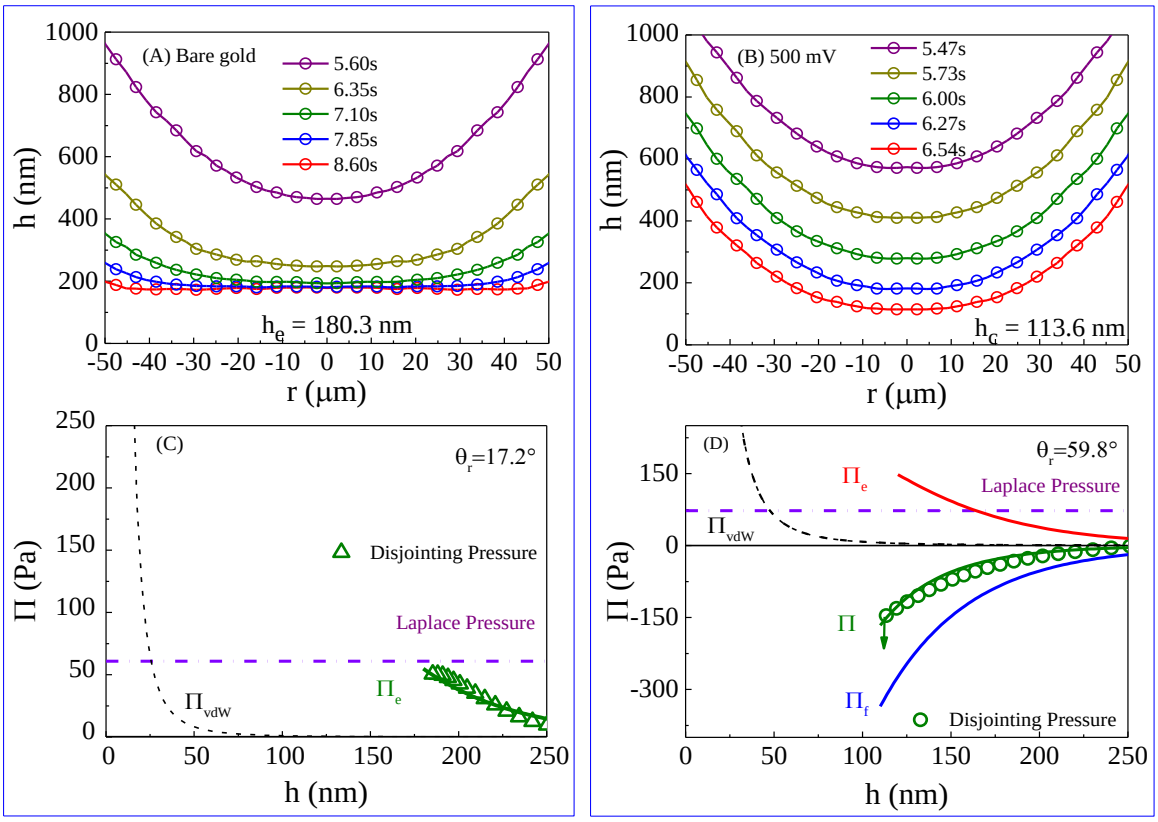

Figure 4.6 A and B show thin water film profile *h(r,t)* variation *vs. t*, during interactions between air bubbles and gold surfaces in pure water. A). An air bubble and fresh gold surface. B) An air bubble and fresh gold surface hydrophobized by KEX with applied potential of 500 mV for 2 minutes. h_{min} represents the thin water thickness before rupture (B) or reaching equilibrium (A). In (C) and (D), they show the variation components of the disjoining pressure with film thickness. Circles are disjoining pressures calculated from the water profile using lubrication approximation. (C) is fitting with DLVO theory and (D) is fitting with exponential function.

have been intensive debates on the origin(s) of the hydrophobic force. In this system, it might be due to the water structure changing and reorganizing on the hydrophobic surface.

From previous analysis, it has been shown that difference of the wetting film behavior between hydrophobic surface and hydrophilic surfaces. Negative disjoining pressure has been confirmed on hydrophobic surfaces, and the disjoining pressure calculated could be explained by extended-DLVO theory perfectly. Besides, the disjoining pressure on hydrophobic surfaces will also changes with gold surface hydrophobicity. It has been shown that the ethyl dixanthogen will adsorb onto gold surfaces and the surface hydrophobicity is different when under different applied potentials. Firstly, a well-orientated monolayer is formed. Afterwards, multilayer of dixanthogen will form on top of the monolayer when the applied potentials exceed 450 mV. At the same time, residual metal xanthate might also be present on the top of dixanthogen. The random orientation of dixanthogen and adsorbed metal xanthate may reduce the gold surface hydrophobicity,[25] and reduce the magnitude of disjoining pressures, which finally becomes too small to overcome the curvature pressure and rupture.

4.5.2 Gold-KAX System

Figure 4.7 shows cyclic voltammogram of gold in 0.05 M $Na_2B_4O_7$ (pH 9.2) solution with and without 10^{-3} M KAX. The sweep rate is 20 mV/s. The adsorption peak of KAX is about 465 mV when the concentration of KAX is 10^{-3} M. The curve without xanthate is the same as that shown in Figure 4.3. The voltammogram curve is similar as that in KEX, and the maximum change peak are both near 450 mV. Both dixanthogen (X_2) and gold xanthate (Au-AX) will form as oxidation product of amyl xanthate-gold reaction, :[26,27]

$$2X^- = X_2 + 2e^- \qquad [4\text{-}17]$$

Where X^- is xanthate ion, and the calculated reversible potential is close to 90mV for the condition used in this study.[26,28] The oxidization of amyl dixanthogen started at about 110 mV as show in Figure 4.7 and it was 100 mV as Mielczarski reported. These values can be considered as consistent. Unlike ethyl dixanthogen reduction reaction that took place at about 400 mV, amyl dixanthogen reduction had a larger overpotential than 400 mV, which indicates that adsorbed amyl dixanthogen is more stable than ethyl xanthate. As reported by Mielczarski,[26] amyl gold xanthate forms monolayer at lower applied potential and multilayer of dixanthogen formed at higher potential.

Figure 4.8 shows the disjoining pressure measured in pure water between air bubble and KAX adsorbed gold substrates. Before being transferred into FADS for wetting film measurement, the gold plate was hydrophobized in 10^{-4} M KAX aqueous solution under differently applied potentials: 200, 400, 450, 500 and 700 mV, and pH value was controlled at 9.2 by 0.05 M sodium tetraborate solution ($Na_2P_4O_7$). Similar to those gold surfaces coated with ethyl xanthate, the magnitude of

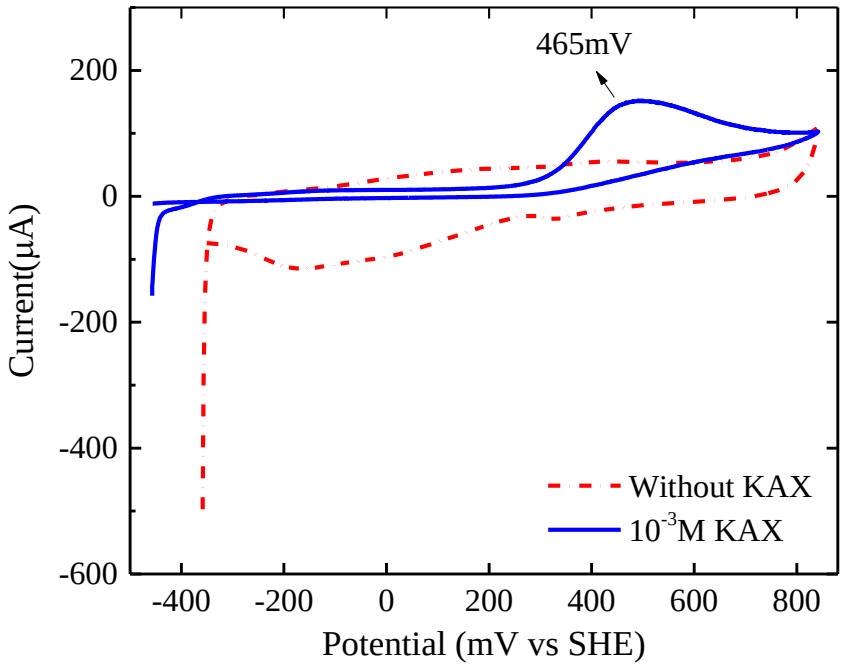

Figure 4.7 Voltammogram of gold in 0.05 M $Na_2B_4O_7$ (pH 9.2) solution with and without 10^{-3} M KAX. Sweep rate was 20 mV·s^{-1}. The adsorption peak of KAX is about 465 mV.

disjoining pressure measured also increased first and then decreased when the applied potential exceeded 450 mV.

Water contact angles are also measured in-situ after the film ruptured, the results of which are shown in Figure 4.9. Obviously, the variation trend is exactly the same as the disjoining pressure. This indicates that the change of disjoining pressure is due to the change of surface hydrophobicity, which is determined by the adsorption properties of amyl xanthate under specific applied electrical potentials. This is consistent with previous deduction that the magnitude of disjoining pressure is closely relate to the surface hydrophobicity. When the applied potential is 700 mV, the receding water contact angle is only about 20º. This value is close to the pure gold surface after cleaning, which is about 15º. When the applied potential is 450 mV, the water contact angle is about 62º. The magnitudes of the disjoining pressures measured in KEX and KAX solutions are different, which may be attributed to the differences in surface coverages. The adsorption mechanisms of KEX and KAX are also different, which is critical in determining surface coverages. As Miekzarski et al.[26] reported, metal ethyl xanthate will form on the metal surface up to a few monolayers. In the case of amyl xanthate, the metal xanthate is produced together with amyl dixanthogen at the beginning of xanthate adsorption. The surface of KAX-coated gold shows more

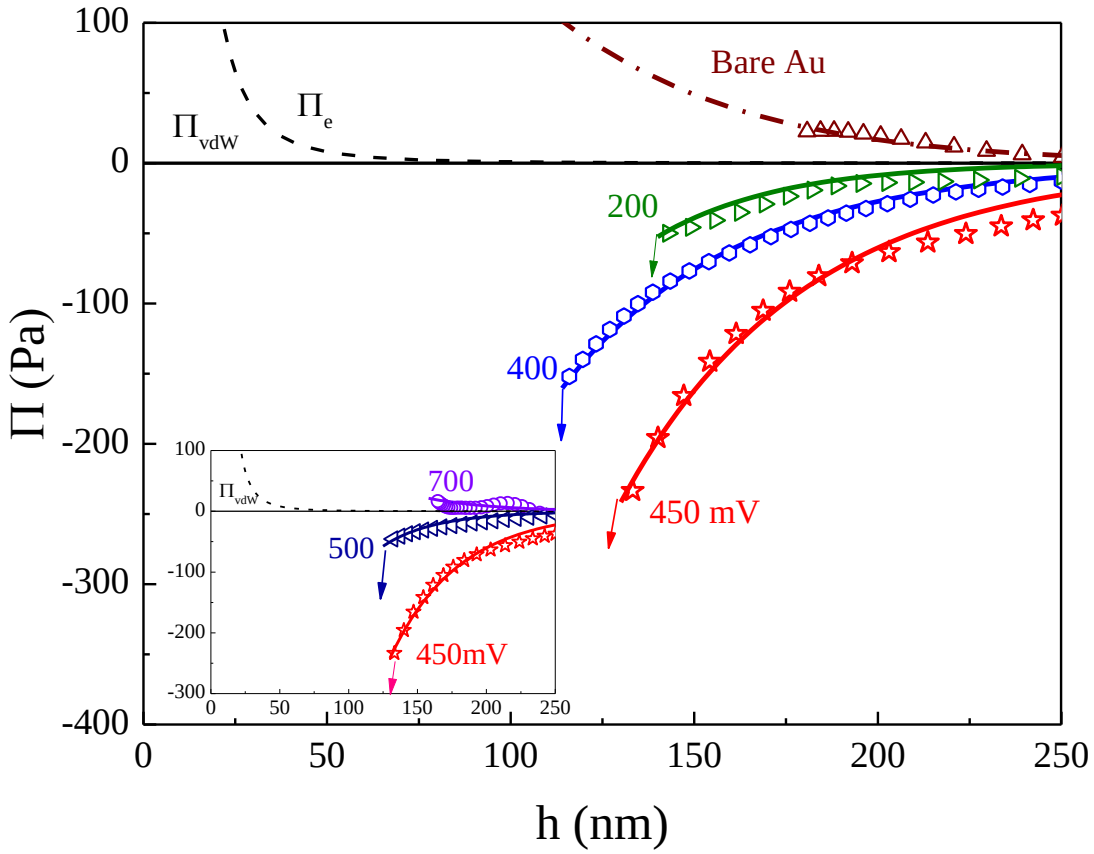

Figure 4.8 Disjoining pressure in pure water between gold coated substrates and probe, treated in 10^{-4} M KAX solution for 2 min at different potentials. Sample of pure gold is measured without KAX treatment. Dash line represents the pressure contributed by van der Waals force and Hamaker constant used here is 1.2×10^{-20} J.

disorder as compared to the KEX-coated gold surface. Thus, it is very possible that the surface hydrophobicity of KAX will be reduced comparison with that of the KEX case.

When the gold surface is free of amyl xanthate, only repulsive forces were present, contributed by the double layer forces and van der Waals forces. And, the DLVO theory fits the curve well if we apply the following parameters: surface potential of gold-alkyl/water surface 40.6 mV[24], surface potential of air-bubble/water 65 mV[29], and CO_2 concentration ~5×10^{-5} M. Thus these values were used for the fitting for all disjoining pressure data as a good approximation. Figure 4.9 shows the fitting result of *C* and *D* values by applying the extended-DLVO theory using Equations [4-6]~[4-10]. Exponential function is applied here and the fitting results match well with the experimental data. It could be seen from the fitting results that long range hydrophobic forces is present. *C* values of this long range force are varying between the range of 0.5 ~1.5 $mN\cdot m^{-1}$. This is close to those data obtained in gold/KEX system. The decay length of *D* is about 35 ~ 50 nm for long range forces. These values vary with the magnitude of disjoining pressure and water contact angle, which means that *C* and *D* parameters are dependent on surface hydrophobicity. From the images, we could see that the magnitude of water contact angle matches well with the *C* and *D* values, all of which have the same variation trend and have the largest value at about 450 mV.

Figure 4.10 (A) and (C) shows the spatiotemporal profile of the water film formed on the bare gold surface, in the same manner as shows in Figure 4.6 (A) and (C). Figure 4.10 (B) and (D) are the profiles formed on the gold surfaces coated with KAX at 500 mV for 2 minutes. The film thinning velocity was approximately 460 nm/s, which decreased as the film thinned, due to the resistance of hydrodynamic pressure and increased hydrophobic force. The disjoining pressure at

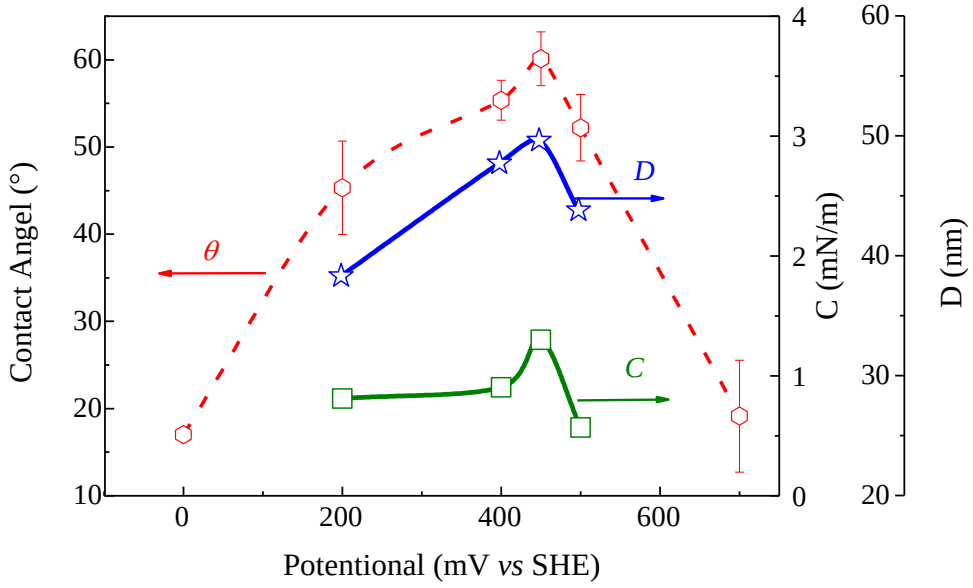

Figure 4.9 Effect of applied potentials on the receding water contact angles and the *C* and *D* constants of the hydrophobic law. The water contact angles were measured directly in the FADS after the wetting film rupture. And the *C* and *D* constants are obtained by fitting with exponential law.

a h = 130 nm was about 60 Pa. The dada were fitted to the extended-DLVO theory as shown in the figure. It has been shown that in the present work that both ethyl xanthate and amyl xanthate chemisorb on gold surfaces.

The results show that gold xanthate (Au-AX) and ethyl dixanthogen ($(AX)_2$) are formed on the surface of gold in a KAX solution, while ethyl dixanthogen is formed on gold in a KAX solution. The coverage of reaction products on gold surfaces will change as the applied potential varies, resulting in different surface hydrophobicity. The results show also that initially adsorbed xanthate and dixanthogen improve surface hydrophobicity. When multilayers form, the surface hydrophobicity decreases possibly due to the exposure of less hydrophobic elements such as oxygen and sulfur to the aqueous phase. Evidence for this was that disjoining pressures decreases at high electrochemical potentials.

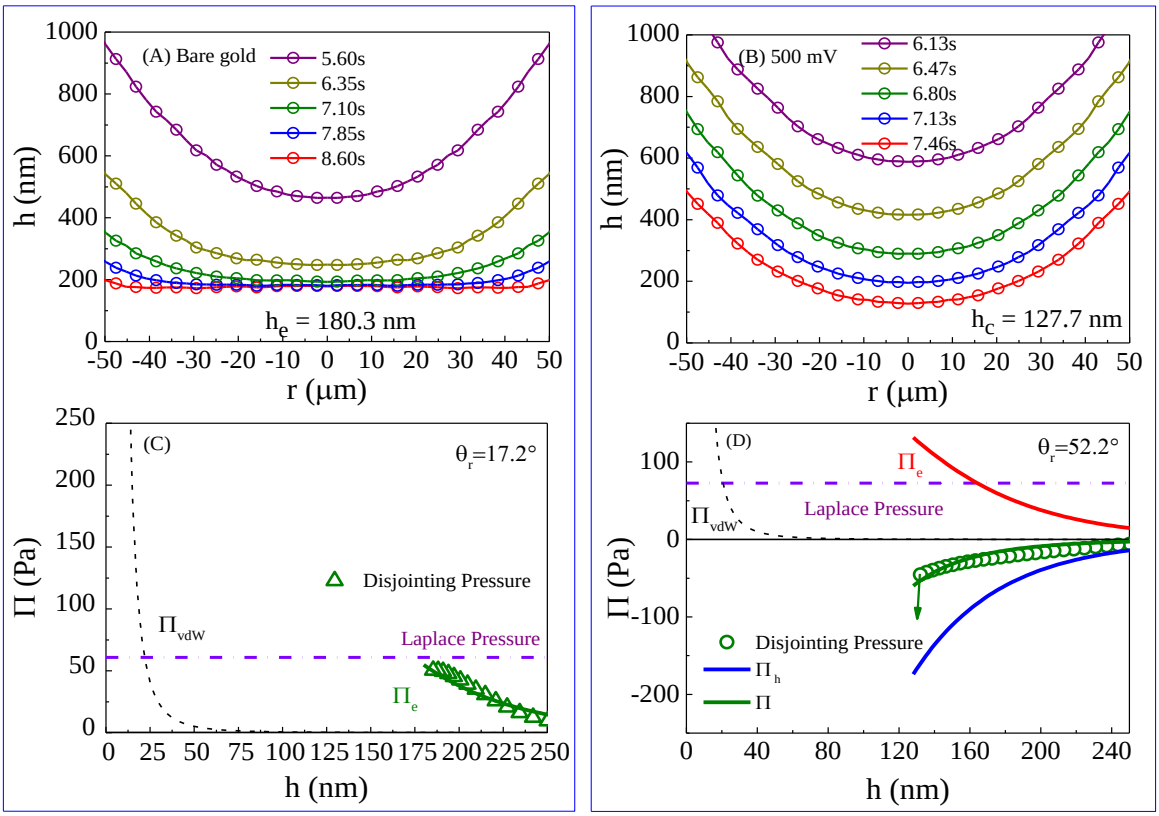

Figure 4.10 A and B show thin water film profile *h(r,t)* variation *vs. t*, during interactions between air bubbles and gold surfaces in pure water. A). An air bubble and fresh gold surface. B) An air bubble and fresh gold surface hydrophobized by KAX with applied potential of 500 mV for 2 minutes. h_{min} represents the thin water thickness before rupture (B) or reaching equilibrium (A). In (C) and (D), they show the variation components of the disjoining pressure with film thickness. Circles are disjoining pressures calculated from the water profile using lubrication approximation. (C) is fitting with DLVO theory and (D) is fitting with exponential function.

4.6 Summary

The surface forces in the wetting films of water from on gold substrates have been measured using a newly developed force apparatus for deformable surfaces (FADS). The kinetics of film thinning has been studied by recording the interference patterns generated during the film thinning process until the film ruptures. Once the film ruptures, however, it is difficult to 'see' the process of film dewetting or retreating to expose the solid/vapor interface. The force measurements are conducted using KAX and KEX as hydrophobizing agents for the gold plate used in the force measurement. Since the adsorption of these reagents are dependent on electrochemical potentials, the surface force measurements were conducted under conditions of controlled potentials. The results show that hydrophobic forces increase with the water contact angles, which indicate that hydrophobic forces are not the artifacts created by nanobubbles and/or cavitation. The contact angles measured under controlled potential conditions are in good agreement reported in the literature.

4.7 Reference

1 Kocabag, D. & Guler, T. Two-liquid flotation of sulphides: An electrochemical approach. *Miner. Eng.* **20**, 1246-1254 (2007).

2 Allan, G. C. & Woodcock, J. T. A review of the flotation of native gold and electrum. *Miner. Eng.* **14**, 931-962 (2001).

3 Prakash, M. & Gershenfeld, N. Microfluidic bubble logic. *Science* **315**, 832-835 (2007).

4 Yotsumoto, H. & Yoon, R.-H. Application of Extended DLVO Theory: II. Stability of Silica Suspensions. *J. Colloid Interface Sci.* **157**, 434-441 (1993).

5 Yoon, R.-H. & Ravishankar, S. A. Application of Extended DLVO Theory: III. Effect of Octanol on the Long-Range Hydrophobic Forces between Dodecylamine-Coated Mica Surfaces. *J. Colloid Interface Sci.* **166**, 215-224 (1994).

6 Yoon, R.-H. & Mao, L. Application of Extended DLVO Theory, IV: Derivation of Flotation Rate Equation from First Principles. *J. Colloid Interface Sci.* **181**, 613-626 (1996).

7 Pan, L. & Yoon, R.-H. Hydrophobic forces in the wetting films of water formed on xanthate-coated gold surfaces. *Faraday Discuss.* **146**, 325-340 (2010).

8 Pan, L., Jung, S. & Yoon, R.-H. A fundamental study on the role of collector in the kinetics of bubble–particle interaction. *Int. J. Miner. Process.* **106–109**, 37-41 (2012).

9 Shi, C. *et al.* Measuring Forces and Spatiotemporal Evolution of Thin Water Films between an Air Bubble and Solid Surfaces of Different Hydrophobicity. *ACS Nano* **9**, 95-104 (2015).

10 Ralston, J., Fornasiero, D. & Hayes, R. Bubble–particle attachment and detachment in flotation. *Int. J. Miner. Process.* **56**, 133-164 (1999).

11 Israelachvili, J. N. *Intermolecular and surface forces: revised third edition*. III edn, 260-261 (Academic press, 2011).

12 Pan, L., Jung, S. & Yoon, R. H. Effect of hydrophobicity on the stability of the wetting films of water formed on gold surfaces. *J. Colloid Interface Sci.* **361**, 321-330 (2011).

13 Shi, C., Chan, D. Y. C., Liu, Q. & Zeng, H. Probing the Hydrophobic Interaction between Air Bubbles and Partially Hydrophobic Surfaces Using Atomic Force Microscopy. *The Journal of Physical Chemistry C* **118**, 25000-25008 (2014).

14 Schönherr, H. Forces and Thin Water Film Drainage in Deformable Asymmetric Nanoscale Contacts. *ACS Nano* **9**, 12-15 (2015).

15 Exerowa, D. & Kruglyakov, P. M. in *Studies in Interface Science* Vol. Volume 5 (eds Exerowa Dotchi & M. Kruglyakov Pyotr) xvii (Elsevier, 1998).
16 Nedyalkov, M., Alexandrova, L., Platikanov, D., Levecke, B. & Tadros, T. Wetting films on a hydrophilic silica surface obtained from aqueous solutions of hydrophobically modified inulin polymeric surfactant. *Colloid. Polym. Sci.* **285**, 1713-1717 (2007).
17 Babar, S. & Weaver, J. H. Optical constants of Cu, Ag, and Au revisited. *Appl. Opt.* **54**, 477-481 (2015).
18 Li, Z. & Yoon, R.-H. AFM force measurements between gold and silver surfaces treated in ethyl xanthate solutions: Effect of applied potentials. *Miner. Eng.* **36–38**, 126-131 (2012).
19 Talonen, P., Rastas, J. & Leppinen, J. Insitu Ftir Study of Ethyl Xanthate Adsorption on Gold, Silver and Copper Electrodes under Controlled Potential. *Surf. Interface Anal.* **17**, 669-674 (1991).
20 Woods, R. Oxidation of Ethyl Xanthate on Plantinum, Gold, Copper, and Galena Electrodes - Relation to Mechanism of Mineral Flotation. *J. Phys. Chem.* **75**, 354-& (1971).
21 Pritzker, M. D. & Yoon, R. H. Thermodynamic Calculations on Sulfide Flotation Systems .1. Galena-Ethyl Xanthate System in the Absence of Metastable Species. *Int. J. Miner. Process.* **12**, 95-125 (1984).
22 Leppinen, J. O., Yoon, R. H. & Mielczarski, J. A. FT-IR studies of ethyl xanthate adsorption on gold, silver and gold—silver alloys. *Colloids and Surfaces* **61**, 189-203 (1991).
23 Woods, R., Kim, D. S., Basilio, C. I. & Yoon, R. H. A Spectroelectrochemical Study of Chemisorption of Ethyl Xanthate on Gold. *Colloids and Surfaces a-Physicochemical and Engineering Aspects* **94**, 67-74 (1995).
24 Li, Z. & Yoon, R.-H. Thermodynamics of Solvophobic Interaction between Hydrophobic Surfaces in Ethanol. *Langmuir* **30**, 13312-13320 (2014).
25 Wang, J. & Yoon, R. H. Surface Forces Measured between Xanthate-Coated Gold Surfaces. *Electrochemistry in Mineral and Metal Processing 8 (Emmp 8)* **28**, 3-14 (2010).
26 Mielczarski, J. A., Mielczarski, E. & Cases, J. M. Influence of chain length on adsorption of xanthates on chalcopyrite. *Int. J. Miner. Process.* **52**, 215-231 (1998).
27 Wang, J. L., Yoon, R. H. & Morris, J. AFM surface force measurements conducted between gold surfaces treated in xanthate solutions. *Int. J. Miner. Process.* **122**, 13-21 (2013).
28 Kakovsky, I. in *Proceedings, 2nd International Congress of Surface Activity.* 225-237 (Butterworths London).
29 Graciaa, A., Morel, G., Saulner, P., Lachaise, J. & Schechter, R. S. The ζ-Potential of Gas Bubbles. *J. Colloid Interface Sci.* **172**, 131-136 (1995).

CHAPTER 5.
Hydrophobic Forces in the Wetting Films of Water Formed on Chalcopyrite Hydrophobized with KAX

5.1 Abstract

Hydrophobic interactions between air bubbles and hydrophobized solid surfaces play an important role in mineral flotation. In this chapter, the disjoining pressures (Π) in the wetting films of water formed on chalcopyrite surface have been measured using the force apparatus for deformable surface (FADS). The chalcopyrite sample conditioned in a 10^{-4} M potassium amyl xanthate (KAX) solution of pH 9.2 at an open circuit potential exhibits negative disjoining pressures, i.e., $\Pi < 0$, due to the presence of the hydrophobic force. The measured hydrophobic forces can be represented by an exponential force law consisting of terms representing long-range force. In general, the hydrophobic force increases with increasing conditioning time of the chalcopyrite surface in the xanthate solution. The measured hydrophobic force reaches a maximum at a 10 min conditioning time. At longer conditioning times, it decreases due to the formation of dixanthogen multilayer. The hydrophobic forces measured under controlled potential conditions show that both the hydrophobic force and the water contact angle increase with increasing potential, reaching a maximum at 450 mV SHE. At higher potentials, dixanthogen is formed on top of the copper xanthate (CuX) monolayer, causing the hydrophobic force and contact angle to decrease.

5.2 Introduction

Flotation behavior of minerals depends critically on mineral hydrophobicity and their interactions with air bubbles. Previous studies have been carried out to study the effect of bubble size and particle size on flotation recovery.[1-4] In addition, many investigators studied the effect of surface hydrophobicity on bubble-particle interactions.[5-8] However, contact angle is a thermodynamic property, which can be directly used to predict flotation kinetics. If one can relate the contact angle to hydrophobic force, it is possible to indirectly relate the thermodynamic property to flotation kinetics. When a particle approaches a bubble surface, the kinetic energy should exceed the energy barrier imposed by a repulsive double-layer force. The role of hydrophobic force is to reduce the force (or energy barrier) by counterbalancing the double-layer repulsion. It is, therefore, the objective of the present work to measure the hydrophobic force present in the wetting film using the force apparatus for deformable surfaces (FADS) developed at Yoon's group of Virginia Tech.

We have chosen to study the wetting film formed on chalcopyrite, which is the most important copper mineral. Furthermore, the mechanism of the mineral becoming hydrophobic using xanthate is well understood.[9-11] Selective flotation of chalcopyrite from other minerals can be achieved using xanthate as a hydrophobizing agent, with proper manipulation of pH, E_h and applied potential.[7] Spectroscopic analysis of the amyl xanthate adsorbed on chalcopyrite showed that both copper xanthate (CuX) and dixanthogen (X_2) are the hydrophobic species formed on the chalcopyrite surfaces.[7,12-15] FTIR spectroscopic studies carried out by Mielczarski[13] showed that CuX begins to form initially and amyl dixanthogen ($(C_5H_{11}OCS_2)_2$) is formed at higher potentials. He showed also that contact angle varies with electrochemical potentials.

In the present work, we have measured the surface forces in the wetting films of water formed on chalcopyrite. The mineral sample is subjected firstly to voltammetry in the presence of

potassium amyl xanthate (KAX) to study the effect of potentials on the collector adsorption. In addition, contact angle measurements have been conducted to determine the condition under which contact angle reaches a maximum. The contact angle data are then compared with the results of the disjoining pressure (or surface force) measurements conducted using the FADS.

5.3 Methods and Materials

5.3.1 FADS and Lubrication Approximation

The scheme of force apparatus of deformable surface (FADS) has been shown in Figure 4.1, in the previous chapter. A flat sample substrate was placed on the upper plate and an air bubble with a radius about 2 mm were fixed on the lower plate, respectively. During the measurement, the plate on the top was driven towards the pate on the bottom using a micro piezo. When they came close enough, interference patterns formed and were recorded by a high speed camera. The images recorded will be analyzed by a self-written program and converted to the air bubble profile *vs.* wetting film thickness, *h(r,t)*. Finally, lubrication approximation will be used to calculate the disjoining pressure *vs.* film thickness. The equation used is as follows,[16-19]

$$\Pi = \frac{2\gamma}{R} - \frac{\gamma}{r}\frac{\partial}{\partial r}\left(r\frac{\partial h}{\partial r}\right) - 12\mu\int_{r=\infty}^{r}\frac{1}{rh^3}\left[\int_{r=0}^{r} r\frac{\partial h}{\partial t}dr\right]dr \qquad [5\text{-}1]$$

Where, μ is viscosity of water, R is the radius of air bubble, r is the radii axis, and h represents air bubble profile, *h(r,t)*.

5.3.2 Materials

The hydrophobizing agent used was potassium ethyl xanthate ($C_2H_5OCS_2^-K^+$, KAX, >90%, TCI America) and potassium amyl xanthate ($C_5H_{11}OCS_2^-K^+$, KEX, >90%, TCI America). Before coated onto gold, they were recrystallized twice using HPLC grade acetone (Fisher Scientific, Inc.) and diethyl ether (99.99%, Sigma-Aldrich, Inc.) following the method used by Pan et al.[20] and Li et al.[21] Then KAX/KEX aqueous solution were prepared and then adjusted to 9.2 by adding 0.05 M sodium tetraborate decahydrate ($Na_2B_4O_7$, Sigma-Aldrich Inc.)

Chalcopyrite (Student Specimens, Ward's Science, USA) was mounted into epoxy and cut into parallel slices with 2 mm thickness. Then a series of polishing steps were applied to make the chalcopyrite as smooth as possible. The final polishing step was using 50 nm alumina particle suspension. The surface roughness measured by AFM was showing roughness only in about 1.09 nm in the smooth region. Before each measurement, the surface of chalcopyrite plates will be polished by 50 nm alumina particle suspension for 2 minutes to make sure the substrates used are 'fresh' chalcopyrite. This will effectively avoid the issue of chalcopyrite oxidization. The receding water contact angle obtained on these 'fresh' chalcopyrite is about 25.2º.

5.3.3 Cyclic voltammogram and Surface Hydrophobization

Cyclic voltammogram was controlled by potentiostat (Model 273A, EG&G, Princeton Applied Research). Before the electrochemical reaction, the KAX aqueous solution (pH 9.2) and the $Na_2B_4O_7$ solution were degassed by ultrapure nitrogen gas (Airgas) for 1 hour. The electrodes and substrate were first cleaned electrochemically by three rounds of cycle potential sweeps in

0.05 M $Na_2B_4O_7$ solution between -950 mV and 850 mV with a sweep rate of 50 mV/s, and then the solution was replaced by potassium amyl xanthate solution (pH 9.2) to obtain the cyclic voltammogram between -950 mV and 850 mV with a sweep rate of 20 mV/s.

When the Cyclic voltammogram was obtained, several conditioning potentials will be applied around the peak with maximum change. Here, we select several potentials from 200 mV to 600 mV. The potentials were held for 2 minutes before adsorption of xanthate reaches equilibrium on chalcopyrite surfaces. Hydrophobization of chalcopyrite in open circuit was also carried out in 10^{-4} M KAX to study the effect of reaction time at pH 9.2. Hydrophobicity was controlled by reaction times: 2 minutes, 5 minutes, 10 minutes, 30 minutes and 60 minutes. One sample was left in the KAX solution for 3hours before wetting film measurement and then measured again after the surface was rinsed with n-Hexane.

5.3.4 Wetting Film and Disjoining Pressure Measurement

When the samples were well prepared, they were transferred in to FDAS immediately for wetting film thinning experiment. DI water is used for wetting film media. The interference pattern will be recorded and the spatiotemporal profile of air bubble will be calculated. After the film ruptured, the water contact angle will also be measured in-situ.

5.4 Results and Discussion

5.4.1 Effect of Surfactant Reaction Time on Hydrophobic Force

Figure 5.1 was the disjoining pressures between air bubbles and chalcopyrite surfaces *vs.* reaction time at open circuit. Dashed lines represent the disjoining pressure contributed by van der Waals force. The Hamaker constant applied here is -2.81×10^{-21} J.[22,23] The surfaces of chalcopyrite were hydrophobized in 5×10^{-5} M KAX aqueous solution for different times and the pH was controlled at 9.2 using 0.05 M borate solutions for all samples. It is already known that the surface hydrophobicity will vary with the reaction time, because more and more xanthate molecules are adsorbed on the chalcopyrite surfaces.

At the beginning 10 minutes, the disjoining pressures measured are increasing as the reaction time increases, indicating the improvement of surface hydrophobicity. Adsorption of KAX on chalcopyrite surface is slow at the beginning 2 minutes, and the water contact angle only increases to about 30º. No attractive disjoining pressure could be observed for the wetting film conducted on this sample. When the reaction time increases to 5 minutes, recognizable disjoining pressures are present, indicating improvement of surface hydrophobicity as more and more hydrophobic species are adsorbed. This could be observed by the increase of receding water contact angle, which becomes as large as 55º. Several possible adsorption mechanisms of amyl xanthate have been reported for this process:[13] formation of cuprous xanthate, dixanthogen, a thick layer of cuprous xanthate complex, as well as a thick layer of dixanthogen. The reaction might be expressed as follows,

$$2AmX^- + Cu^{2+} = CuAmX + 0.5AmX_2 \qquad [5\text{-}2]$$

It is likely that the formation of metal xanthate will be primary at the initial stage and then the formation of amyl dixanthogen will dominate at later stages.[13]

The disjoining pressure is largest when the reaction time is 10 minutes, with the largest water contact angle of 63º. At the film thickness of 100 nm, the disjoining pressure reaches about 1000 Pa, while the sample reacts for 5 minutes is only about 500 Pa. It might be due to that the surfactant coverage of the sample 5 minutes is not as good as that of 10 minutes. When more and more xanthate is adsorbed on the surface, multilayer dixanthogen forms on the chalcopyrite surfaces. The water contact angle decreases to 55º when the reaction time extends to 30 minutes. The disjoining pressure measured is also smaller as a result of the decreased hydrophobicity of chalcopyrite surfaces, as seen in Figure 5.1.

Formation of amyl dixanthogen multilayers can be confirmed by immersing the chalcopyrite in KAX aqueous solution for long hours, which has been shown in the inset of Figure 5.2 on the left. From the inset, a lot of droplet oil shape substances can be observed, and there are reports stating this is amyl dixanthogen.[24] The disjoining pressure measurement carried out on the chalcopyrite surface with the presence of massive dixanthogen is also shown in Figure 5.2. Surprisingly, no attractive disjoining pressure could be observed. It is well known that amyl Dixanthogen have long carbon chains and it should behave as hydrophobic matter. The hydrophilic surface properties could be a result of cuprous xanthate or potassium amyl xanthate adsorbed on the surface dixanthogen agglomeration. Due to hydrophobic interaction between carbon chains,

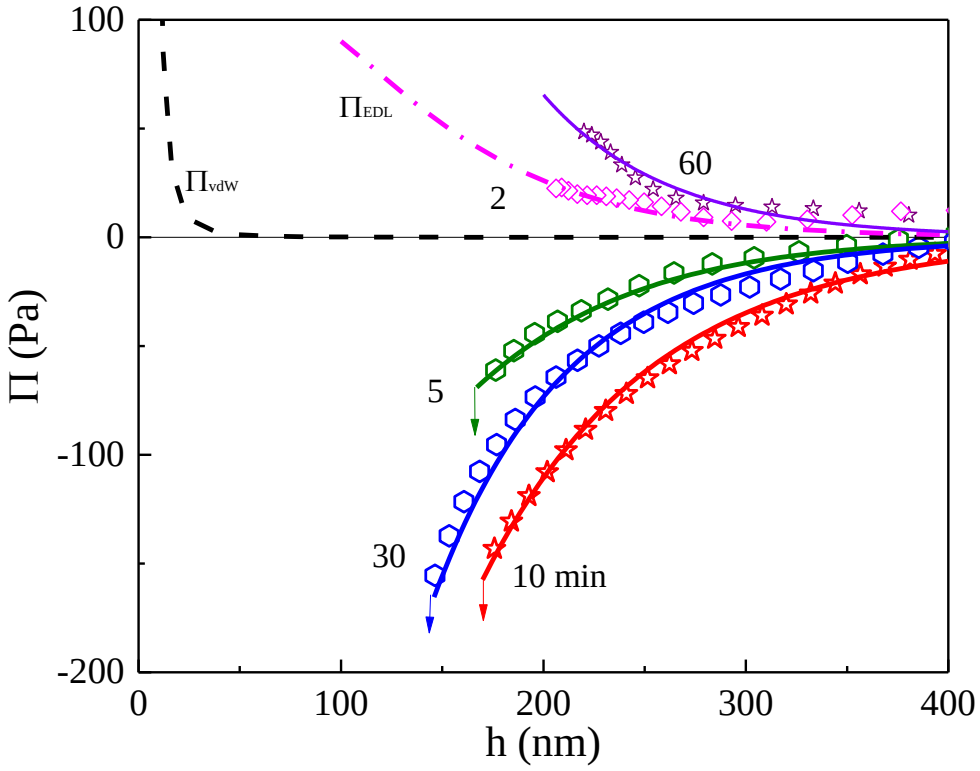

Figure 5.1 Disjoining pressures measured between air bubble and chalcopyrite interaction, hydrophobized in 5×10^{-5} M KAX at pH 9.2 for different time under condition of open circuit potential. The surface hydrophobicity increase first and then decrease as reaction continues. Dash line represents the disjoining pressure contributed by van der Waals force, with Hamaker constant of -2.81×10^{-21} J.

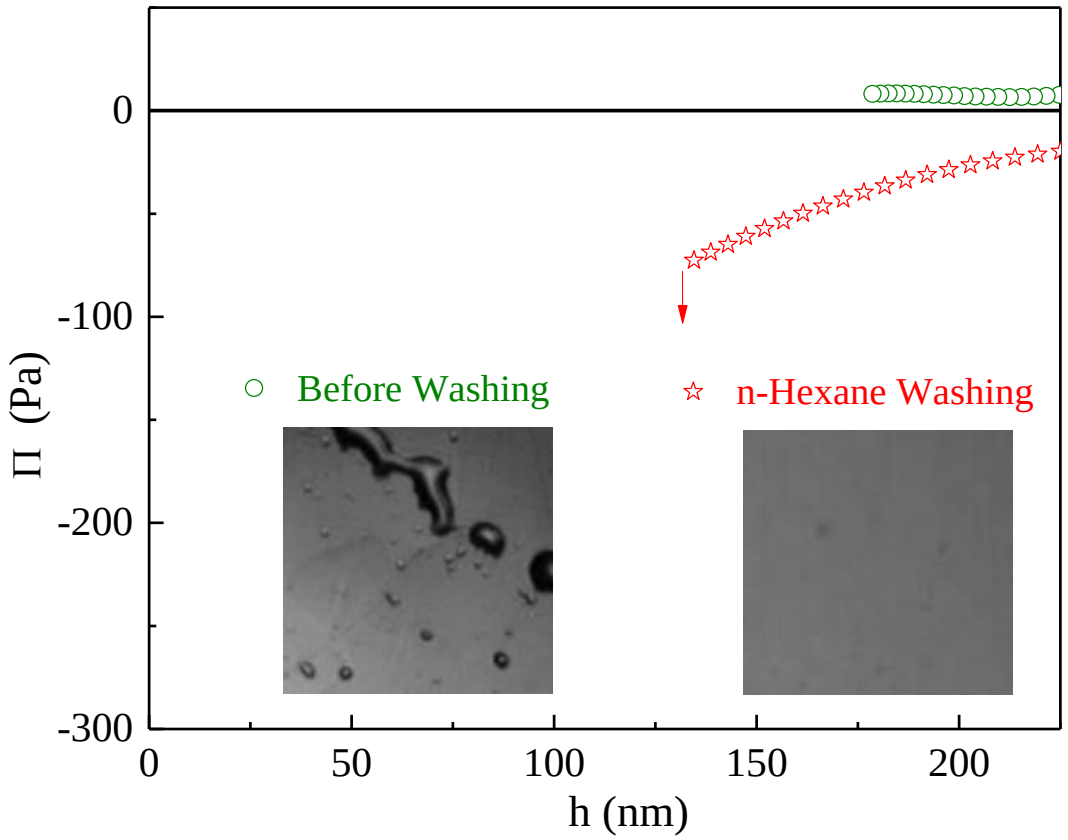

Figure 5.2 Significant disjoining pressures are difference between air bubble and chalcopyrite: (a) Reaction time is 3 hour and droplet oil shape substance formed and, (b) the same chalcopyrite, but the surface was washed in n-Hexane for 1minute. The dimension of images is 30 μm×30 μm.

the hydrophilic head of these metal xanthate will face towards bulk water, which made the surface of amyl dixanthogen hydrophilic instead of hydrophobic.

The dixanthogen agglomeration on the chalcopyrite surface can be dissolved in an organic solvent, such as n-Hexane. The right inset image shown in Figure 5.2 is the surface chalcopyrite when washed in n-Hexane. Most oil substances disappeared after the washing. Interestingly, the disjoining pressure measurement carried out on the washed chalcopyrite surface shows strong negative disjoining pressure, indicating the surface of chalcopyrite with hydrophobic properties. Both the disjoining pressures measured before n- and after n-Hexane washing are also shown in Figure 5.2. It is very likely that such large hydrophobicity is raised from the cuprous amyl xanthate monolayer chemisorbed on the chalcopyrite surface. Thus, it is fair to say that results shown in Figure 5.2 are evidence of multilayers of amyl dixanthogen formed on the top of a well-ordered monolayer of cuprous amyl xanthate. And the surface of the dixanthogen agglomeration might be mixed with metal xanthate, which makes the surface properties hydrophilic.

5.4.2 Effect of Applied Potential on Hydrophobic Force

Electrochemical has been considered as a reliable method for controlling surface reaction, after the systematic investigation on collectors with sulfide minerals[25-27]. In this approach, the

surfactant species is firstly chemisorbed onto mineral surface during anodic scanning. Different reaction products will be produced as the electrochemical potential changes during cyclic voltammogram sweeping.

Figure 5.3 shows cycle voltammogram of chalcopyrite in $Na_2P_4O_7$ aqueous solution (pH 9.2), for presence or absence 10^{-3} M KAX. Three adsorption peaks during anodic scanning can be observed when there is no collector presence. These peaks are due to the oxidization of mineral ($CuFeS_2$) and this curve is consistent with those reported by Woods and others.[28-30] During anodic potential sweeps, three potential-dependent stages were observed. Stage I *ca.* -0.1V to 0.1V might be due to the formation of metastable CuS_2*:[28]

$$CuFeS_2 + 3OH^- \rightarrow CuS_2^* + Fe(OH)_3 + 3e^- \quad [5\text{-}3]$$

$$2CuFeS_2 + 6H^+ \rightarrow 2CuS_2^* + Fe_2(O)_3 + 6H_2O + 3e^- \quad [5\text{-}4]$$

Stage II starts at about 0.1 V and to 0.5 V, which involves the formation of $Fe(OH)_3$ and Fe_2O_3.[25,28]. It is also possible that the iron oxide was oxidized to iron hydroxide.[25] In the alkaline solution, stage III represented the formation of sulfur,[11,25,28-30] which can be expressed by:

$$CuFeS_2 + 3H_2O \rightarrow CuS + Fe(OH)_3 + S + 3H^+ + 3e^- \quad [5\text{-}5]$$

The standard potential for this reaction is 0.547 V. During negative-going sweeps, observed reduction peaks are due to the reduction of iron oxides and iron hydroxide, as reverse reactions of reactions [5-3], [5-4] and [5-5].

When there is KAX present in the solution, the anodic reaction is different from that of without KAX. The oxidization peak is due to the formation of amyl dixanthogen and cuprous xanthate,[13]

$$AmX^- \rightarrow 0.5AmX_2 + e^- \quad [5\text{-}6]$$

$$2AmX^- + Cu^{2+} \rightarrow Cu(Am)_2 \quad [5\text{-}7]$$

According to the thermodynamic data (E^0 = -0.158 V) reported by Mu and others,[31,32] the reversible potential of amyl dixanthogen formation at 10^{-3} M KAX can be calculated using Nernst equation to be E_r=19.0 mV at room temperature. The adsorption peaks of amyl dixanthogen start at 80 mV high the reversible potential. And the cathodic peaks indicate the reverse reactions of reaction [5-6] and [5-7]. Obviously, the oxidization of iron at low potentials was inhibited by the oxidization of xanthate. FTIR spectroscopy and XPS have confirmed that the formation of cuprous amyl xanthate and amyl dixanthogen were formed on the surface of chalcopyrite.[7,12,13,15] Besides, the sulfur is also present on the chalcopyrite surface at high applied potentials.

Figure 5.4 shows the disjoining pressure measured using FADS on the surfaces of hydrophobized chalcopyrite. As demonstrated previously, the magnitude of disjoining pressure is related to surface hydrophobicity. For all measurements between air bubbles and chalcopyrite interaction carried out in this study, the properties of air bubbles are considered as a constant. Thus, the disjoining pressures measured reflect the surface hydrophobicity of chalcopyrite after electrochemical reaction. From Figure 5.4, we can see that the disjoining pressure increases from 200 mV to 400 mV and then decreases at higher applied potentials. Because the formation of

cuprous amyl xanthate and dixanthogen begins as low as 44.6 mV, it is very surprising that no negative disjoining pressure can be observed on the chalcopyrite surface conditioned at 200 mV. The reason might be due to the adsorption rate being too slow, and when the potential is about 200 mV, there are still not many hydrophobic species adsorbed.[7,13] Disjoining pressure becomes largest when the sample is conditioned at 400 mV, which is consistent with prediction of cyclic voltammogram. This indicates the best surface hydrophobicity, due to a well-orientated monolayer of cuprous amyl xanthate. However, when more amyl dixanthogen forms multilayer on top of the first layer cuprous amyl xanthate at higher applied potential. It is also very likely that the hydrophobic head of potassium amyl xanthate and cuprous amyl xanthate will be adsorbed on the surface of the multilayer of amyl dixanthogen, without ordered molecular level configuration. Part of these hydrophilic moieties of these species might face towards bulk water and result in worse surface hydrophobicity. This is a multistage model, which is very similar to those promoted on ethyl xanthate adsorbed on chalcocite.[15]

Water contact angle have also been measured on these chalcopyrite surfaces hydrophobized by KAX under different applied potential, shown in Figure 5.5. The water contact angles obtained change consistently with disjoining pressure measured. When the applied potential is about 400mV, the water contact angle becomes largest (57º). This shows the thermodynamic properties of wetting film match well with the kinetics properties.

Figure 5.4 shows the disjoining pressures of wetting film carried out on the chalcopyrite surface, conditioned under the applied potential above. The pressure contributed by hydrophobic force are much larger than those pressures contributed by van der Waals force, presented by a

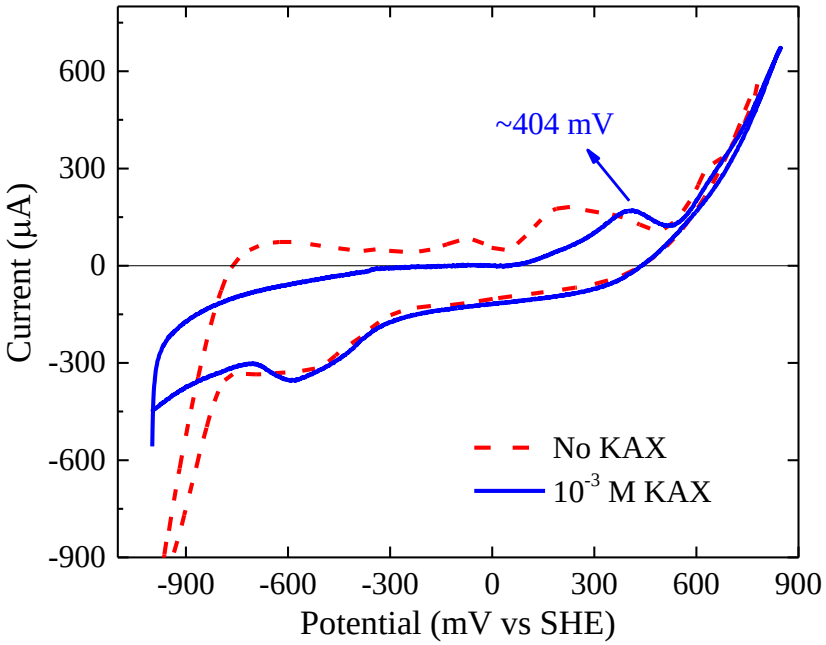

Figure 5.3 Cyclic voltammogram for chalcopyrite in $Na_2P_4O_7$ aqueous solution (pH 9.2), with or without 10^{-3} M KAX. The sweep rate is controlled at 50 mV/s. The maximum charge is located at about 400 mV when the presence of KAX. While there was no KAX, several adsorption peaks appeared indicating oxidization of chalcopyrite.

dashed line, using the Hamaker constant of A_{131}=-2.74×10^{-21} J.[23] The contribution of electrical double layer forces can be expressed as,

$$\Pi_e = -\frac{\xi\varepsilon\kappa^2}{2\sinh(\kappa h)}\left[\left(\psi_1^2+\psi_2^2\right)\csc(\kappa h) - 2\psi_1\psi_2\coth(\kappa h)\right] \qquad [5\text{-}8]$$

Where ψ_1 and ψ_2 are the surface potentials on the air /water interface and water/substrate interfaces, κ is the Debye length, h is the separation distance of air bubble and substrate, $\zeta\varepsilon$ is the dielectric permittivity of water. Here, we assume the concentration of CO_2 is 4.78×10^{-5} M as a good approximation from the disjoining pressure on pure chalcopyrite. The surface potential between air/water is 30.4 mV and water/chalcopyrite surface is 40.6 mV.[33] According to the extended-DLVO theory, disjoining pressure contributed by hydrophobic interaction can be calculated by using the disjoining pressure measured minus the pressures contributed by van der Waals and double layer electrical forces. In this chapter, the hydrophobic interactions are fitted using exponential law, and the contribution can be expressed as:

$$\Pi_h = -\frac{C}{2\pi D}\exp\left(-\frac{h}{D}\right) \qquad [5\text{-}9]$$

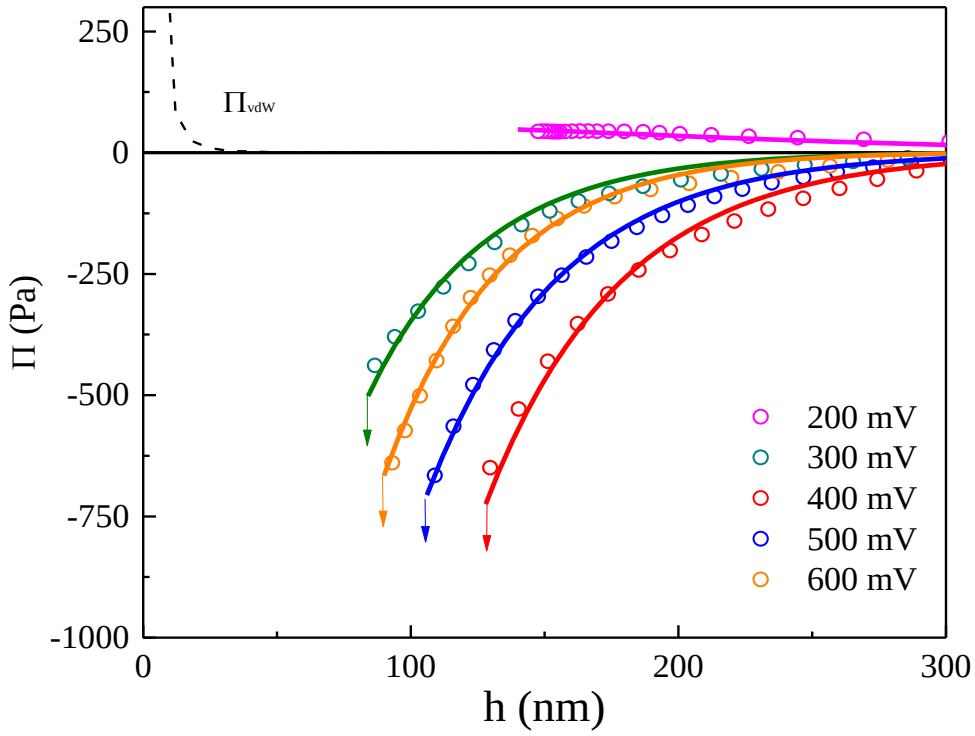

Figure 5.4 Disjoining pressures measured between air bubble and chalcopyrite interaction, hydrophobized in 10^{-4} M KAX at pH 9.2 under differently applied potential. Dash line represents the disjoining pressure contributed by van der Waals force, with Hamaker constant of -0.274×10^{-20} J.

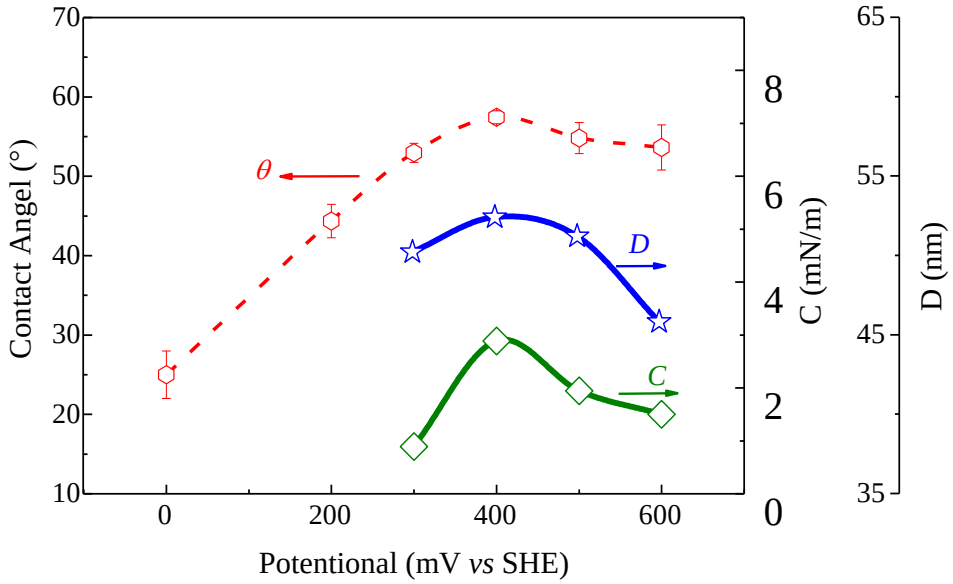

Figure 5.5 Receding water contact angle of chalcopyrite *vs.* applied potential. The surfaces of chalcopyrite were hydrophobized in 10^{-4} M KAX at pH 9.2 and the conditioning time were 2 minutes. *C* and *D* values of disjoining pressures between air bubble and chalcopyrite, fitted using exponential fitting. Both long range and short range hydrophobic interaction was observed, the range of which were about 80nm and 20 nm, respectively.

Where *h* is the film thickness between air bubbles and chalcopyrite surfaces and *C, D* are fitting parameters. The fitting results have been shown in Figure 5.5. Two kinds of hydrophobic interaction are present in this system. Interestingly, both *C*- and *D*- values obtained from FADS agree with the contact angle well. This indicates that the magnitude and range of hydrophobic interactions are both closely related to the surface hydrophobicity.

It is also very interesting that the variation trend of fitting parameters C and D values are consistent with the water contact angle. This indicates that the disjoining pressure obtained are crucially dependent on the substrate surface hydrophobicity. In other words, these negative disjoining pressures are raised from hydrophobic force, rather than the artifact of nano-bubble.

Figure 5.6 (A) shows spatiotemporal profiles of the wetting films formed on the chalcopyrite conditioned at 500 mV for 2 minutes in a 10^{-4} M KAX solution at pH 9.2. The receding water contact angle was 53.6º. The approaching speed of the micro piezo in this experiment was 1 μm/s. The film thinning velocity at larger distance was close to this value. When the wetting film became thinner, it decreased due to increased hydrophobic force. The hydrodynamic force also increased at short separations. Figure 5.6 (B) shows the changes in disjoining pressure as calculated based on the spatiotemporal film profiles, by applying Reynolds lubrication approximation. The wetting film ruptured at film thickness about 91.2 nm. The disjoining pressure at this point was about 700 Pa. The extended DLVO theory was then applied to calculate the contribution from disjoining pressure, as described in previous section.

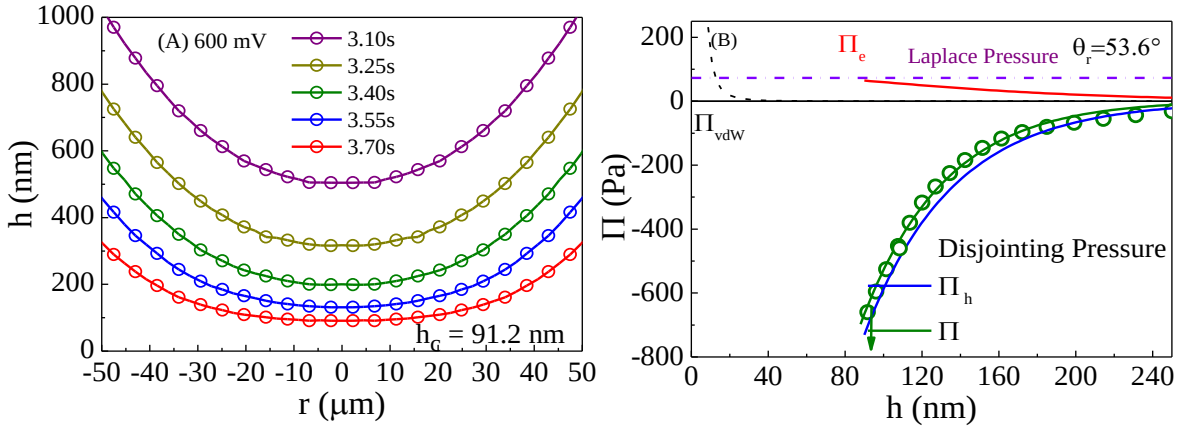

Figure 5.6 A and B show thin water film profile *h(r,t)* variation *vs. t*, during interactions between air bubbles and chalcopyrite surfaces in pure water: An air bubble and fresh chalcopyrite surface hydrophobized by KAX with applied potential of 500 mV for 2 minutes. h_c represents the thin water thickness before rupture. Extended DLVO theory fitting result is shown in (B).

5.5 Conclusion

The force apparatus for deformable surface (FADS) developed at Virginia Tech has been used to measure the disjoining pressure in the thin films of water formed between air bubbles and chalcopyrite surfaces, hydrophobized in a 10^{-4} M KAX solution at pH 9.2. The results showed the presence of a strong and long ranged hydrophobic force. The measured forces can be represented by the exponential force law, representing a long-range hydrophobic force.

It has been found that the magnitudes of these long-range hydrophobic forces are crucially dependent on the surface hydrophobicity of the substrate (chalcopyrite). The adsorption mechanism of KAX on chalcopyrite plays a key role in determining the surface hydrophobicity. At open circuit, the hydrophobicity of chalcopyrite is increased with increasing immersion time, reaching a maximum at a 10 min immersion time. At longer immersion times, surface hydrophobicity decreased due to the formation of dixanthogen on top of the copper xanthate (CuX_2) formed at shorter immersion time. After an excessively long immersion time, visible oil drops are formed, with the measured disjoining pressure becoming very small. When the oil droplets are washed off with an organic solvent, strong hydrophobic force is observed, which can be attributed to the exposure of a CuX_2 monolayer.

The FADS measurements conducted under controlled potential conditions show that disjoining pressure decreases with applied potentials, becoming most negative at 400 mV. At higher potentials, dixanthogen is formed on top of the CuX_2 adsorbed in the monolayer. Thus, the results show that dixanthogen formation is detrimental to hydrophobizing chalcopyrite. This finding is contrary to what has been known in the literature that dixanthogen formation increases contact angle and hence increase flotation recovery.

5.6 Reference

1 Sarkar, M. S. K. A., Evans, G. M. & Donne, S. W. Bubble size measurement in electroflotation. *Miner. Eng.* **23**, 1058-1065 (2010).

2 Shahbazi, B., Rezai, B. & Koleini, S. M. J. Bubble-particle collision and attachment probability on fine particles flotation. *Chem. Eng. Process.* **49**, 622-627 (2010).

3 Basarova, P., Machon, V., Hubicka, M. & Horn, D. Collision processes involving a single rising bubble and a larger stationary spherical particle. *Int. J. Miner. Process.* **94**, 58-66 (2010).

4 Tran, D. N. H., Whitby, C. P., Fornasiero, D. & Ralston, J. Selective separation of very fine particles at a planar air-water interface. *Int. J. Miner. Process.* **94**, 35-42 (2010).

5 Wang, J. L., Yoon, R. H. & Morris, J. AFM surface force measurements conducted between gold surfaces treated in xanthate solutions. *Int. J. Miner. Process.* **122**, 13-21 (2013).

6 Wang, J. & Yoon, R. H. Surface Forces Measured between Xanthate-Coated Gold Surfaces. *Electrochemistry in Mineral and Metal Processing 8 (Emmp 8)* **28**, 3-14 (2010).

7 Mielczarski, J. A., Mielczarski, E. & Cases, J. M. Influence of chain length on adsorption of xanthates on chalcopyrite. *Int. J. Miner. Process.* **52**, 215-231 (1998).

8 Yoon, R.-H. & Mao, L. Application of Extended DLVO Theory, IV: Derivation of Flotation Rate Equation from First Principles. *J. Colloid Interface Sci.* **181**, 613-626 (1996).

9 Gardner, H. A. & Wood, E. M. Variation in Chromosome-19. *Journal of Medical Genetics* **16**, 79-80 (1979).

10 Chanturiya, V., Vigdergauz, V., Sarkisova, L. & Dorofeev, A. The hydrophilic-hydrophobic transitions on chalcopyrite: electrochemical study. *Fizykochemiczne Problemy Mineralurgii/Physicochemical Problems of Mineral Processing*, 65-78 (2004).

11 Chander, S. & Khan, A. Effect of sulfur dioxide on flotation of chalcopyrite. *Int. J. Miner. Process.* **58**, 45-55 (2000).

12 Mielczarski, J., Mielczarski, E. & Cases, J. Infrared evaluation of composition and structure of ethyl xanthate monolayers produced on chalcopyrite, tetrahedrite, tennantite at controlled potentials. *J. Colloid Interface Sci.* **188**, 150-161 (1997).

13 Mielczarski, J., Mielczarski, E. & Cases, J. Interaction of amyl xanthate with chalcopyrite, tetrahedrite, and tennantite at controlled potentials. Simulation and spectroelectrochemical results for two-component adsorption layers. *Langmuir* **12**, 6521-6529 (1996).

14 Andreev, G. N. & Barzev, A. Raman spectroscopic study of some chalcopyrite-xanthate flotation products. *J. Mol. Struct.* **661**, 325-332 (2003).

15 Mielczarski, J. XPS study of ethyl xanthate adsorption on oxidized surface of cuprous sulfide. *J. Colloid Interface Sci.* **120**, 201-209 (1987).

16 Pan, L., Jung, S. & Yoon, R.-H. A fundamental study on the role of collector in the kinetics of bubble–particle interaction. *Int. J. Miner. Process.* **106–109**, 37-41 (2012).

17 Pan, L. & Yoon, R.-H. Hydrophobic forces in the wetting films of water formed on xanthate-coated gold surfaces. *Faraday Discuss.* **146**, 325-340 (2010).

18 Shi, C., Chan, D. Y. C., Liu, Q. & Zeng, H. Probing the Hydrophobic Interaction between Air Bubbles and Partially Hydrophobic Surfaces Using Atomic Force Microscopy. *The Journal of Physical Chemistry C* **118**, 25000-25008 (2014).

19 Shi, C. *et al.* Measuring Forces and Spatiotemporal Evolution of Thin Water Films between an Air Bubble and Solid Surfaces of Different Hydrophobicity. *ACS Nano* **9**, 95-104 (2015).

20 Pan, L., Jung, S. & Yoon, R. H. Effect of hydrophobicity on the stability of the wetting films of water formed on gold surfaces. *J. Colloid Interface Sci.* **361**, 321-330 (2011).
21 Li, Z. & Yoon, R.-H. AFM force measurements between gold and silver surfaces treated in ethyl xanthate solutions: Effect of applied potentials. *Miner. Eng.* **36–38**, 126-131 (2012).
22 Sharma, P. K. & Hanumantha Rao, K. Adhesion of Paenibacillus polymyxa on chalcopyrite and pyrite: surface thermodynamics and extended DLVO theory. *Colloids and Surfaces B: Biointerfaces* **29**, 21-38 (2003).
23 Vilinska, A. & Rao, K. H. Surface thermodynamics and extended DLVO theory of Acidithiobacillus ferrooxidans cells adhesion on pyrite and chalcopyrite. *The Open Colloid Science Journal* **2**, 1-14 (2009).
24 Wang, J. & Yoon, R.-H. AFM forces measured between gold surfaces coated with self-assembled monolayers of 1-hexadecanethiol. *Langmuir* **24**, 7889-7896 (2008).
25 Gardner, J. & Woods, R. An electrochemical investigation of the natural flotability of chalcopyrite. *Int. J. Miner. Process.* **6**, 1-16 (1979).
26 Trahar, W. J. A Laboratory Study of the Influence of Sodium Sulfide and Oxygen on the Collectorless Flotation of Chalcopyrite. *Int. J. Miner. Process.* **11**, 57-74 (1983).
27 Woods, R. Electrochemical potential controlling flotation. *Int. J. Miner. Process.* **72**, 151-162 (2003).
28 Yin, Q., Vaughan, D. J., England, K. E. R., Kelsall, G. H. & Brandon, N. P. Surface oxidation of chalcopyrite (CuFeS2) in alkaline solutions. *J. Electrochem. Soc.* **147**, 2945-2951 (2000).
29 Güler, T., Hiçyılmaz, C., Gökağaç, G. & Ekmekçi, Z. Electrochemical behaviour of chalcopyrite in the absence and presence of dithiophosphate. *Int. J. Miner. Process.* **75**, 217-228 (2005).
30 Buckley, A. N. & Woods, R. An X-Ray Photoelectron Spectroscopic Study of the Oxidation of Chalcopyrite. *Aust. J. Chem.* **37**, 2403-2413 (1984).
31 Mu, Y., Peng, Y. & Lauten, R. A. Electrochemistry aspects of pyrite in the presence of potassium amyl xanthate and a lignosulfonate-based biopolymer depressant. *Electrochim. Acta* **174**, 133-142 (2015).
32 Guo, B., Peng, Y. & Espinosa-Gomez, R. Effects of free cyanide and cuprous cyanide on the flotation of gold and silver bearing pyrite. *Miner. Eng.* **71**, 194-204 (2015).
33 Fullston, D., Fornasiero, D. & Ralston, J. Zeta potential study of the oxidation of copper sulfide minerals. *Colloids and Surfaces a-Physicochemical and Engineering Aspects* **146**, 113-121 (1999).

CHAPTER 6.
Measurement of Hydrophobic Forces Present in the Wetting Films of Water Formed on Galena Surfaces Treated with Potassium Amyl Xanthate

6.1 Abstract

The stability of the wetting films of water formed between air bubble and galena have been studied using the force apparatus for deformable surfaces (FADS). It has been found that a stable wetting film forms on an untreated hydrophilic galena surface with an equilibrium film thickness of 160 nm. When the galena surface is rendered hydrophobic by treating the mineral in a 10^{-5} M potassium amyl xanthate (KAX) solution, wetting films become unstable and rupture quickly at film thicknesses in the range of at 80-160 nm, depending on the surface hydrophobicity. Analysis of the spatiotemporal film profiles in view of the Reynolds lubrication theory and the extended DLVO theory, it is possible to determine the contributions from the hydrophobic force to the disjoining pressure of a wetting film. It has been found that hydrophobic forces increase with increasing water contact angles, which in turn vary with the potentials at which the mineral is conditioned in the xanthate solution.

6.2 Research Background

When a particle meets an air bubble in a flotation cell, the wetting film formed in between must rupture. The rupture should occur while the bubble and particle are in contact with each other. Since the pulp in a flotation cell is strongly agitated to keep the particles in suspension and to create small air bubbles, the contact times are very short, typically in tens of milliseconds or less. Thus, it is important to facilitate the kinetics of film thinning and rupture. In the flotation industry, hydrophobizing agents, called collectors, are used to selectively hydrophobize the mineral particles to be floated. Rendering a mineral hydrophobic causes the wetting film to be labile so that it thins fast and eventually rupture. Thermodynamically, a wetting film ruptures when contact angle is greater than zero and the disjoining pressure (Π) in the film is negative or the disjoining pressure gradient with respect to film thickness, h, becomes positive, *i.e.*, $\partial\Pi/\partial h > 0$.

In this chapter, the disjoining pressures in the wetting films of water formed on galena surface have been measured using the force apparatus for deformable surfaces (FADS). Galena is chosen as many investigators studied the adsorption mechanisms of xanthate, which is most widely used hydrophobizing agent for sulfide minerals. As is well known, xanthate ions (X^-) adsorb on galena *via* a mixed potential reaction mechanism involving a cathodic reaction,

$$PbS + 2X^- \rightarrow Pb(X)_2 + S^0 + 2e^- \qquad [6\text{-}1]$$

$$1/2O_2 + H_2O + 2e^- \rightarrow 2OH^- \qquad [6\text{-}2]$$

in which lead xanthate is the hydrophobic species formed upon xanthate adsorption.

In this chapter, the hydrophobic forces measured using the FADS are compared with the contact angles measured at different electrochemical potentials. In addition, voltammetry studies are conducted to identify the xanthate species formed at different potentials.

6.3 Materials and Experiments

6.3.1 Materials

Galena (New York State Regents: Mineral and Rock Identification Package, Ward's Science, USA) is used for the current study. The samples were mounted into epoxy (Buehler, USA) and cut into parallel plates with 2.5 mm thickness. Then these plates were polished smoothly following standard steps with the final step using suspension of 50 nm alumina particle (Buehler, USA). These plates could be reused if the surface of galena plates were polished by 50 nm alumina particle suspension before usage because these substrates would become 'fresh' galena.

Potassium amyl xanthate ($C_5H_{11}OC\,S_2^-K^+$, KEX, >90%, TCI America) was used as hydrophobizing agent. Before coated onto galena, it was recrystallized twice using HPLC grade acetone (Fisher Scientific Inc.) and diethyl ether ($(CH_3CH_2)_2O$, >99.99%, Sigma-Aldrich Inc.) as described previously by Pan et al.[1] and Li et al.[2] Then KAX aqueous solutions were prepared by dissolving in DI water (Nanopure, 18.2 MΩ) and the pH value was adjusted to 9.2 by adding 0.05 M sodium tetraborate decahydrate ($Na_2B_4O_7$, >99.5%, Sigma-Aldrich Inc.)

6.3.2 Cyclic voltammogram

The electrodes and substrate were first cleaned electrochemically by three rounds of cycle potential sweeps in 0.05 M $Na_2B_4O_7$ solution between -750 mV and 1100 mV with a sweep rate of 50 mV/s, and then the solution was replaced by potassium amyl xanthate solution (pH 9.2) to obtain the cyclic voltammogram with a sweep rate of 50 mV/s, conducted by potentiostat (Model 273A, EG&G, Princeton Applied Research). Before the electrochemical reaction, KAX aqueous solution (pH 9.2) and $Na_2B_4O_7$ solution was degassed with ultrapure nitrogen gas (Airgas) for 1 hour.

When the cyclic voltammogram curve was obtained, and based on the adsorption information obtained, several potentials, 50, 100, 150 and 250 mV, were applied for chalcopyrite and KAX electrochemical reactions. Each 'fresh' galena flat plate was cleaned using electrical cycle in $Na_2B_4O_7$ solution (pH 9.2) for three rounds. Then the sample was held at a set-up potential 2 minutes for the adsorption of xanthate reaching equilibrium.

6.3.3 Wetting Film

The illustration of experimental device (FADS) has been shown in previous chapter. When the galena sample is ready, it will be transferred to FDAS for wetting film experiments in DI water. The air bubble was fixed, and the other plate is driven towards the air bubble at a constant speed of 1 μm/s. As the separation distance between air bubble and galena plate became thinner, the air bubble deformed, indicating some interaction between the air bubble and galena substrate. Interference pattern also formed due to the reflection of air bubble and galena surface. The evolution of air bubble was recorded with a high speed camera. The light source used is a monochromatic green light with wavelength of 546 nm (USH-1030L, Olympus, Japan), equipped in an inverted microscope and recorded with a high-speed video camera (HiSpec4 2G, GigE Vision, Germany). This interference pattern obtained could be used to generate information of the bubble spatial profile, which is identical to the 3D separation distance of the bubble and galena substrate. The wetting film will rupture on hydrophobic galena surface if the separation distance between the

air bubble and the galena was close. After the wetting film ruptured, the water contact angle was recorded in-situ.

6.4 Theoretical models

Disjoining pressure could be defined as the derivative of the Gibbs energy of per unit area in respect to distance, at constant pressure, temperature and chemical potential, expressed as following,[3]

$$\Pi(h) = -(\partial G / \partial h)_{p,T,\mu_2} \qquad [6\text{-}3]$$

It is now realized that disjoining pressure was the interaction result of both DLVO forces and non-DLVO forces,

$$\Pi = \Pi_e + \Pi_d + \Pi_h \qquad [6\text{-}4]$$

Where Π_d is contributed by van der Waals force, Π_e double layer electrical forces and Π_h hydrophobic forces. The pressure contributed by van der Waals force between sphere and flat plate is,[4]

$$\Pi = -\frac{A_{132}}{6\pi h^3} \qquad [6\text{-}5]$$

Where A132 is Hamaker constant of solid/water/air interaction and h the closest separation distance of air bubble and substrate. The pressure contributed by electrical double layer forces between sphere and flat plate is as follows,

$$\Pi_e / R = -\frac{\xi\varepsilon\kappa^2}{2\sinh(\kappa h)}\left[(\psi_1^2 + \psi_2^2)\csc h(\kappa h) - 2\psi_1\psi_2 \coth(\kappa h)\right] \qquad [6\text{-}6]$$

Where ψ_1 and ψ_2 are the surface potentials on the air /water interface and water/substrate interfaces, κ is the Debye length, $\zeta\varepsilon$ is the dielectric permittivity of water. And the disjoining pressure, raised from the hydrophobic force, can be written in exponential form as,

$$\Pi_h = -\frac{C}{2\pi D} exp\left(-\frac{h}{D}\right) \qquad [6\text{-}7]$$

Where *C is* fitting parameters regarding to interfacial tension and *D is* the decay lengths.

Besides the theoretical fitting, the disjoining pressure could also be calculated from experimental data, the spatial profile of air bubble *h(r,t)*. By applying the lubrication approximation and Yong-Laplace equation, the disjoining pressure can be derived as,

$$\Pi = \frac{2\gamma}{R} - \frac{\gamma}{r}\frac{\partial}{\partial r}\left(r\frac{\partial h}{\partial r}\right) - 12\mu\int_{r=\infty}^{r}\frac{1}{rh^3}\left[\int_{r=0}^{r} r\frac{\partial h}{\partial t}dr\right]dr \qquad [6\text{-}8]$$

By fitting disjoining pressure calculated from Equation [6-8] with the theoretical DLVO force and non-DLVO force, the *C* and *D* parameters could be fitted with system parameters.

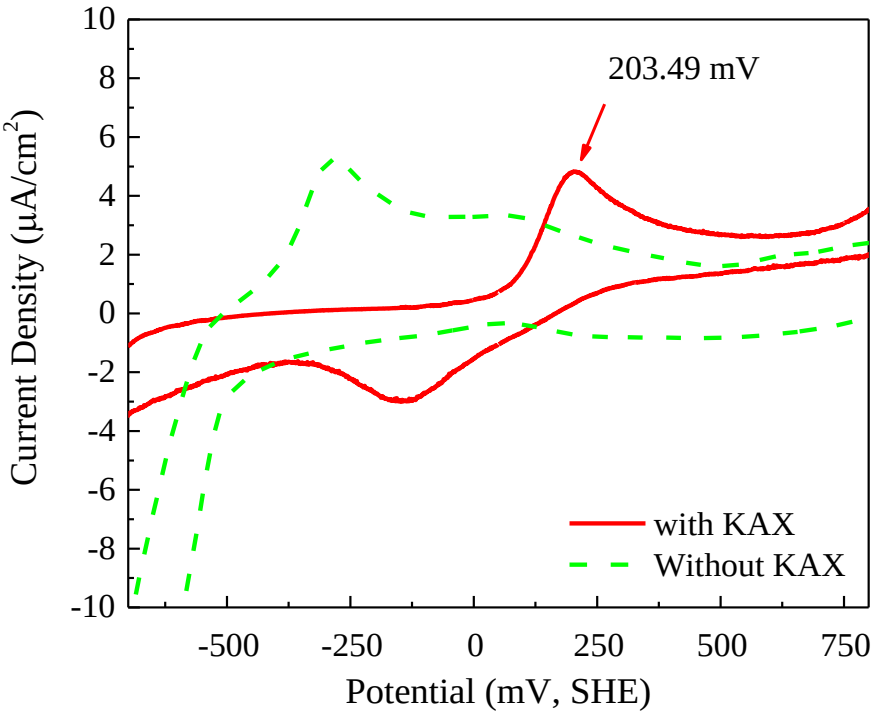

Figure 6.1 Voltammograms for galena in $Na_2P_4O_7$ aqueous solution (0.05 M, pH 9.2) when absent of oxygen. Red curve presents cycle under 10^{-3} M KAX solution and green curve without KAX solution. The sweep rates are controlled at 50 mV/s. The maximum charge is located at about 200mV when the presence of KAX.

6.5 Results and Discussion

6.5.1 Electrochemical Reaction of Galena-KAX

Linear sweep voltammogram have been obtained on polished galena flat substrates in $Na_2P_4O_7$ aqueous solution (0.05 M, pH 9.2) with or without amyl xanthate, and the results are shown in Figure 6.1. Red curve presents cycle voltammogram obtained under 10^{-3} M KAX and green curve is that of without KAX presence. The sweep rates in both cycles are controlled at 50 mV/s.

When absent of xanthate, the primary cycle of galena oxidation is as follows,[5,6]

$$PbS \rightarrow Pb^{2+} + S^0 + 2e^- \qquad [6\text{-}9]$$

In alkaline solutions, $Pb(OH)_2$ will form on the surface of galena as a passive layer and sulfide species are very likely in the form of SH^-.[7] Ahlberg et al. argued that the oxidization of galena at low overpotential would yield PbOH surface complexes and metal deficient sulfide at the initial stages of oxidation.[8] The reduction peak was also observed at the potential of about 500 mV.

The red curve shown in Figure 6.1 represents the cyclic voltammogram of galena at pH 9.2, which involves an anodic oxidation galena and xanthate. The anodic reaction processes are different at various stages.[5,9] Chemical adsorption might start at a lower potential (-100 mV to 200 mV)[10] than reverse potential of metal xanthate formation,[5,11-13]

$$PbS + 2AX^- + 4H_2O \rightarrow Pb(AX)_2 + SO_4^{2-} + 8H^+ + 8e^- \quad [6\text{-}10]$$

In the reaction of xanthate and galena, a sub-monolayer of metal xanthate is formed on the mineral surface, according to the XPS spectroscopy study carried out by Woods.[14] Then, multiple layer of lead xanthate is formed on top of the lead xanthate at higher applied potentials. Kari suggested that the distribution of xanthate in the galena-xanthate system was irregular and three dimensional aggregates of lead xanthate occurred. However, this is not observed in the conditions carried out in present study. At low applied potential, the formation of the hydroxide layer of $Pb(OH)_2$ will be inhabited by xanthate ions. However, at higher applied potential, galena will be oxidized to lead oxides/hydroxides, as shown in the large peak observed in anodic sweeping at high potential.[15,16] During cathodic scanning, a reduction peak, starting at about -44 mV, is observed as a reverse process of equation [6-10].

6.5.2 Wetting film of Galena and Air Bubble

Based on the cyclic voltammogram curve of galena in $Na_2P_4O_7$ aqueous solution (0.05 M, pH 9.2), polished galena substrates were conditioned under several different potentials: 50, 100, 150, 200 and 250 for 2 minutes before the adsorption reaction reached equilibrium. During wetting film measurement, an air bubble with radius about 2.5 mm will be fixed on one plate and galena substrates on anther plate. The air bubble was immobilized, while the plate with galena was driven by a pizeo-electric transducer and moved toward the air bubble. The approach speed of the plate was kept constant at 1 μm/s; however, the actual speed at which the wetting film thins would become slower as the film thinning progresses. The kinetics of wetting film should vary depending on surface hydrophobicity. On the hydrophilic galena surface, the kinetics decreases dramatically as the film becomes thinner. However, on a hydrophobic galena surface, the kinetics does not change much. Nevertheless, the interference patterns would form on all wetting films confined between galena substrates and air bubbles. The interference patterns were processed with MATLAB to obtain the spatiotemporal film profile using the method introduced by Michail and Shceludko et al.[17,18]

a. Hydrophilic Galena Surface and Air Bubble

Interaction between fresh galena (hydrophilic) and air bubble is carried out prior to the interaction between hydrophobized galena and air bubble, since it is a relatively simple system. More importantly, the forces involved in this process are DLVO forces, which could be well described using DLVO theory.[19,20] The process is also helpful to establish experimental protocol and DLVO fitting parameters. Figure 6.2 (A) shows in water film profile *h(r,t)* during film thinning between hydrophilic galena surface and an air bubble with radius about 2.5 mm in DI water. Figure 6.2 (B) shows the forces contributing to the disjoining pressure and theoretical prediction using DLVO theory. In the case of pure water, CO_2 is the major origination of electrolyte and contributes to the electrical double layer forces. When the separation distance is larger than 100 nm, the contribution of van der Waals force is very small and negligible. The Hamaker constant (A_{132}) used in the present work was -1.92×10^{-20} J obtained from combing rule, using Hamaker constant of galena/water/galena (A_{131}) and water/air/water (A_{232})[21] with the following expression,[20]

$$A_{132} = -\sqrt{A_{121}}\sqrt{A_{232}} \quad [6\text{-}11]$$

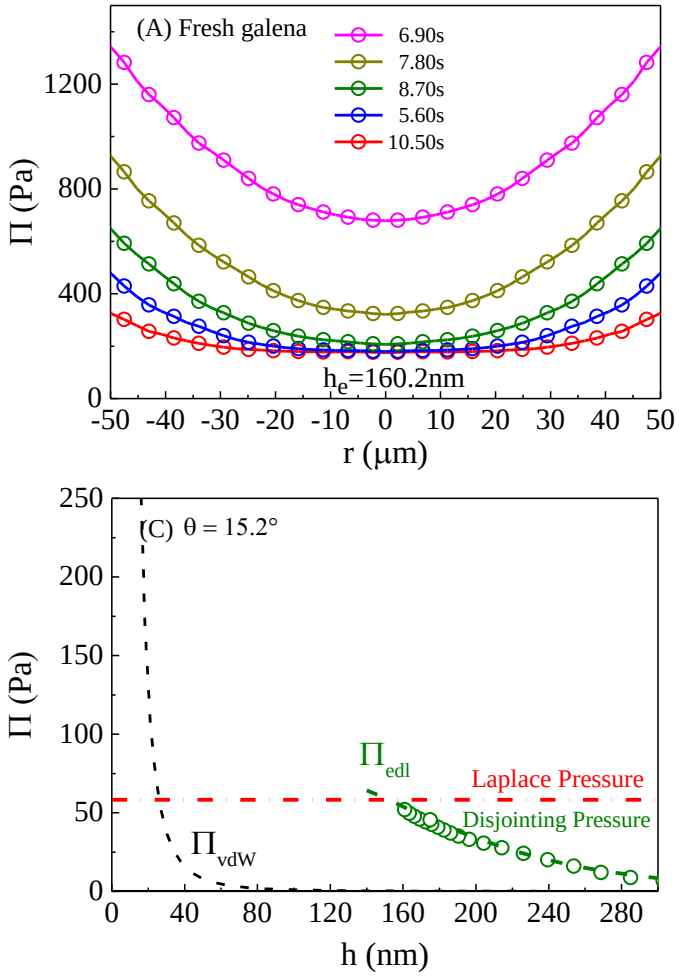

Figure 6.2 (A) Thin water film profile *h(r,t)* during interaction between the air bubble and 'fresh' hydrophilic galena surface in water. The receding water contact angle of fresh galena is about 15º. The radius of air bubble was about 2.5 mm, and the approaching speed of air bubble and galena is 1μm/s. Finally, the separation distance will be stabilized at about 132 nm. (B) shows the variation component of the disjoining pressure with film thickness. Circles are disjoining pressure (Π) calculated from the water profile using lubrication approximation. And the dashed line represents van der Waals force (Π_{vdW}) with Hamaker constant of -1.92×10^{-20} J. Red line is pressure contributed by electrical double layer forces(Π_{EDL}).

In the initial seconds of the wetting film experiment, the separation distance between the air bubble and galena is large (>1 μm), and the film thinning kinetics of air bubbles is crucially dependent upon the approaching speed of the micro-piezo. In this stage, the profile of the air bubble stays spherical and the film thinning rate is the same as the approaching speed. However, when the separation distance of the air bubble and galena comes closer, *e.g.* from t=6.9 s to t=7.8 s, the film thinning velocity is only about 500 nm/s. At this separation distance, both van der Waals force and the electrical double layer force are still negligible. The reduced film thinning velocity is due to the increase of hydrodynamic resistance and the repulsive surface force. When the air bubble and galena separation distance comes much closer (160 nm < h < 300 nm), film thinning velocity

is greatly reduced because the repulsive electrical double layer force. On the hydrophilic sample studied, the air bubble is stabilized at air/galena separation distance of about 160 nm. At this point, the hydrodynamic effect could be totally ignored and the profile maintained by the disjoining pressure and Laplace pressure. From Figure 6.2 (B), at the equilibrium film thickness of wetting film, the disjoining pressure equals Laplace pressure. As the air bubble continues to be driven towards the galena plate, the center region is kept flat and stabilized, while the outer region keeps moving towards the substrate; this process was clearly shown in the spatiotemporal film profile of the air bubble. In the center area, the film thinning velocity was almost zero and no hydrodynamic interaction should be considered. The air bubble is stabilized due to the interactions of electrical double layer force and the pressure caused by the deformation of air bubble. These conclusion was consistent with those reported on the small air bubble radius of 98 μm in AFM,[22,23] however, in their system, it was the pressure caused by repulsive van der Waals force supporting the Laplace pressure of air bubble, while the double layer forces were inhabited by a high concentration of NaCl solution.

The FADS experimental result discussed above clearly validates the DLVO theory model for wetting film thinning on hydrophilic surfaces, and the disjoining pressure is calculated using Reynolds lubrication approximation. The equilibrium thickness of the wetting film was about 160 nm, and the disjoining pressure equals to Laplace pressure at this point.

b. Hydrophobic Galena Surfaces and Air Bubble

Galena-xanthate system is one of the most in the flotation industry. In present study, galena substrates are hydrophobized with KAX by applying electrochemical reaction, as introduced previously. Galena surfaces with different hydrophobicity are achieved by processing the galena samples in KAX solution under various applied potentials, which are selected according to cyclic voltammogram shown in Figure 6.1.

The wetting film experiment on hydrophobic galena surface have been carried out in FADS. The disjoining pressures were calculated by applying Reynolds lubrication approximation, Equation [6-8]. Results of disjoining pressures obtained are shown in Figure 6.3, with the following conditioning potentials: 50, 100, 150, 200 and 250 mV. The disjoining pressures are mainly contributed by electrical double layer forces and hydrophobic forces; because Van der Waals force could be ignored at large film separation distance. At low conditioning potential (50 mV), no negative disjoining pressure was measured. When the conditioning potential was increased to 100 mV, negative disjoining pressure with a small magnitude could be observed. The disjoining pressure measured continued to increase as the conditioning potential increased and the maximum disjoining pressure was observed at 250 mV for all the potentials studied in the present work. None of these pressure curves showed any discontinuous step, and this is evidence that they are not attributed to the artifact of nano-bubble on the surface.

Extended DLVO (eDLVO) theory is used to analyze these data obtained and the C and D parameters are shown in Figure 6.4. More importantly, these disjoining pressures measured change with the water contact angle, as show in Figure 6.4. Disjoining pressure is a kinetics property, and the water contact angle is a thermodynamics property. The variation trend of eDLVO fitting parameters is the same as that of water contact angle. Present study disclosed a connection between the kinetics property and thermodynamics properties of the wetting film, which is due to the

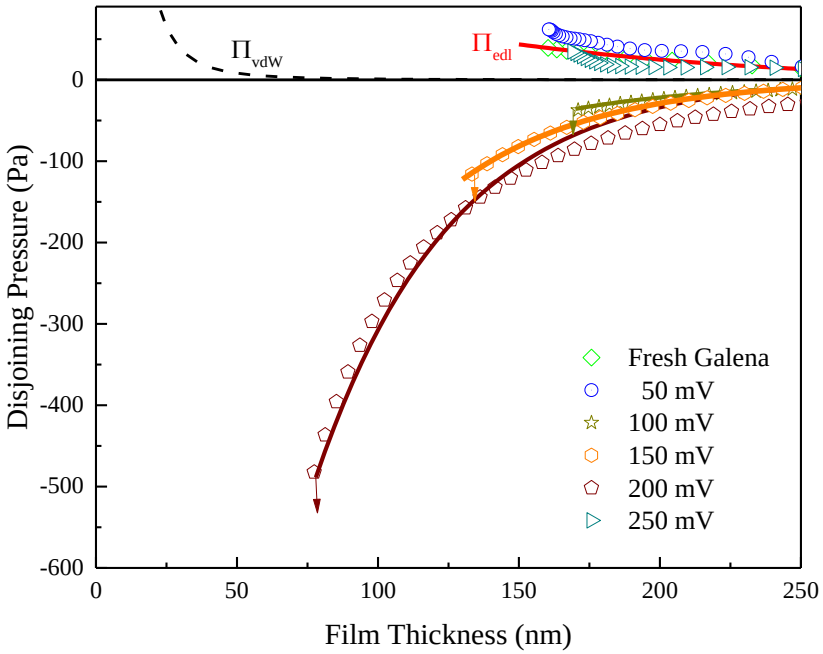

Figure 6.3 Disjoining pressures measured between air bubbles and galena surfaces, hydrophobized in 10^{-5} M KAX at pH 9.2 under differently applied potentials. Dash line represents the disjoining pressure contributed by van der Waals force, with Hamaker constant of -1.92×10^{-20} J.

intrinsic properties of the hydrophobic surfaces. This might have important contribution for industry application.

The spatiotemporal profile of two hydrophobized galena samples, hydrophobized under100 mV and 200 mV, are show in in Figure 6.5. Reynolds lubrication approximation has also been applied to calculate the disjoining pressure based on the air bubble spatiotemporal profiles obtained. The disjoining pressures calculated and the fitting process of eDLVO is also shown in Figure 6.5 (C) and (D). For convenience purpose, these two galena samples are designated as "galena-KAX-100" and "galena-KAX-200", respectively.

Figure 6.5 (A) and (B) show the interactions between an air bubble of radius of 2.5 mm in pure water and galena-KAX-100 and another air bubble and galena-KAX-200 surface. The curve of disjoining pressure shown is continuous, and thus the disjoining pressure measured is not raised from preexistence nanobubble. And, nanobubbles are not observed during the experiments. The profiles of air bubbles on the surface these two hydrophobic samples are different from that observed on hydrophilic galena surface. On hydrophobic surfaces, the air bubble will rupture instead of becoming stable when the separation distance is small. The film rupture distances are 170.2 nm and 81.2 nm for galena-KAX-100 and galena-KAX-200, respectively. The film thinning kinetics is also much faster on the hydrophobic surface than on the hydrophilic surface, which could be estimated from the air bubble profile and time label. The central film thinning velocity for the air bubble on galena-KAX-100 is about 700 μm/s and galena-KAX-200 is 800 μm/s. On the case of hydrophilic surfaces, the film thinning velocity reduces dramatically when the air bubble comes close to the substrates. The film thinning velocity on hydrophobic substrates does not change much. Because both electrical double layer forces and van der Waals forces were

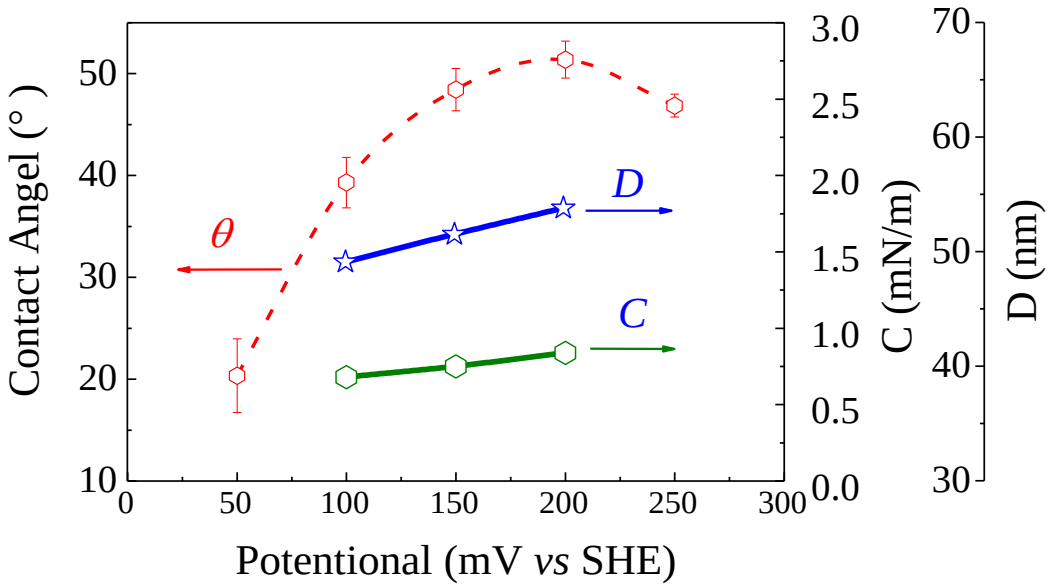

Figure 6.4 Effect of applied potentials on the receding water contact angles on galena surface. The water contact angles were measured directly in the FADS after the wetting film rupture. And the fitting parameter of C and D.

repulsive in this system, there must be some other attractive forces present in this system to drive the air bubble moving towards the galena surfaces and finally trigger the air bubble rupture. The force present is the so-called hydrophobic force. As introduced in the introduction section, there has been a wide debate concerning the origin of the hydrophobic force. In the study, it might be due to the water structure changing and reorganizing on the hydrophobic surface. Low density liquid (LDL) forms on the vicinity of the hydrophobic surfaces and this process cost free energy which result in the film wetting spontaneously on the hydrophobic surface. The physical nature of this process is due to the antipathy of water molecular and the hydrophobic xanthate species and the reorientation of 3D H-bonding configuration.

As shown in Figure 6.4, the receding water contact angles of galena-KAX-100 and galena-KAX-200 are 39.3º and 51.4º, respectively. This shows that the surface hydrophobicity of sample galena-KAX-200 is better than galena-KAX-100. Thus, it is very convincing that larger hydrophobic forces measured on the surface of galena-KAX-200 sample than that of galena-KAX-100 sample. The film thinning velocity on galena-KAX-200 is also larger than that of galena-KAX-100 in all film thickness, which could be confirmed from the spatiotemporal profiles. All of these data are consistent, and this further confirmed that the disjoining pressure measured is due to the presence of hydrophobic forces.

In Figure 6.5 (C) and (D), circles present the data calculated from the lubrication theory while the solid curves are the result of theoretical calculation using extended-DLVO theory. Exponential law is applied to describe the hydrophobic interaction[4] in this system,

$$\Pi_h = -\frac{C}{2\pi D}\exp\left(-\frac{h}{D}\right) \qquad [6\text{-}12]$$

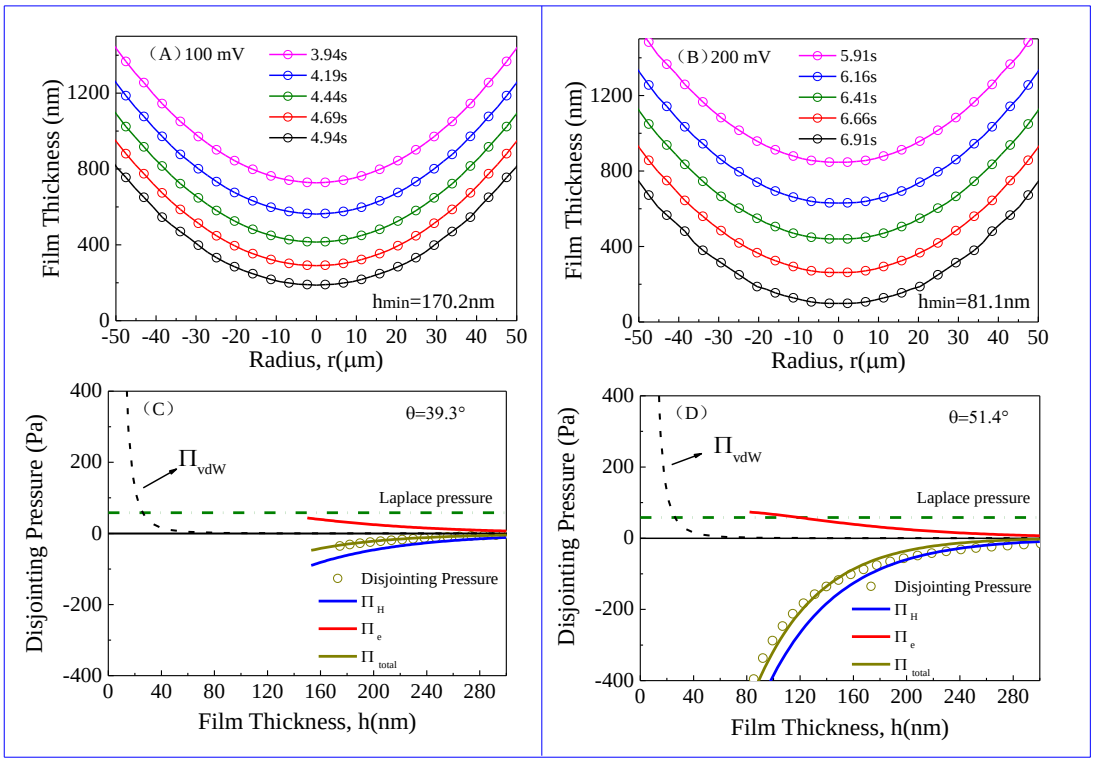

Figure 6.5 A and B show thin water film profile *h(r,t)* variation *vs. t*, during interactions between air bubbles and hydrophobized galena surfaces in pure water. Galena is conditioned in $Na_2P_4O_7$ aqueous solution (pH 9.2) for 2 minutes under: A, 100 mV and B, 200 mV. The radius of the air bubble was about 2.5 mm, and the approaching speed of the air bubble and galena is 1 μm/s. h_{min} represents the thin water thickness before rupture. In (C) and (D), they show the variation components of the disjoining pressure with film thickness. Circles are disjoining pressures calculated from the water profile using lubrication approximation, and the purple line through the circles are theoretical results by applying extended-DLVO theory. Blue lines are the disjoining pressure raised from hydrophobic force from hydrophobic surfaces.

C is a fitting parameter relating to the excess of surface tension, while *D* is the decay length. The fitting values of *C* and *D* are calculated using Mathematica (Wolfram, USA). Not surprisingly, all values of *C* and *D* of galena-KAX-200 are larger than galena-KAX-100, as shown in Figure 6.4.

All the values of *C* and *D* for the disjoining pressures shown in Figure 6.3 were calculated by applying the same methodology. These values are depended on the surface hydrophobicity ad reach maximum when the surface of galena is treated at 200 mV for 2 minutes. And this is evidence that the disjoining pressures are raising form the substrate surface hydrophobicity. In other words, the difference of decay length and the magnitude of *C* and *D* values is a result of hydrophobicity difference of the galena substrates. It is already known that the molecular level organization of KAX is different if galena substrates is conditioned under different applied potentials. If the applied potential is low, KAX ions are chemisorbed on the galena. If the applied potential is about 50 mV, monolayer of lead xanthate will start to form on the galena surfaces. When the applied potential reached about 200 mV, the monolayer formed will become well-ordered. And the

formation of this well-order monolayer will greatly increase the surface hydrophobicity of galena surfaces. As the applied potential continues to increase, multiple layers of metal xanthate will form on top of the monolayer metal xanthate. Potassium amyl xanthate or lead amyl xanthate will be also adsorbed on the outmost layer, with the hydrophilic part heading into bulk liquid, reducing the surface hydrophobicity of galena surfaces.

It is already well accepted that the hydrophobic effect is raised from the interfacial water molecules rearranging their position and orientation to compensate the loss the 3D hydrogen bonding on hydrophobic surfaces.[24,25] Though there are reports arguing that the adjustment of water molecules is effective only within 1 nm, our results clearly show that the influence of hydrophobic surface could be extended to tens of nanometers, as evidenced by the presence of long range hydrophobic forces. It is very likely that water rearrangement due to the loss of hydrogen bonding had some other effects and a mechanism made this effect effective for a longer range. A plausible mechanism is the formation of water clusters,[26] which significantly changes the entropy and enthalpy of the wetting film. As the free energy decreases, the wetting film will be thinning spontaneously. However, future work is required to analyze the hydrophobic force origination systematically.

6.6 Conclusion

In this chapter, spatiotemporal profiles of the wetting films confined between air bubble and galena surfaces have been obtained using the FADS and subsequently analyzed using the Reynolds lubrication approximation. When the galena surface is hydrophilic, the wetting film reaches an equilibrium at a film thickness of about 130 nm. The measured surface forces can be fitted to the classical DLVO theory as there no surface forces other than the double-layer and van der Waals forces in the wetting film.

When the galena surface is hydrophobized by immersing the mineral in a 10^{-5} M potassium amyl xanthate (KAX) solution at pH 9.2, the film ruptures at thicknesses in the range of 40 to 60 nm, depending on surface hydrophobicity. In the present work, the surface hydrophobicity is varied by control of the electrochemical potential of the mineral specimen. It can be said that film rupture occurs due to the presence of the hydrophobic force in the wetting film formed on hydrophobic surfaces. In general, both the hydrophobic force and contact angle increase with potential until it reaches ~200 mV. At higher potentials, galena surface becomes less hydrophobic due to formation of multiple layer of metal xanthate. At very high applied potential, galena would be oxidized to lead oxides/hydroxides according to the Eh-pH diagram.

6.7 References

1 Pan, L., Jung, S. & Yoon, R. H. Effect of hydrophobicity on the stability of the wetting films of water formed on gold surfaces. *J. Colloid Interface Sci.* **361**, 321-330 (2011).

2 Li, Z. & Yoon, R.-H. AFM force measurements between gold and silver surfaces treated in ethyl xanthate solutions: Effect of applied potentials. *Miner. Eng.* **36–38**, 126-131 (2012).

3 Butt, H.-J., Graf, K. & Kappl, M. *Physics and chemistry of interfaces*. (John Wiley & Sons, 2006).

4 Pan, L. & Yoon, R.-H. Hydrophobic forces in the wetting films of water formed on xanthate-coated gold surfaces. *Faraday Discuss.* **146**, 325-340 (2010).

5 Eslami Andargoli, M. B., Jannesar Malakooti, S., Doulati Ardejani, F. & Abdollahi, H. Effect of galvanic contact on the flotability of galena in the presence and absence of a collector. *International Journal of Mining Science and Technology* **22**, 629-632 (2012).
6 Paul, R. L., Nicol, M. J., Diggle, J. W. & Saunders, A. P. The electrochemical behaviour of galena (lead sulphide) — I. Anodic dissolution. *Electrochim. Acta* **23**, 625-633 (1978).
7 Fornasiero, D., Li, F. S. & Ralston, J. Oxidation of Galena .2. Electrokinetic Study. *J. Colloid Interface Sci.* **164**, 345-354 (1994).
8 Ahlberg, E. & Broo, A. E. Anodic Polarization of Galena in Relation to Flotation. *Int. J. Miner. Process.* **33**, 135-143 (1991).
9 Rao, M. Y. & Natarajan, K. Effect of electrochemical interactions among sulphide minerals and grinding medium on the flotation of sphalerite and galena. *Int. J. Miner. Process.* **29**, 175-194 (1990).
10 Page, P. W. & Hazell, L. B. X-ray photoelectron spectroscopy (XPS) studies of potassium amyl xanthate (KAX) adsorption on precipitated PbS related to galena flotation. *Int. J. Miner. Process.* **25**, 87-100 (1989).
11 Laajalehto, K., Nowak, P. & Suoninen, E. On the XPS and IR identification of the products of xanthate sorption at the surface of galena. *Int. J. Miner. Process.* **37**, 123-147 (1993).
12 Pritzker, M. D. & Yoon, R. H. Thermodynamic Calculations on Stable and Metastable Pbs-Ethyl Xanthate Systems. *J. Electrochem. Soc.* **131**, C98-C98 (1984).
13 Pritzker, M. D. & Yoon, R. H. Thermodynamic Calculations on Sulfide Flotation Systems .1. Galena-Ethyl Xanthate System in the Absence of Metastable Species. *Int. J. Miner. Process.* **12**, 95-125 (1984).
14 Buckley, A. N. & Woods, R. X-ray photoelectron spectroscopic and electrochemical studies of the interaction of xanthate with galena in relation to the mechanism proposed by Page and Hazell. *Int. J. Miner. Process.* **28**, 301-311 (1990).
15 Pritzker, M. D. & Yoon, R. H. The Relationship between the Open-Circuit Potential of a Galena Electrode and the Dissolved Lead Concentration. *Hydrometallurgy* **23**, 341-352 (1990).
16 Woods, R. The anodic oxidation of ethylxanthate on metal and galena electrodes. *Aust. J. Chem.* **25**, 2329-2335 (1972).
17 Exerowa, D. & Kruglyakov, P. M. in *Studies in Interface Science* Vol. Volume 5 (eds Exerowa Dotchi & M. Kruglyakov Pyotr) xvii (Elsevier, 1998).
18 Nedyalkov, M., Alexandrova, L., Platikanov, D., Levecke, B. & Tadros, T. Wetting films on a hydrophilic silica surface obtained from aqueous solutions of hydrophobically modified inulin polymeric surfactant. *Colloid. Polym. Sci.* **285**, 1713-1717 (2007).
19 Derjaguin, B. V. & Churaev, N. V. STRUCTURE OF WATER IN THIN-LAYERS. *Langmuir* **3**, 607-612 (1987).
20 Israelachvili, J. N. *Intermolecular and surface forces: revised third edition*. III edn, 260-261 (Academic press, 2011).
21 Bergström, L. Hamaker constants of inorganic materials. *Adv. Colloid Interface Sci.* **70**, 125-169 (1997).
22 Shi, C., Chan, D. Y. C., Liu, Q. & Zeng, H. Probing the Hydrophobic Interaction between Air Bubbles and Partially Hydrophobic Surfaces Using Atomic Force Microscopy. *The Journal of Physical Chemistry C* **118**, 25000-25008 (2014).
23 Shi, C. *et al.* Measuring Forces and Spatiotemporal Evolution of Thin Water Films between an Air Bubble and Solid Surfaces of Different Hydrophobicity. *ACS Nano* **9**, 95-104 (2015).

24 Chandler, D. Interfaces and the driving force of hydrophobic assembly. *Nature* **437**, 640-647 (2005).
25 Tabor, R. F., Grieser, F., Dagastine, R. R. & Chan, D. Y. C. The hydrophobic force: measurements and methods. *PCCP* **16**, 18065-18075 (2014).
26 Wang, J. & Yoon, R.-H. AFM forces measured between gold surfaces coated with self-assembled monolayers of 1-hexadecanethiol. *Langmuir* **24**, 7889-7896 (2008).

CHAPTER 7.
Conclusions and Recommendations

7.1 Conclusions

Stability of the thin liquid films (TLFs) confined between two hydrophobic surfaces have been studied. An atomic force microscope has been used to measure the surface forces in the colloidal film formed between two solid surfaces, while the force apparatus for deformable surfaces (FADS) recently developed at Virginia Tech has been used to measure the forces in wetting films.

The AFM force measurements have been conducted in two different H-bonding liquids including water and ethanol and the mixtures of the two at different ethanol mole fractions. Gold plates pretreated with potassium amyl xanthate (KAX) to obtain equilibrium water contact angles of 95.3º have been used as confining surfaces. The measurements are conducted at several different temperatures to derive thermodynamic functions associated with the macroscopic hydrophobic interaction. The results show that attractive forces not considered in the DLVO theory are present in the colloid films.

The FADS measurements have been conducted to measure the surface hydrophobic forces in the wetting films formed on gold, chalcopyrite, and galena. The measurement are carried out under conditions of applied potentials and compared with the water contact angles measured under the same conditions.

The major findings of the present work may be summarized as follows,

a. Long range attractive forces not considered in the classical DLVO theory have been measured in the colloid films confined between two hydrophobic gold surfaces in both pure water and pure ethanol, and also in the ethanol solutions of varying mole fractions. The non-DLVO forces are observed in all three cases, with the measured forces decaying exponentially with film thickness (h). It is the first time that hydrophobic forces have been measured systematically at different temperatures over a wide range of solution compositions.

b. It has been found that the measured non-DLVO forces increase with decreasing temperature in all liquids and solutions used in the present work. Thermodynamic analysis of the forces measured at different temperatures shows that the changes in excess film free energy (ΔG^f), excess film enthalpy (ΔH^f), and excess film entropy (ΔS^f) become increasingly negative with decreasing film thickness. The loss of system enthalpy is an evidence of water forming H-bonded clusters. The enthalpy loss is compensated by the decrease in configurational entropy. Despite the large enthalpy-entropy compensation observed in the present work, the free energy changes remain negative, indicating that the macroscopic interaction between two hydrophobic surfaces in the H-bonding liquids used in the present work is spontaneous. It is suggested, therefore, that the hydrophobic interaction is solvent mediated. In this regard, hydrophobic force is a solvophobic force created by the antipathy between the hydrophobic surface and the H-bonding solvent. At the face of the antipathy, the only way for the solvent molecules in the vicinity of a hydrophobic surface may be to form H-bonded clusters, resulting in losses of enthalpy, entropy, and free energy. It has been found that the enthalpy and entropy compensation is significant, which is the reason

that the solvophobic (or hydrophobic) interaction at macroscopic scale is relatively week. That the hydrophobic forces are weak may be precisely the reason that biology chooses structures, *e.g.*, cell membranes, proteins, vesicles, *etc*., using hydrophobic forces. Other forces are either too weak to hold the structures together or too strong for the biological structures to grow and sustain life.

c. The magnitudes of the solvophobic forces measured in colloid films are maximum in pure H-bonding liquids, *e.g.*, pure water and pure ethanol. When one type of H-bonding liquid is added to another type of H-bonding liquid, the solvophobic forces decrease, which may be attributed to the likelihood that the cohesive energy of one type of liquid is compromised in the presence of the other, which in turn reduces the propensity of the former to form H-bonded clusters.

d. It has been found for the first time that adding a small amount of ethanol to water causes the hydrophobic force to decrease sharply. This new finding may be attributed to the ethanol adsorption on hydrophobic surfaces with inverse orientation. Exposure of the OH groups of the adsorbed ethanol molecules toward the aqueous phase reduces the antipathy between the hydrophobic surface and the vicinal water molecules, which should in turn cause the propensity of the water molecules to form H-bonded clusters to decrease and hence cause the hydrophobic force to decrease.

e. The solvophobic forces measured in ethanol solutions are minimum at mole fractions of ~0.18, at which surface excess of ethanol is maximum. This finding may also be attributed to the inverse orientation of ethanol on hydrophobic surfaces.

f. Surface forces in the wetting films of water have been measured successfully using the FADS developed at Virginia Tech. The results obtained with gold and chalcopyrite substrates show that hydrophobic forces increase with increasing contact angles. The contact angles are less than 90^{o}, which minimizes the probability bubbles and cavitation being responsible for the long-range hydrophobic forces measured in the present work using the FADS.

g. The surface forces measured using the FADs show that hydrophobic forces decrease when dixanthogen is formed on chalcopyrite and gold, which is contrary to what has been reported on the bases of contact angle, electrochemistry, and spectroscopic methods. Further research may be needed for clarification.

h. Hydrophobic forces measured with xanthate-coated galena increases with increasing potentials. At potentials above 200 mV, however, both contact angle and hydrophobic force decrease due to oxidation of the substrates.

i. Hydrophobic forces measured in the wetting films of water formed chalcopyrite at open circuit in a 10^{-4} M KAX solution increases with increasing conditioning time. The measured force reaches a maximum at 10 min conditioning time and then decreases at longer conditioning times. The detrimental effect of the longer contact time is due to the adsorption of dixanthogen on top of the copper xanthate monolayer.

However, detrimental effect disappears when the dixanthogen is washed off by solvent wash.

7.2 Recommendation for Further Work

a. In the present work, solvophobic forces have been measured in water, ethanol and mixtures thereof. The measurements should be extended to other H-bonding and non-H-bonding liquids. It will be interesting to see the implication of the new information obtained in the present work to biology and biochemistry. I have shown that a tiny amount of ethanol greatly reduces the hydrophobic force.

b. The AFM force measurements suggest that hydrophobic force decreases substantially in the presence of a small amount of ethanol. This new finding has been attributed to the inverse orientation of ethanol on hydrophobic surfaces. However, no spectroscopic evidence has been given. It will be useful to conduct spectroscopic analysis of the surfaces treated with ethanol.

c. I have suggested that solvophobic forces are solvent mediated and suggested further that H-bonding molecules form clusters. It will be useful if one can detect the structural changes using advanced spectroscopic methods. To detect the structural changes, the solvents may need to be confined in nanotubes at very low temperatures.

d. I have shown that hydrophobic interaction at macroscopic scale is enthalpic. If so, one should be able to use a micro-calorimetry technique to measure the heat of macroscopic interaction.

e. It has been shown that FADS is a powerful tool to study hydrophobic interactions at macroscopic scale. Since it is a very new instrument, the measurement should be extended to many other minerals.

f. The surface forces measured using the FADS show that dixanthogen formation on gold and chalcopyrite is detrimental to hydrophobic force and hence to flotation. This finding is contrary to what has been known in the literature. Further studies is need to confirm the new finding.